Bárbara Almeida Rebelo

Bachelor degree in Biochemistry

Chemical synthesis of new histone deacetylase inhibitors and their evaluation as inducers of recombinant protein production in plants

Dissertation to obtain the Master Degree in Biochemistry for Health

Supervisor: Rita Ventura, PhD, ITQB-NOVA

Co-supervisor: Rita Abranches, PhD, ITQB-NOVA

Outubro, 2017

Bárbara Almeida Rebelo

Bachelor degree in Biochemistry

Chemical synthesis of new histone deacetylase inhibitors and their evaluation as inducers of recombinant protein production in plants

Dissertation to obtain the Master Degree in Biochemistry for Health

Supervisor: Rita Ventura, PhD, ITQB-NOVA

Co-supervisor: Rita Abranches, PhD, ITQB-NOVA

Jury

President: Dr. Pedro Manuel H. M. Matias, Senior Researcher, ITQB-NOVA
Main examiner: Dr. Hélder João Ferreira Vila Real, Postdoc Researcher, IBET
Examiner (s): Dr. Margarida Archer Franco Frazão, Auxiliary Researcher, ITQB-NOVA
Dr. Maria Rita Mendes Bordalo Ventura, Auxiliary Researcher, ITQB-NOVA

Instituto de Tecnologia Química e Biológica António Xavier da Universidade Nova de Lisboa

Outubro, 2017

Chemical synthesis of new histone deacetylase inhibitors and their evaluation as inducers of recombinant protein production in plants

ACKNOWLEDGMENTS

First of all, I would like to express gratitude for my supervisor Rita Ventura, for having believed in me from the beginning, for her concern for my work, for her availability, for her dedication and for her advice. Thank you for having me in your group, allowing me to enter the world of research. I would like to thank my other supervisor, Rita Abranches, for all her dedication, trust and support that always showed me and for gather all the necessary conditions for the development of this study. Thank you for all the knowledge and confidence I gained during this time.

I must thank Diana Lousa from Protein Modelling Lab at ITQB for all the knowledge transmitted for this project. For all the willingness to help me whenever I needed, I cannot thank you enough.

A special thank you to all the people at Bioorganic Chemistry Lab and Plant Cell Biology Lab for welcoming me and teach me. I am grateful especially to Osvaldo Ascenso and Rita Santos for their valuable help in the development of my work, Vanessa Miranda for being always available and João Cascão and Márcia Rénio for their friendship, companionship and tireless support.

To all my friends from Mangualde, Covilhã and Lisboa, especially to António Lopez, for all the support and affection that have always given to me. To everyone with whom I always smile, studied and enjoyed myself over the years.

Finally, I cannot never express my totally gratitude to family for the support in my decisions; to my parents for allowing me to finish another important stage in my life and to my brother for the love and confidence, and just for being there.

This is for you. Thank you!

ABSTRACT

Transgenic plants offer several advantages for the production of recombinant proteins with pharmaceutical value. Moreover, plant suspension cell cultures combine the benefits of plants with the advantages of recombinant protein production by microbial cell cultures.

Histones are proteins that are essential in gene expression control through several modifications like acetylation, phosphorylation and methylation. Histone acetyltransferases and histone deacetylases regulate the expression levels via acetylation and deacetylation of lysine residues in histones. Therefore, histone acetylation is associated with an increase in transcription levels, resulting in higher protein production levels. Inhibitors of these HDACs have been associated with the treatment of prostate and lymphoma cancer, reactivation of latent HIV cells and they also behave as small molecular enhancers for recombinant protein production.

The purpose of this work was to synthesise new HDAC inhibitors derived from the commercial inhibitors SAHA and Belinostat. Overall, forty compounds were successfully synthesised where key aspects of the HDACis structure were altered. *Nicotiana tabacum* BY2 cell suspension cultures expressing a human lipocalin-type prostaglandin D_2 synthase were used in order to evaluate the newly synthesised compounds as production enhancers of this protein.

Results show that compounds N'-(2-fluorophenyl)-N-hydroxyoctanediamide (**12**) and (2E)-N'-(2-bromo-4-fluorophenyl)-N-hydroxybut-2-enediamide (**6**) were efficient HDACis. They increased the acetylation levels and were functional as L-PGDS production enhancer. Commercial N-Hydroxy-N'-phenyloctanediamide (SAHA) significantly increased the acetylation levels but not L-PGDS production. The present work paves the way for employing epigenetic strategies to improve recombinant protein production by plant cell cultures.

Keywords: Molecular Farming, tobacco BY2 cell cultures, chemical synthesis, HDAC inhibitors, L-PGDS, histone acetylation

RESUMO

As plantas transgénicas possuem características vantajosas para a produção de proteínas recombinantes com valor farmacêutico. As culturas de células vegetais em suspensão combinam os benefícios das plantas com as vantagens de produção de proteínas recombinantes por culturas de células microbianas.

As histonas são proteínas essenciais para o controlo da expressão genética através de modificações na acetilação, fosforilação ou metilação. As histonas acetiltransferases e histonas deacetilases regulam os níveis de expressão através da acetilação e deacetilação de resíduos de lisinas presentes nas histonas. Por sua vez, a acetilação de histonas está associada a um aumento dos níveis de transcrição, resultando num aumento de produção de proteínas. Os inibidores das HDACs estão associados ao tratamento do cancro da próstata e linfoma, reactivação de células de HIV latentes e como potenciadores da produção de proteínas recombinantes.

Um dos objectivos deste trabalho foi a síntese de novos inibidores de HDAC derivados de inibidores comerciais, como o SAHA e o Belinostat. Foram sintetizados quarenta compostos com êxito, com alterações nos domínios-chave da estrutura dos inibidores. Neste estudo utilizou-se culturas de células de *Nicotiana tabacum* BY2 em suspensão, expressando a proteína recombinante prostaglandina D2 sintetase humana do tipo lipocalina, para avaliar o efeito dos compostos sintetizados na produção desta proteína.

Os resultados demostram que os compostos N'-(2-fluorofenil)-N-hidroxoctanediamida (**12**) e (2E)-N'-(2-bromo-4-fluorofenil)-N-hidroxibut-2-enediamida (**6**) funcionaram eficientemente como HDACis. Estes compostos produziram um aumento dos níveis de acetilação e potenciaram a produção de L-PGDS. O composto comercial N-hidroxi-N'-feniloctanediamida (SAHA) aumentou significativamente os níveis de acetilação, mas não a produção de L-PGDS. O presente trabalho demonstra a validade para a aplicação de estratégias epigenéticas com o objectivo de melhorar a produção de proteínas recombinantes em culturas de células vegetais.

Palavras-chave: *Molecular Farming*, culturas celulares BY2 de tabaco, síntese química, inibidores de HDAC, L-PGDS, acetilação de histonas.

LIST OF CONTENTS

FIGURE INDEX

TABLE INDEX

ABBREVIATIONS

APS - Ammonium persulfate
Ar – Aromatic
BBr_3 – Boron tribromide
BFE – binding free energy
BLAST – Basic local alignment search tool
BnOH – Benzyl alcohol
BSA – Bovine serum albumin
BY2 – Bright yellow 2
CCl_4 – Carbon tetrachloride
$CDCl_3$ – Deuterated chloroform
CH_3CN - Acetonitrile
CLA-1 – Lysosomal integral membrane protein-II analogous-1
DBU – 1,8-Diazabicyclo[5.4.0]undec-7.ene
DCM – Dichloromethane
DIPEA – *N*,*N*-diisopropylethylamine
DMF – Dimethylformamide
DMSO – Dimethyl sulfoxide
DMSO-d_6 – Deuterated dimethyl sulfoxide
DNA – Deoxyribonucleic acid
EDC – 1-Ethyl-3-(3-dimethylaminopropyl)carbodiimide
EtOAc – Ethyl acetate
EtOH – Ethanol
FDA – Food and Drug Administration
FT-IR – Fourier transform infrared spectroscopy
GMP – Good manufacturing practice
h – Hours
HAT(s) – Histone acetyltransferase(s)
HCl – Hydrochloric acid
HDAC(s) – Histone deacetylase(s)
HDACi(s) – Histone deacetylase inhibitor(s)
Hex – Hexane
HIV – Human immunodeficiency virus
Hz – Hertz
KH_2PO_4 – Monopotassium phosphate
L-PGDS – Lipocalin-type prostaglandin D2 synthase
MARs – Matrix attachment regions
MeOH – Methanol
$MgCl_2$ – Magnesium chloride
$MgSO_4$ – Magnesium sulphate
MHz – Megahertz
Min – Minute

MS – Murashige & Skoog
Na_2HPO_4 – Disodium hydrogen phosphate
NaCl – Sodium chloride
NAD – Nicotinamide adenine dinucleotide
$NaHCO_3$ – Sodium bicarbonate
NaOH – Sodium hydroxide
NH_2OH – Hydroxylamine
$NH_2OH{\cdot}HCl$ – Hydroxylamine Hydrochloride
NMR – Nuclear magnetic resonance
PBS – Phosphate-buffered saline
PBS-T - Phosphate-buffered saline with tween-20
PDB – Protein data bank
PGDS – Prostaglandin-D synthase
PMSF – Phenylmethanesulfonyl fluoride
Ppm – Parts per million
PTM – Post-translational modification
RNA – Ribonucleic acid
RT – Room temperature
SAHA - Vorinostat
SDS – Sodium dodecyl sulfate
SDS-PAGE – Sodium dodecyl sulfate – polyacrylamide gel electrophoresis
SME(s) – Small molecular enhancer(s)
THF – Tetrahydrofuran
TLC – Thin-layer chromatography
TSA – Trichostatin A
TSP – Total soluble protein

1 INTRODUCTION

1.1 Molecular farming

Plants are a simple and efficient bioproduction system for human survival, producing fibers, foods, wood and secondary metabolites with therapeutic effects. The evolutionary development of plants caused these metabolites to play a protective role against pathogens or predators, because of their anti-inflammatory, antimicrobial and psychoactive properties. Nowadays, it is imperative to produce new and effective compounds for further applications, so modern biotechnology pursues and investigates new paths to obtain these therapeutics in a controlled environment using cell cultures originated from the respective plant (Boehm, 2007).

Plant molecular farming is a branch of biotechnology, where plants are engineered to produce industrial and recombinant pharmaceutical proteins in large quantities. This technology involves several steps, such as the growing, harvesting, transport, storage, downstream process and protein purification (Boehm, 2007; Obembe et al., 2011). Advances in genomics and proteomics facilitate the identification and characterization of useful genes for placing into plant expression vectors, transforming the plants into transgenic plants to further administrate as need, as demonstrated in Figure 1-1 (Yao et al., 2015).

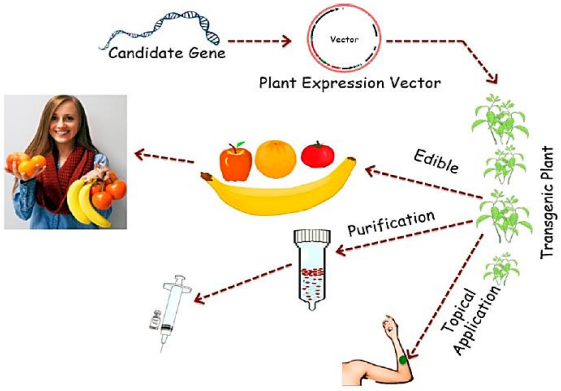

Figure 1-1- *Simple illustration of the process of molecular farming, including the process of transformation and the applicability of the product, topical, intravenous or edible vaccines administration (adapted from Yao et al., 2015).*

The development of genetic systems expressing foreign proteins in plants is facilitated by recombinant deoxyribonucleic acid (DNA) technology (Moustafa et al., 2015). Furthermore, alterations in specific genes or regulatory DNA sequences of the plant genome allowed to improve the products of therapeutic value that were already produced by the plant (Boehm, 2007; Obembe et al., 2011). The plants have the capability to perform post-translational modifications (PTM) that allow the recombinants

proteins to fold correctly, preserving their functional and structural integrity. Because of that, plants are able to produce complex functional mammalian proteins, as demonstrated in Table 1-1, (Obembe et al., 2011; Yao et al., 2015).

The market for biopharmaceutical products has grown substantially since 1994 and, over the past decades, roughly 250 biopharmaceuticals have received licenses in the United States and European Union (Figure 1-2) and several more are currently in clinical trials. These products, traditional vaccines, proteins and biomolecules extracted from the biological source material, represent an important category of the pharmaceutical product before the era of molecular biology, because they are produced in biological systems instead of chemical synthesis (Walsh, 2014). One of the main and attractive advantages in plant molecular farming is the low cost for large scale production. The plants are photoautotrophic, producing their biomass using inorganic substances and sunlight, which results in the low energy cost in production (Ma et al., 2003). However, when a cell suspension cultures established from plants are used, other obstacles are encountered. Low yield, purification and downstream processing hurdles have limited the progress of pharmaceuticals production on a clinical scale (Yao et al., 2015).

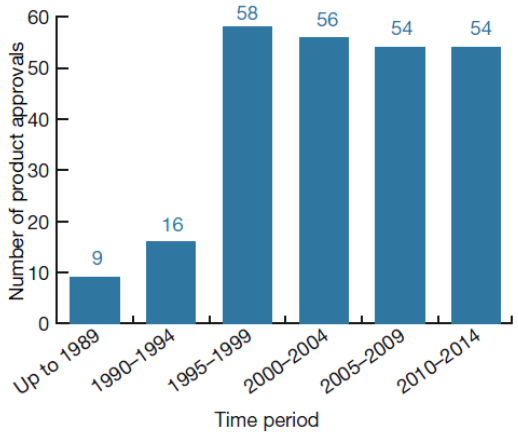

Figure 1-2- *Approval numbers for biopharmaceuticals products in the United States and European Union until 2014 (adapted from Walsh, 2014).*

Table 1-1- *List of biopharmaceuticals produced in several plant cell suspension cultures (reviewed in Santos et al., 2016).*

Host cell	Species	Protein	Application
Tobacco	*Nicotiana tabacum* BY2	Hepatitis B Surface Antigen (HBsAg)	Hepatitis B vaccine
		PRX-102(α-Galactosidase-A)	Fabry disease
		EPO	Tissue protective function
		Granulocyte-Macrophage Colony-Stimulating Factor (GM-CSF)	Production of white cells
		IL-4	Immunoregulation
		α -HBsAgMab	Hepatitis B antibody
		2G12 monoclonal α -HIVAb	Anti-HIV antibody
		Human Growth Hormone	Growth hormone
		IL-10	Immunoregulation
		Norwalk virus capsid protein	Acute gastroenteritis vaccine
		IL-12	Immunoregulation
Rice	*Oryza sativa*	Human α 1-antitrypsin	Emphysema
		hCTLA4Ig	Immunosuppressive agent
		Derp2-FIP-*fve* fusion protein	Immunomodulator and immunotherapeutic for allergies
		hGM-CSF	Production of white cells
		Human Serum Albumin	Treatment of hypoalbuminemia
		Human CTLS4Ig	Immunosuppressive agent
		Human Growth Hormone	Growth Hormone
Medicago	*Medicago truncatula*	EPO	Tissue protective
		Prostaglandin D_2 Synthase (PGDS)	Clinical marker
Carrot	*Daucus carota*	Taliglucerase α	Gaucher disease
		PEGylated recombinant human acetylcholinesterase (PRX-105)	Biodefense program
		α1-antitrypsin (PRX-107)	Emphysema
Tomato	*Lycopersicon esculentum*	hGM-CSF	Immunosuppressive and immunomodulator
Soybean	*Glycinemax*	HBsAg	Vaccine against Hepatitis B
Siberian Ginseng	*Acanthopanax senticosus*	Human lactoferrin	Immunosuppressive and immunomodulator
Korean ginseng	*Panax ginseng*		
Sweet Potato	*Ipomoea batatas*		

The pharmaceutical industry produces recombinant proteins in prokaryotic and eukaryotic systems. Bacteria and yeast expression systems are economically attractive because of their short cell cycle and well characterized genome, making the process of production and optimisation faster and efficient. However, the lack of glycosylation and accumulation of endotoxins in bacteria, and reduced secretion rates in yeast is the barrier for microbial-based production platforms (reviewed in Schmidt, 2004 and Terpe, 2006). The main reason for most therapeutical proteins being produced in eukaryotic systems is that one-third or more of biopharmaceuticals are glycoproteins which need glycosylation.

Despite being more expensive and highly favourable to contamination, mammalian cell culture systems produce the same PTM that occur in humans (Buyel, 2015; Schmidt, 2004). So, efforts are being made in the plant glycosylation pathway to improve the therapeutic safety of recombinant proteins and overall production process. One example is the enzyme taligucerase alfa produced for the treatment of Gaucher's disease, by the company Protalix, which is already in the market (Paul and Ma, 2011). An equivalent product is produced in Chinese Hamster Ovary cell-based systems, a mammalian expression platform, that remains the most commonly used expression system (Walsh, 2014). They express recombinant proteins with a terminal sialic residue, that prevents uptake, and it is necessary to be removed. In plant-based systems, the recombinant protein that is targeted to vacuole of carrot cells already exhibited the mannose residue. There is no need for an enzyme to remove it, so the cost is reduced (Yao et al., 2015).

1.1.1 Plant cell suspension cultures

High costs and some inefficiency of existing production systems, briefly explained in Table 1-2, coupled with increasing demand, highlights the potential of transgenic plant-based production platforms as an alternative protein production system (Obembe et al., 2011, Yao et al., 2015).

Plant cell suspension culture systems offer many advantages when compared with whole plants. They have a faster growth, more efficient secretion (Hellwig et al., 2004, Xu et al., 2012), they only require simple nutrients to grow, they have high-level containment, controlled and sterile production conditions and the risk of contamination with pathogens or endotoxins, dangerous to human health, is non-existent (Horn et al., 2004; Moustafa et al., 2015; Twyman et al., 2003). The downstream processing is simpler as the protein can be secreted into the culture medium, cheaper, there is no need to acquire highly specialized apparatus or hire highly qualified personnel to manage them. It should be noted that this expression system complies with GMP (good manufacturing practice) (Obembe et al., 2011; Santos et al., 2016; Walsh, 2014; Xu et al., 2012). In order to further improve this system, strategies such as to increase

Table 1-2- *Comparison of different aspects of several expression platforms for the production of pharmaceuticals (adapted from Yao et al., 2015).*

	Transgenic plants	**Plant cell culture**	Bacteria	Yeast	Mammalian cell culture	Transgenic animals
Overall cost	Very low	Medium	Low	Medium	High	High
Scale-up capacity	High	Medium	High	High	Very low	Low
Protein fold accuracy	High	High	Low	Medium	High	High
Glycosylation	Minor differences	Minor differences	-	Incorrect	Correct	Correct
Product quality	High	High	Low	Medium	High	High
Contamination risks	Low	Low	Endotoxins	Low	Virus, oncogenic DNA	Virus, oncogenic DNA
Safety	High	Non-specific	Low	Unknown	Medium	High
Storage cost	Inexpensive	Moderate	Moderate	Moderate	Expensive	Expensive

transcription rate to improve protein expression and addition of protease inhibitors to prevent protein degradation are currently under study at the Plant Cell Biology Laboratory.

Within the therapeutic space, perhaps plant-based systems may yet make the most influence upon healthcare applications. The production of therapeutic pharmaceuticals at an affordable market price is an important combination, between economics and scale production. Goals that plant systems can achieve (Walsh, 2014).

1.1.2 Limitations and optimisation of downstream processing

As in all production systems, also in plant systems, about 80% of the production cost is related to the cost of downstream processing, depending on product type and application. The downstream process is divided in primary recovery and purification, being influenced by the recombinant protein concentration, required product purity and plant extracts/cell-free culture medium (Wilken and Nikolov, 2012). Primary recovery serves for maximizing product yield and titter in extract/cell homogenate, to reduce extract/medium volume and to develop a clarified feed stream for purification. For plant cell suspension cultures, where the protein is secreted into the medium, the culture medium is concentrated,

clarified, conditioned and then separated by chromatography. Purification of protein produced by plant systems is dependent on protein properties and host cell impurities (Fischer et al., 2015; Wilken and Nikolov, 2012).

Even though the optimisation of protein production is essential, a more significant factor for the final product yields is the protein stability (Abranches et al., 2005). There are less recombinant proteins produced in the late stationary phase, because of increased proteolytic activity, that can be responsible for protein instability, therefore, a lower overall yield. Some differences in protein glycosylation or sometimes the long time needed to generate a stable transgenic line are challenges that need to be overcome by the implementation of new techniques and further research, in order to exploit plants as alternative bioreactors instead of mammalian cell cultures (Obembe et al., 2011; Xu et al., 2011).

According to Obembe et al., 2011, to increase the stability of the recombinant protein, one of the strategies to adopt would be subcellular targeting to and retaining in other subcellular compartments, such as the endoplasmic reticulum. This is accomplished by including the fusion of the endoplasmic reticulum-retention signal KDEL. Another strategy would be the addition of fusion and affinity tags to enhance the process of isolation and purification of proteins, as long as the tags can be removed to restore the native structure of the protein (Fischer et al., 2004). In general, these strategies can serve to increase the yield of biopharmaceuticals production using plant molecular farming.

1.1.3 Post-translational modifications

PTMs increase protein complexity and dynamics, causing an intricate regulation of biological events. They modify the primary structure of proteins by the removal and reversible addition of functional groups, by phosphorylation, acylation, glycosylation (most common modification) or ubiquitination. Structural changes occur in the protein, like interactions with proteins/other molecules, modulation of the activity and subcellular localization (Sun et al., 2006). Recombinant proteins usually contain some form of PTMs, which can affect protein properties important for their therapeutic application, such as product equivalence, i.e. the production of biopharmaceuticals already on the market using plant-based systems, without losing the fundamental characteristics of the drug, biological activity and immunogenicity (Walsh and Jefferis, 2006).

Glycosylation is the most common PTM found in natural and biopharmaceutical proteins, hence, changes in the glycosylation profiles can function as disease markers. These profiles and the functional activity of glycoproteins differ depending on the tissue in which the protein is expressed (Walsh and Jefferis, 2006). In plants, glycosylation takes place in the secretory pathway (in the Golgi apparatus and endoplasmic reticulum) and it is defined by the covalent link of sugar moieties to proteins, improving their

bioavailability, folding and biological activity (Gomord et al., 2010; Obembe et al., 2011). Glycocomponents, that are attached to individual glycosylation sites, can direct a protein to its final destination; sugar side chains can stabilize a glycoprotein, improve solubility, shield hydrophobic patches on its surface and protect from proteolysis; high concentration of sialic acid can enhance glycoprotein's plasma half-life; galactose residues exposed decrease plasma half-life (Walsh and Jefferies, 2006).

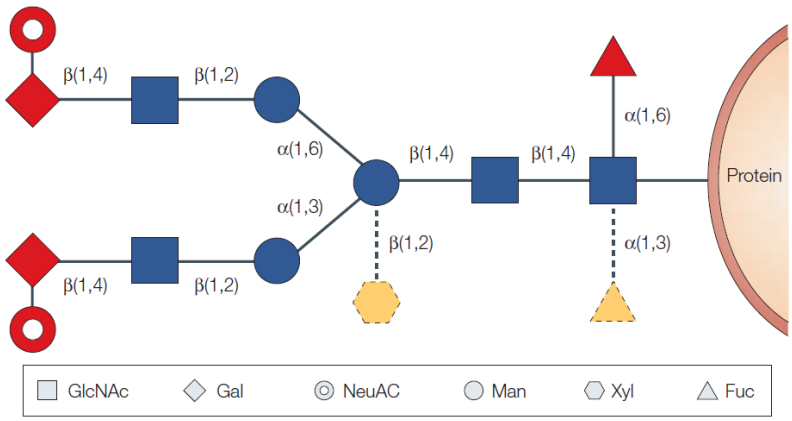

Figure 1-3- *Structure of the glycan chain in humans and plants. Blue residues are common to plants and humans. Yellow residues are only found in plants while red residues are only found in humans. GlcNAc: N-acetylglucosamine; Gal: galactose; NeuAC: sial acid; Man: manose; Xyl: xylose; Fuc; fucose. Adapted from Ma et al., 2003.*

All eukaryotes add different glycan chains, according to their taxonomy, to the proteins as they pass through the secretory pathway (Ma et al., 2013). Between animals and plants, there is in some cases a different glycosylation pattern. Mammals have β(1,4)galactose, α(1,6) fucose and sialic acid residues to the N-glycan of their glycoproteins whereas plants have α(1,3) and α(1,4) fucose and β(1,2) xylose residues to the N-glycan, as briefly explain in Figure 1-3 (Gomord et al., 2010; Obembe et al., 2011). Owing to these differences, complications may arise such as allergic reactions, or immunogenicity due to sugar moieties immunogenic in humans (Obembe et al., 2011; Walsh, 2014).

To overcome this problem, several strategies have been tested with the aim of manipulating plant N-glycans to produce humanized recombinant proteins, so they can be administrated to humans/animals without adverse effects. Knockout or silencing of α(1,3) fucose and β(1,2) xylose with ribonucleic acid (RNA) interference was tried to prevent the production of plant glycan moieties (Ma et al, 2013). Also, the targeting of recombinant proteins to the endoplasmic reticulum where non-immunogenic N-glycans are produced, is a way to avoid accumulations of these sugars because these proteins are located in the Golgi apparatus. Besides removal of fucose and xylose residues, galactose and silica-acid residues must be added in order to "humanize" recombinant proteins. All the efforts to optimise the glycosylation pathway

have improved the safety of recombinant proteins and reduce fears about glycan immunogenicity (Castilho and Steinkellner, 2012; Ko et al., 2008, Ma et al, 2013, Yao et al, 2015).

The fundamental phase when evaluating a new biopharmaceutical product should not be the structure of the PTM itself, but rather that the recombinant protein is functional and does not cause adverse effects, regardless of whether or not there are the same PTMs as mammals. One can take into account the functionality and safety consequences of any PTM or altered PTM profile (Walsh and Jefferis, 2006).

1.2 *Nicotiana tabacum* as an expression platform for recombinant proteins

A vital choice for the success of molecular farming technology is the selection of a suitable host, taking into account the biological factors, amenability to transformation and regeneration, and the economic factors, like the value of the recombinant protein itself, scale-up, maintenance and downstream processing cost, among others (reviewed in Obembe et al., 2011 and Abranches et al., 2005).

A plant with a simple transformation protocol, well-established growth parameters and shorter production cycle and good scale-up capacity is ideal. To further reduce the purification cost, cell suspension cultures are created from plants with those characteristics. This leads to advantages such as high biomass yield and secretion of recombinant proteins into the culture medium. That can be the solution for safer and cost-effective plant-based expression platforms. For these reasons, *Nicotiana tabacum* L. cv. Bright Yellow 2 (BY2) cell suspension cultures is one of the favourite systems for molecular farming (Yao et al., 2015).

Nicotiana belongs to de Solanaceae family and is naturally distributed through Southern Hemisphere and North America, with the exception of *N. fragrans, which* found in the South Pacific Ocean and the *N. Africana* that is restricted to Africa (Aoki, 2000). A callus induced from *Nicotiana tabacum* L. cv. BY2 in Tobacco Science Research Laboratory, Japan Tobacco, Inc., originated a BY2 cell line (Nagata et al., 1992).

Tobacco is a successful crop for molecular farming as a result of well-established gene transfer and expression, the existence of a large-scale processing infrastructure and high biomass yield. Even though tobacco cultivars produce some toxic alkaloids, there are low-alkaloid varieties that can be employed for the production of biopharmaceutical proteins. Fortunately, tobacco cell suspension cultures lack these metabolites (Twyman et al., 2003). BY2 and NT-1 cell lines are the most popular to be used as bioreactors for molecular farming. The recombinant protein expressed is secreted to the culture medium, simplifying the purification process (Yao et al., 2015).

The first therapeutic protein expressed in plants, precisely in transgenic tobacco, was a human growth hormone normally isolated from blood. The hormone gene was flanked by DNA fragments containing the promoter and polyadenylation site of the nopaline synthase gene (Barta et al., 1986).

1.2.1 Prostaglandin-D synthase (PGDS, lipocalin type)

PGDS is involved in a diversity of physiologic pathologies and functions. This enzyme catalyses the isomerization of prostaglandin H2 into to prostaglandin D2, in the presence of sulfhydryl compounds. PGDS comes from phylogenetically distinct proteins families and is divided in two classes: the hematopoietic PGDS type, a glutathione-requiring enzyme, and the lipocalin-type (L-PGDS), the glutathione-independent enzyme or previously known as brain-type enzyme (Urade, Hayaishi, 2000).

L-PGDS is an N-glycosylated monomeric protein and belongs to the lipocalin superfamily, which are secretory proteins partly responsible for the binding and transportation of small hydrophobic molecules. It was first purified out of a rat brain in the soluble form and the full amino acid sequence was determined to be identical to β-trace, a major protein of human cerebrospinal fluid (Urade, Hayaishi, 2000). It operates as a carrier protein, binding small lipophilic molecules (Pires et al., 2014).

L-PGDS can be found in the heart, central nervous systems and male genital organs (Inoue et al., 2008) and it is involved in inflammatory responses, sleep and pain regulation and progression of Alzheimer's disease. Besides, L-PGDS protects against hypoxemia, ischemia and its deficiency leads to obesity and facilitates atherosclerosis (reviewed in Pires et al., 2014).

Inoue et al., 2008, hypothesized that serum concentration of L-PGDS could function as a specific biomarker for atherosclerotic coronary artery disease. Given the number of potential application for this enzyme, recombinant L-PGDS is a powerful research tool for the progress of new therapies and novel diagnostic methods (Pires et al., 2014).

1.3 Epigenetic modifications

Eukaryotic organisms have their genetic information packaged inside the cell nucleus and this arrangement is mediated by histones. DNA is organized around histones, basic nuclear proteins rich in lysine and arginine residues, to form the chromatin that is essential for DNA replication and repair, transcription and recombination (Kim et al., 2006). The basic unit of eukaryotic chromatin is the nucleosome core particle, a repeating element consisting of a histone octamer with DNA wrapped around it, formed by histones H2A, H2B, H3 and H4 (Bieliauskas and Pflum, 2008; Lusser et al., 2001; Ruijter et al., 2003).

After years of research, many transcriptional regulators and co-regulators have been identified as histone acetyltransferases (HATs) and histone deacetylases (HDACs). Histone tails are positively charged due to amino groups present in the lysine and arginine amino-acids; hyperacetylation potentially neutralizes this charge and thus weakens the interaction of the histone octamer with the DNA, negatively charged because of phosphate groups. This could destabilize the nucleosomes and expand the chromatin, enabling transcriptional regulators to access the DNA. Also, acetylation, transfer of an acetyl group from acetyl coenzyme A to the amine group of a lysine residue at the N-terminal tail, could act as a specific signal to alter protein-histone interaction (Lusser et al., 2001). HDACs remove the acetyl groups, encouraging the affinity binding between histones and DNA backbone. Increased binding to DNA condenses the structure of DNA, blocking the accessibility of binding of transcription factors to target genes, thus avoiding transcription (Liu et al., 2016; Lusser et al., 2001; Ma et al., 2013; Verdin and Ott, 2014; Wu et al., 2008).

The reversible acetylation of lysine residues found in the amino-terminal tails of histone proteins, highly conserved and flexible, plays an important role in transcriptional activation and repression. There is an equilibrium in the activities of HAT and HDAC enzymes that balance the regulation of PTM, as seen in Figure 1-4 (Bieliauskas and Pflum, 2008; Lusser et al., 2001; Salmi-Smail et al., 2010).

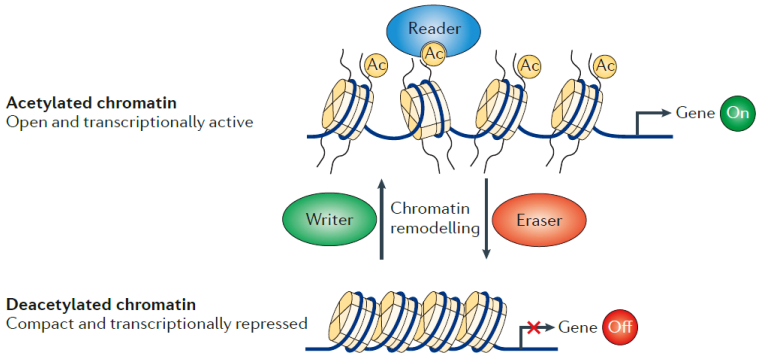

Figure 1-4- *Histone acetylation, chromatin condensation and gene expression. On the top of the image is the effect of HAT and the effect of HDAC at the bottom. When acetylated, the string of nucleosomes is illustrated with the tails protruding (adapted from Verdin and Ott, 2014).*

HDAC proteins are enzymatic components of chromatin modifying complexes and they are able to regulate mitosis, chromatin organization, cell differentiation, apoptosis, metabolism and immune response in eukaryotes (Bieliauskas and Pflum, 2008; Hendricks et al., 2011). Due to size, number of catalytically active sites, homology and cellular localization, HDAC proteins are grouped into four classes. Sirtuins proteins belong to the class III, the only class that operates by a NAD^+ (nicotinamide adenine dinucleotide) - dependent mechanism. In contrast, classes I, II and IV HDAC proteins operate by

a metal ion-dependent mechanism, a crucial point for most inhibitors. Class I consists of HDAC1, HDAC2, HDAC3 and HDAC8 and shares homology with yeast transcriptional regulator RDP3. Class II, homologue to yeast HDAC1, includes two subclasses, IIa which includes HDAC4, HDAC5, HDAC7, HDAC9 and IIb that includes HDAC6 and HDAC10; the first has a single catalytic site and the other has two. Based on phylogenetic analysis and because it shares features with class I and II, HDAC11 is the sole member of class IV (Bieliauskas and Pflum, 2008; Ruijter et al., 2003). Cumulative information regarding HDAC function through genetic studies allowed elucidation of the different roles for different isoforms (Hendricks et al., 2011).

Histone acetylation and deacetylation play an imperative role in the regulation of gene expression by modulating chromatin topology. Consequently, HDAC inhibitors (HDACis) affect gene transcription by hyperacetylating histones. The role of HDAC function in cellular processes has been deduced by the effects seen after enzymatic activity inhibition (reviewed in Dietz and Casaccia, 2010). A broad-spectrum of molecules have been tested as HDACis, in addition to their initial function. For example, trichostatin A (TSA) was isolated from *Streptomyces hygroscopicus* and was originally used as an antifungal antibiotic.

The majority of HDACis undergoing clinical trials inhibit non-specifically all HDAC isoforms, also known as pan-inhibitors, like SAHA and TSA (Marks, 2007). So, selective HDACis would be the ideal drugs to elucidate the individual functions of each HDAC isoform. A practical example is the development of class-selective or isoform-selective HDAC inhibitor (HDACi) that could define the molecular mechanism behind HDAC activity, in order to provide a more effective treatment (Bieliauskas and Pflum, 2008).

1.4 Design and development of HDAC inhibitors.

Increasing HAT activity facilitates gene expression and, therefore protein production, which can also be achieved by HDAC inhibition. In fact, higher HDAC activity levels have been associated with transcriptional repression (Salmi-Smail et al., 2010). In this context, a handful of HDACi drugs (see Table 1-3 for more detailed information) are in clinical trials or have gained FDA (Food and Drug Administration) approval for the treatment of several dysfunctions, as explained in the next sub-section.

HDACis are grouped into four major structural families: hydroxamic acids (e.g. SAHA), short-chain aliphatic acids (e.g. Valproic acid), cyclic tetrapeptides (e.g. Romidepsin) and benzamides (e.g. Entinostat) (Shirakawa et al., 2013). The first choice for the design of a metal-related inhibitor is the target metal ion and, depending on its electronic/ionic characteristics, to define the type of electron donating or chelating groups like –CONHOH or –COOH, which should be included in a given molecular unit, thus resulting in an HDACi with one or more chelating groups. The design of these inhibitors is formulated to

structurally mimic the HDAC aliphatic acetyl-lysine substrate and can be divided in three essential domains (Figure 1- 5). The capping group is solvent-exposed and interacts with amino acid residues at the entrance region of the active site, it is responsible for differentiating the HDAC isoforms and its size may govern HDAC class selectivity. The metal binding moiety resides in the protein interior. This domain coordinates with the zinc atom within the HDAC active site. In this case, in addition to the drug containing a chelating group, it is also important that it includes other functional groups capable of establishing interactions, within the subcavities of the active site, in particular through H bonds or hydrophobic interactions with amino acid residues.

The linker positions the other two domains for interaction in the active site because it is structurally related to the carbon chain of the acetyl-lysine substrate. It has been diversified by changing the length and creating unsaturation points along the chain.

Optimisation of these domains is crucial for the construction of compounds that better fit into the catalytic center of the enzyme HDAC and, therefore, with higher potency as HDACi (Bieliauskas and Pflum, 2008; Gediya et al., 2005; Salmi-Smail et al., 2010; Santos, 2014).

.

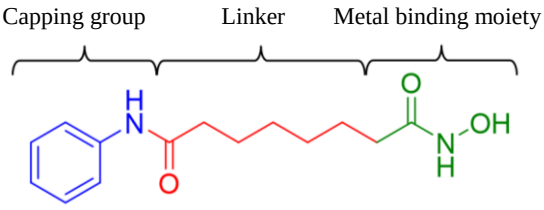

Figure 1-5- *Structure of suberoylanilide hydroxamic acid (SAHA) with its three important domains: capping group, linker and metal binding moiety. SAHA is adopted as a reference inhibitor.*

Table 1-3- *List of HDACis, including their structure, and information about the treatment applications.*

HDAC inhibitor	Structure	Treatment
Trichostatin A	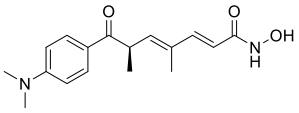	Cutaneous T-cell lymphoma (Bieliauskas and Pflum, 2008)
SAHA (Vorinostat) *Approved by FDA*	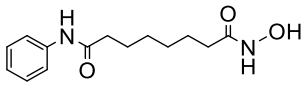	Cutaneous T-cell lymphoma (Bieliauskas and Pflum, 2008)
Belinostat *Approved by FDA*	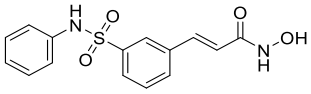	Relapsed or refractory peripheral T-cell lymphoma (Mottamal et al., 2016)
Givinostat	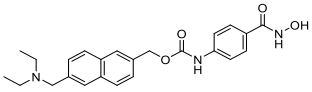	Hodgkin's lymphoma, chronic lymphocytic leukaemia and multiple myeloma (Mottamal et al., 2016)
Panobinostat *Approved by FDA*	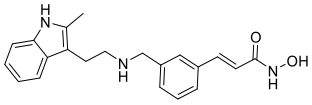	Solid tumours or cutaneous T-cell lymphoma, multiple myeloma (Mottamal et al., 2016)
Sodium butyrate	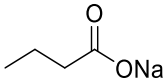	Neurodegenerative conditions (Chuang et al., 2009)
Valproic acid	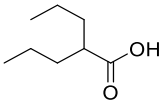	Refractory solid or central nervous system tumours (Mottamal et al., 2016)
Mocetinostat (MGCD0103)	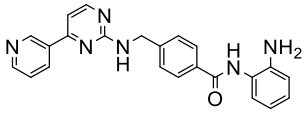	Chronic lymphocytic leukaemia (Mottamal et al., 2016)
Entinostat (MS-275)	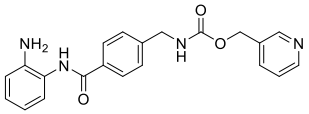	Refractory solid tumours and lymphomas (Mottamal et al., 2016)
Romidepsin (FK228, depsipetide) *Approved by FDA*	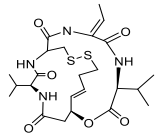	T-cell malignancies (Hendricks et al., 2011)

1.4.1 HDACi synthesis

To obtain compounds that could potentially act as HDACi and, thus, increase the production of recombinant proteins, key aspects were altered in order to assess which structure may be of added value to the activity of the compound. Based on previously published synthesis of HDACis and derivates, like TSA

and SAHA, a small library of hydroxamic and carboxylic acid derivates can be achieved by following the synthetic scheme represented in Figure 1-6 (Chen et al., 2011).

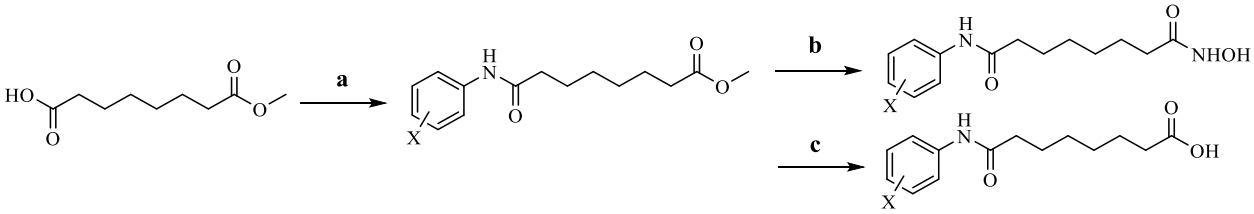

Figure 1-6- *The synthetic route of the target compounds using suberic acid monomethyl ester as starting material. Similar syntheses were performed with mono-ethyl fumarate as starting material. Reagents: (a) Preparation of ester - XArNH$_2$, DMF, EDC; (b) Preparation of hydroxamic acid - MeOH, NH$_2$OH·HCl, NaOH; (c)Preparation of carboxylic acid - THF, NaOH.*

The first step (a) consists in a typical coupling reaction for amide bond formation using the aniline derivate and a carboxylic acid with a coupling agent, 1-Ethyl-3-(3-dimethylaminopropyl)carbodiimide, (EDC) in dimethylformamide (DMF). The ester produced may follow two synthetic routes, so as to produce two different compounds with a minimal structural difference. While hydroxamic acids could be prepared from the corresponding carboxylic acid precursor in the presence of a dehydration agent and hydroxylamine (NH_2OH), the direct hydroxylaminolysis from methyl/ethyl substrates is a simpler reaction. Foremost, hydroxamic acid (b) can be prepared by mixing the ester and hydroxylamine hydrochloride ($NH_2OH·HCl$) with sodium hydroxide (NaOH) in methanol (MeOH). The ester, dissolved in tetrahydrofuran (THF) and after NaOH addition, can be converted in a carboxylic acid (c) (Beillard et al., 2016; Chen et al., 2011).

As mentioned in sub-section **1.4**, a library of compounds with structural differences in the three principal domains was designed and synthesised. The starting material with 4 and 8-carbon linker was used to form amides with different anilines, containing different substituents, mostly halogens or functional groups in the aromatic ring (Ar), at different positions. Considering the extreme importance of the metal chelator moiety and the carboxylic acid being a good metal chelator, it was tested along with the very good metal chelating group hydroxamic acid in BY2 cell suspension cultures.

Many metal ions play a crucial role in biological and biomedical processes because of their interaction with proteins or DNA. Thus, the pharmacological activity of these synthesised compounds, also known as ligands, results from their coordination with existing metal ions in biological systems. Zinc is present in an extensive variety of proteins, including in the catalytic center of histones, and is significant to the metabolism of most organisms (Santos, 2014; Santos-Martins et al., 2014).

To investigate the potential binding of the synthesised HDACis in an HDAC system, molecular docking studies were performed.

1.4.2 HDACis: multitarget compounds

The diversity of medical dysfunctions or pathologies, its complexity, comes as a challenge for compounds to have a diversified performance, a criterion that HDACis fulfil. In the field of cancer, HDACi suppress tumour cell proliferation by inducing cell differentiation and regulating genes associated with anti-cancer effects; they can be conjugated to pre-existing therapies in order to optimise their effectiveness, whether it is synergistic or additive (several compounds are represented in Table 1-3) vitro (Bieliauskas and Pflum, 2008; Gediya et al., 2005, Mottamal et al., 2016).

An example of a case study was reported by Chen et al., 2011, preliminary discovered that TSA and SAHA up-regulate a lysosomal integral membrane protein-II analogous-1(CLA-1) that mediate selective uptake of cholesteryl ester from peripheral tissues to the liver. They regulated the CLA-1 transcriptional activity in HepG2 cells and the HDAC inhibition rate (Chen et al., 2011).

In the field of neuroscience, quite a few HDACis described above have been tested to combat neurodegenerative conditions. Valproic acid, with mood stabilizing and anticonvulsant activities, crosses the blood brain barrier so it can be administered orally. Another pioneering study showed, as preliminary results, that treatment with TSA/SAHA protected against glutathione depletion-induced oxidative stress, a neuroprotection mechanism (Chuang et al., 2009).

A new study under development is the reactivation of latent HIV (Human Immunodeficiency Virus) cells by HDACi. Inhibition of HDACs activity reactivates a fraction of latent HIV, associated with transcriptional silencing of the integrated provirus. By forcing the transcriptional activation of HIV it will possibly lead to virus expression, virus/host-induced cell death of the reactivated cells and to the extinction of the pool of latently infected cells (Shirakawa et al., 2013).

1.4.2.1 HDACis as small molecular enhancers (SMEs)

Commercial HDACis have been used in mammalian cells as SME to potentially increase the production of recombinant proteins (reviewed in Allen et al., 2008). Sodium butyrate and SAHA are small molecule additives to cell culture medium that improve the expression of recombinant proteins with significant utility in the production and manufacture of biopharmaceuticals. To identify these SMEs in mammalian-based expression systems, the compounds are tested for their capability to enhance the expression of either a specific protein or a monoclonal antibody. Furthermore, it is important to know the effect of SME addition on the expression system with several classes of recombinant proteins, in order to

evaluate if it regulates the transcriptional activation, the level of acetylation or if it regulates other mechanisms that can be involved (Allen et al., 2008; Gorman and Howard, 1983).

There have been several experiments with SME that demonstrate its potential as an enhancer of protein production. Backliwal et al., 2008 verified that Valproic acid enhanced the yield of transient antibody 25% more than sodium butyrate, which alone increases the production of recombinant proteins. Sodium butyrate has been reported to enhance total protein production in CHO-Tag and 293-EBNA cell lines and to increase production of the GFP protein in NSO and NSO-Tag mammalian cell lines (Parham et al., 1998). In plants, these HDACis are only used for fundamental biology studies, but recent work in the Plant Cell Biology Lab at ITQB, revealed that one of the compound, SAHA, can act as SME in *Medicago truncatula* cell cultures (Santos et al Submitted). They demonstrated that this compound enhances L-PGDS production in *M. truncatula* and that this was related with the ability of SAHA to inhibit the activity of HDACs.

Some HDACis behave as SME that are useful for generating protein reagents needed for pre-clinical investigations or for large-scale therapeutic protein manufacturing. Sodium butyrate, SAHA or VPA are capable of enhancing the expression of recombinant proteins in mammalian cells and is also being studied in plant cell cultures, with the same purpose (Allen et al., 2008; Santos et al., submitted).

1.5 Objectives

The main goal of this project is to synthesise analogues of HDACis and test them in plant cell cultures, in order to evaluate their potential as enhancers of recombinant protein production. The work will be divided in two parts. Firstly, SAHA and Belinostat will be the starting point for the design of our new compounds with modifications in the capping group by introduction of halogens and other functional groups. Also, the size of the linker will have four to ten carbons, with/without double bonds. This work will be performed at the Bioorganic Laboratory at ITQB. Secondly, there will be a biological evaluation where the synthesised compounds will be tested in a transgenic tobacco cell suspension line, which produces the human recombinant protein L-PGDS, with the aim of increasing its yield through transcriptional enhancement. This will include establishment of growth curves, measurement of total soluble protein, determination of cell viability, quantification of the recombinant product and checking the effect of the best performing HDACi in histone H3 acetylation levels. This part of the work will be carried out at the Plant Cell Biology Laboratory at ITQB.

2 MATERIAL AND METHODS

2.1 Chemistry

2.1.1 Compound characterization and purification

Organic solutions, intermediate reagents and solvents were prepared, distilled, dried and purified by conventional techniques. For more details, check sub-section **6.1** in chapter **6**. Analytical thin layer chromatography (TLC) was carried out on aluminum-backed Merck 60 F254 silica gel plates. The spots corresponding to the compound or reagents were identified by ultraviolet radiation (254 nm) and then the TLC immersed in a respective reagent for staining: phosphomolybdic acid (FLUKA^{TM}) (5%) in ethanol (EtOH, CARLO ERBA) for the amides and carboxylic acids, (5%) iron (III) chloride (SIGMA-ALDRICH) in hydrochloric acid (HCl, Riedel-de Haën) (0.5 M) for hydroxamic acids and (0.3%) ninhydrin (MERCK) in 100 ml 1-butanol (MERCK) plus 3 ml glacial acetic acid (MERCK) for anilines.

Purification of each product was done by recrystallization, silica flash-column chromatography on Silica gel Merck 60 or preparative thin layer chromatography. In silica flash-column chromatography, the product is dissolved in dichloromethane (DCM, MERCK) /MeOH (CARLO ERBA) and the solution applied to a column of flash silica, eluting with ethyl acetate (EtOAc, CARLO ERBA):hexane (Hex, CARLO ERBA), with an increasing polarity gradient, depending on the compound polarity in the TLC of the reaction mixture (1:9 EtOAc:Hex, 2:8 EtOAc:Hex, 3:7 EtOAc:Hex for more polar compounds). Each preparative thin layer chromatography needs 20 g of dissolved silica per plate (2 mL of water per g of silica).

Nuclear magnetic resonance (NMR) spectra were acquired on a Bruker 400 spectrometer. Chemical shifts for **^{1}H-NMR**, acquired at 400 MHz, are given in parts per million (ppm) and calibrated by reference to signals from the solvent [7.26 ppm for deuterated chloroform ($CDCl_3$) and 2.5 ppm for deuterated dimethyl sulfoxide (DMSO-d_6)]. For **^{13}C NMR**, the spectras were acquired at 101 MHz and calibrated according to the respective solvent from Cambridge Isotope Laboratories, Inc. (77.16 ppm for $CDCl_{3+}$, 39.52 ppm for DMSO-d_6). NMR spectra peaks were ascribed with the assistance of 2D NMR spectroscopy, COSY and HMQC. Coupling constants (J) are calculated in hertz (Hz) and the multiplicity of each signal is given as singlet (s), doublet (d), triplet (t), quartet (q), doublet of doublets (dd), doublet of doublet of doublets (ddd), triplet of doublets (td), doublet of triplets (dt), doublet of doublet of triplets (ddt) or multiplet (m). When needed, spectras of **^{19}F NMR** or **^{31}P NMR** were performed.

Infrared (IR) spectroscopy was performed in Bruker Optics - IFS 66v/S FT-IR spectrometer.

Melting points of the compounds were obtained using a BUCHI 530 equipment.

2.1.2 General procedure for the amide bond formation

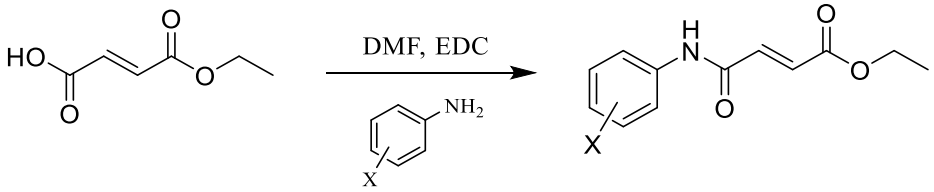

[1]

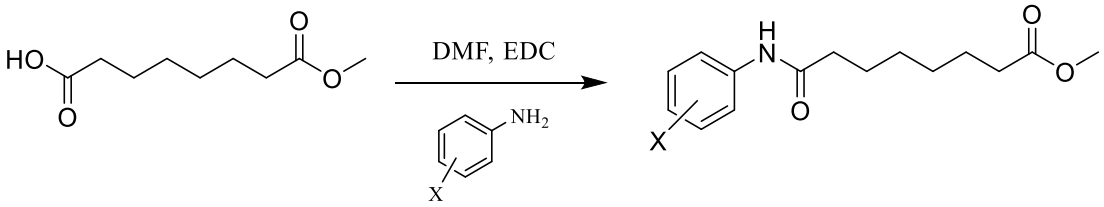

[2]

All the compounds described in section **2.1.2** were obtained by dissolving the starting material (E)-4-ethoxy-4-oxobut-2-enoic acid **[1]** (SIGMA-ALDRICH) or 8-methoxy-8-oxooctanoic acid **[2]** (SIGMA-ALDRICH), commercially known as mono-ethyl fumarate and suberic acid monomethyl ester, respectively, in dry DMF (BHD) in a two-neck round-bottom flask, under argon atmosphere. The respective aniline for each reaction and EDC [Tokyo Chemical Industry Co., Ltd. (TCI)], a coupling agent, were added afterward and the reaction stirred overnight at room temperature (RT). To confirm if the starting material was consumed, TLC was performed (3:7 EtOAc:Hex). The overall work-up involved quenching the reaction with water and liquid-liquid extraction with EtOAc (x3). The organic phases were combined, dried with anhydrous magnesium sulfate ($MgSO_4$, LaborSpirit) and the solvents removed by evaporation under vacuum. All the compounds were purified by recrystallization, with the exception of compound **[32]** and compound **[40]**, with Hex:EtOAc (Chen et al., 2011).

<u>Experiment 1:</u> Ethyl (2E)-3-[(2-fluorophenyl)carbamoyl]prop-2-enoate [3]

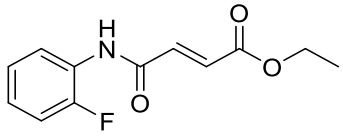

[3]

To a stirred solution of mono-ethyl fumarate **[1]** (3.47 mmol; 500 mg) in DMF (3.50 mL) was added 2-fluoroaniline (SIGMA-ALDRICH) (5.21 mmol; 0.50 mL) and EDC (5.21 mmol; 997 mg) portionwise. Recrystallization provided the compound **[3]**, as a yellow solid (83%; 687 mg).

^{1}H NMR (400 MHz, $CDCl_3$): δ 8.40 (t, *J* = 7.8 Hz, 1H, Ar), 7.86 (s, 1H, NH), 7.20 – 7.06 (m, 4H, Ar and CH=CH), 6.96 (d, *J* = 15.2 Hz, 1H, CH=CH), 4.29 (q, *J* = 7.1 Hz, 2H, OCH_2CH_3), 1.34 (t, *J* = 7.1 Hz, 3H, OCH_2CH_3).

^{13}C NMR (101 MHz, $CDCl_3$) δ 165.2 (C=O, quaternary), 161.4 (C=O, quaternary), 158.3 (C-F, quaternary), 144.1 (C-NH, quaternary), 135.8 (CH=CH), 132.1 (CH=CH), 125.2 (CH, Ar), 124.7 (CH, Ar), 121.8 (CH, Ar), 114.9 (CH, Ar), 61.4 (OCH_2CH_3), 14.2 (OCH_2CH_3).

Melting Point – 78 – 80 ºC

FT-IR (ATR): (vmax/cm-1) 3356 (NH), 1710 (C=O), 1677 (C=O, amide).

Experiment 2: Ethyl (2E)-3-[(2-bromo-4-fluorophenyl)carbamoyl]prop-2-enoate [5]

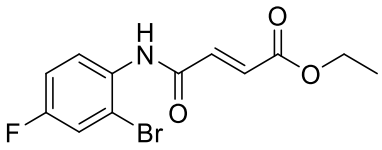

[5]

To a stirred solution of **[1]** (6.94 mmol; 1g) in DMF (5 mL) was added 2-bromo-4-fluoroaniline (SIGMA-ALDRICH) (10.35 mmol; 1.18 mL) and EDC (10.35 mmol; 1.994 g). The resulting solution was stirred overnight and the crude residue purified by recrystallization. This afforded the expected derivative as a beige powder (63% yield, 1.378 g).

^{1}H NMR (400 MHz, $CDCl_3$): δ 8.42 (dd, J = 8.9, 5.6 Hz, 1H, Ar), 7.77 (s, 1H, NH), 7.33 (dd, J = 7.7, 2.8 Hz, 1H, Ar), 7.14 – 7.08 (m, 1H, Ar), 7.08 – 7.04 (m, 1H, CH=CH), 6.96 (d, J = 15.3 Hz, 1H, CH=CH), 4.30 (q, J = 7.1 Hz, 2H, OCH_2CH_3), 1.35 (t, J = 7.1 Hz, 3H, OCH_2CH_3).

^{13}C NMR (101 MHz, $CDCl_3$) δ 165.1 (C=O, quaternary), 161.4 (C=O, quaternary), 160.1 (C-F, quaternary), 135.9 (CH=CH), 132.2 (CH=CH), 131.5 (C-NH, quaternary), 123.2 (CH, Ar), 119.4 (CH, Ar), 115.5 (CH, Ar), 113.8 (Br-C, Ar, quaternary), 61.4 (OCH_2CH_3), 14.1 (OCH_2CH_3).

Melting Point – 196 – 200 ºC

FT-IR (ATR): (vmax/cm-1) 3266 (NH), 1713(C=O), 1643 (C=O, amide).

Experiment 3: Ethyl (2E)-3-[(3-methoxyphenyl)carbamoyl]prop-2-enoate [8]

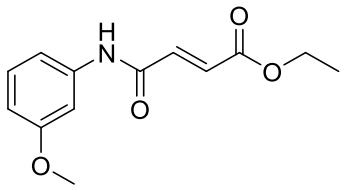

[8]

DMF (5 mL) and **[1]** (6.94 mmol; 1 g) were mixed together, followed by the addition of 4-methoxyaniline (SIGMA-ALDRICH) (10.35 mmol; 1.17 mL) and EDC (10.35 mmol; 1.994 g). The mixture was stirred at RT, overnight. The final compound was a gold granulate solid with 79% yield (1.364 g).

^{1}H NMR (400 MHz, $CDCl_3$) δ 7.91 (s, 1H, NH), 7.39 (s, 1H, Ar), 7.23 (t, J = 8.2 Hz, 1H, Ar), 7.12 (d, J = 15.3 Hz, 1H, C<u>H</u>=CH), 7.08 (d, J = 8.0 Hz, 1H, Ar), 6.95 (d, J = 15.3 Hz, 1H, CH=C<u>H</u>), 6.71 (d, J = 8.0 Hz, 1H, Ar), 4.28 (q, J = 7.1 Hz, 2H, OC<u>H$_2$</u>CH$_3$), 3.81 (s, 3H, Ph-OC<u>H$_3$</u>), 1.33 (t, J = 7.1 Hz, 3H, OCH_2C<u>H$_3$</u>).

^{13}C NMR (101 MHz, $CDCl_3$) δ 165.7 (<u>C</u>=O, quaternary), 161.7 (<u>C</u>=O, quaternary), 160.3 (<u>C</u>OCH$_3$, quaternary), 138.7 (<u>C</u>-NH, quaternary), 136.8 (<u>C</u>H=CH), 131.5 (CH=<u>C</u>H), 129.9 (<u>C</u>H, Ar), 112.3 (<u>C</u>H, Ar), 111.1 (<u>C</u>H, Ar), 105.9 (<u>C</u>H, Ar), 61.5 (O<u>C</u>H$_2$CH$_3$), 55.4 (Ph-OC<u>H$_3$</u>), 14.2(OCH$_2$<u>C</u>H$_3$).

Melting Point – 105 - 107 ºC

FT-IR (ATR): (vmax/cm-1) 3354 (NH), 1679 (C=O), 1606 (C=O, amide).

Experiment 4: Methyl 7-[(2-fluorophenyl)carbamoyl]heptanoate [11]

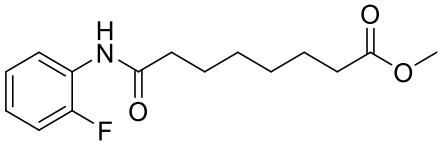

[11]

2-Fluoroaniline (7.26 mmol; 0.53 mL) was mixed with **[2]** (4.84 mmol; 0.87 mL) in DMF (4.600 mL); then EDC (7.26 mmol; 1.380 g) added. The purified product was a white powder (54%, 0.740 g).

^{1}H NMR (400 MHz, $CDCl_3$) δ 8.33 (t, J = 7.8 Hz, 1H, Ar), 7.33 (s, 1H, NH), 7.15 – 6.99 (m, 3H, Ar), 3.67 (s, 3H, OC<u>H$_3$</u>), 2.40 (t, J = 7.5 Hz, 2H, C<u>H$_2$</u>), 2.32 (t, J = 7.5 Hz, 2H, C<u>H$_2$</u>), 1.70 (m, C<u>H$_2$</u>-C<u>H$_2$</u>), 1.39 (dd, J = 7.7, 4.3 Hz, 4H, C<u>H$_2$</u>-C<u>H$_2$</u>).

^{13}C NMR (101 MHz, $CDCl_3$) δ 174.1 (C=O, quaternary), 171.2 (C=O, quaternary), 153.4 (C-F, quaternary), 126.4 (C-NH, quaternary), 124.6 (CH, Ar), 124.1 (CH, Ar), 121.7 (CH, Ar), 114.8 (CH, Ar), 51.4 (OCH_3), 37.6 (CH_2), 33.9 (CH_2), 28.7 (CH_2- CH_2), 25.2(CH_2), 24.7 (CH_2).

Melting Point – 52 - 60 ºC

FT-IR (ATR): (vmax/cm-1) 3305 (NH), 2923 (OCH_3), 1726 (C=O), 1667 (C=O, amide).

Experiment 5: Methyl 7-[(2-iodophenyl)carbamoyl]heptanoate [14]

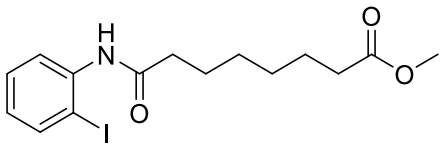

[14]

2-Iodoaniline (TCI) (8.34 mmol; 1.84 g) and **[2]** (5.56 mmol; 1 mL) were dissolved in DMF (5 mL) and, then, EDC (8.34 mmol; 1.61 g) was added. The solution was stirred overnight. The residue was purified by recrystallization to afford the target compound, a white powder (30%, 0.656 g).

^{1}H NMR (400 MHz, $CDCl_3$) δ 8.23 (d, J = 7.6 Hz, 1H, Ar), 7.78 (d, J = 8.0 Hz, 1H, Ar), 7.42 (s, 1H, NH), 7.34 (t, J = 7.8 Hz, 1H, Ar), 6.84 (t, J = 7.1 Hz, 1H, Ar), 3.67 (s, 3H, OCH_3), 2.38 (dt, J = 43.5, 7.5 Hz, 4H, CH_2-CH_2), 1.71 (ddt, J = 45.8, 14.6, 7.3 Hz, 4H, CH_2-CH_2), 1.39 (ddd, J = 16.0, 11.0, 7.6 Hz, 4H, CH_2-CH_2).

^{13}C NMR (101 MHz, $CDCl_3$) δ 174.1 (C=O, quaternary), 171.2 (C=O, quaternary), 138.7 (CH, Ar), 138.1 (C-NH, quaternary), 129.2 (CH, Ar), 125.9 (CH, Ar), 122.0 (CH, Ar), 89.9 (C-I, quaternary), 51.5 (OCH_3), 37.8 (CH_2), 33.9 (CH_2), 28.8 (CH_2- CH_2), 25.3 (CH_2), 24.7 (CH_2).

Melting Point – 76 - 78 ºC

FT-IR (ATR): (vmax/cm-1) 3265 (NH), 2947 (OCH_3), 1729 (C=O), 1656 (C=O, amide).

Experiment 6: Methyl 7-[(4-fluorophenyl)carbamoyl]heptanoate [17]

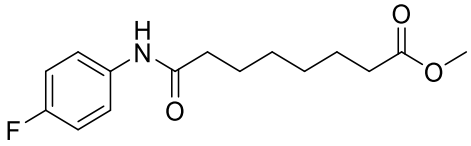

[17]

4-fluoroaniline (FLUKA™) (5.58 mmol; 0.53 mL) was added to a solution of **[2]** (3.72 mmol; 0.700 g) in DMF (3.50 mL). EDC (5.58 mmol; 1.069 g) was added portionwise. The mixture was left to stir overnight followed by work-up, to afford a white powder (87%, 0.910 g).

^{1}H NMR (400 MHz, $CDCl_3$) δ 7.47 (dd, J = 8.8, 4.8 Hz, 2H, Ar), 7.29 (s, 1H, NH), 7.00 (t, J = 8.6 Hz, 2H, Ar), 3.67 (s, 3H, OCH_3), 2.33 (q, J = 7.7 Hz, 4H, CH_2-CH_2), 1.78 – 1.59 (m, 4H, CH_2-CH_2), 1.43 – 1.32 (m, 4H, CH_2-CH_2).

^{13}C NMR (101 MHz, $CDCl_3$) δ 174.2 (C=O, quaternary), 171.2 (C=O, quaternary), 160.4 (C-F, quaternary), 133.9 (C-NH, quaternary), 121.6 (CH, Ar), 121.5 (CH, Ar), 115.6 (CH, Ar), 115.4 (CH, Ar), 51.5 (OCH_3), 37.3 (CH_2), 33.9 (CH_2), 28.7 (CH_2), 28.6 (CH_2), 25.2 (CH_2), 24.6 (CH_2).

Melting Point – 81 - 84 ºC

FT-IR (ATR): (vmax/cm-1) 3382 (NH), 2943 (OCH_3), 1723 (C=O), 1692 (C=O, amide).

Experiment 7: Methyl 7-[(2-bromo-4-fluorophenyl)carbamoyl]heptanoate [20]

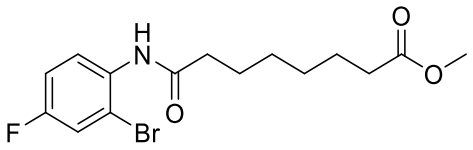

[20]

2-bromo-4-fluoroaniline (3.81 mmol; 0.43 mL) and **[2]** (2.54 mmol; 0.50 mL) were dissolved in DMF (2.50 mL) and EDC was added (3.81 mmol; 0.719 g). Purification via recrystallization gave a white power (46%, 0.421 g).

^{1}H NMR (400 MHz, $CDCl_3$) δ 8.30 (dd, J = 9.0, 5.6 Hz, 1H, Ar), 7.47 (s, 1H, NH), 7.29 (dt, J = 6.8, 3.4 Hz, 1H, Ar), 7.10 – 7.01 (m, 1H, Ar), 3.67 (s, 3H, OCH_3), 2.37 (dt, J = 39.6, 7.5 Hz, 4H, CH_2-CH_2), 1.70 (ddt, J = 40.7, 14.5, 7.3 Hz, 4H, CH_2-CH_2), 1.48 – 1.33 (m, 4H, CH_2-CH_2).

^{13}C NMR (101 MHz, $CDCl_3$) δ 174.1 (C=O, quaternary), 171.1 (C=O, quaternary), 159.6 (C-F, quaternary), 132.1 (C-NH, quaternary), 123.1 (CH, Ar), 121.5 (C-Br, quaternary), 119.1 (CH, Ar), 115.1 (CH, Ar), 51.5 (OCH_3), 37.7 (CH_2), 33.9 (CH_2), 28.7 (CH_2), 28.7 (CH_2), 25.2 (CH_2), 24.7 (CH_2).

Melting Point – 60 - 62 ºC

FT-IR (ATR): (vmax/cm-1) 3279 (NH), 2923 (OCH_3), 1725 (C=O), 1663 (C=O, amide).

Experiment 8: Methyl 7-[(3-methoxyphenyl)carbamoyl]heptanoate [23]

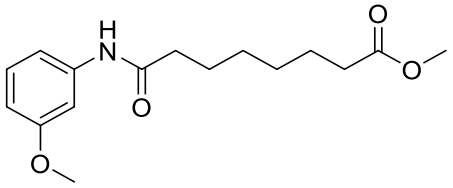

[23]

In a round-bottom flask, 3-methoxyaniline (8.34 mmol; 0.94 mL) and **[2]** (5.56 mmol; 1 mL) were placed in DMF (5.20 mL). The mixture was stirred and EDC (8.34 mmol; 1.610 g) was added. This procedure afforded the expected product as a brown powder (87% yield, 1.411 g).

^{1}H NMR (400 MHz, $CDCl_3$) δ 7.39 (s, 1H, NH), 7.33 (s, 1H, Ar), 7.19 (t, J = 8.1 Hz, 1H, Ar), 6.97 (d, J = 7.9 Hz, 1H, Ar), 6.65 (d, J = 7.0 Hz, 1H, Ar), 3.79 (s, 1H, Ph-OCH_3), 3.67 (s, 1H, OCH_3), 2.32 (dt, J = 10.9, 7.5 Hz, 4H, CH_2-CH_2), 1.78 – 1.58 (m, 4H, CH_2-CH_2), 1.43 – 1.31 (m, 4H, CH_2-CH_2).

^{13}C NMR (101 MHz, $CDCl_3$) δ 169.5 (C=O, quaternary), 166.6 (C=O, quaternary), 155.3 (C-OCH_3, quaternary), 134.5 (C-NH, quaternary), 124.8 (CH, Ar), 107.0 (CH, Ar), 105.3 (CH, Ar), 100.6 (CH, Ar), 50.5 (Ph-OCH_3), 46.7 (OCH_3), 32.8 (CH_2), 29.1 (CH_2), 23.9 (CH_2.CH_2), 20.5 (CH_2), 19.9 (CH_2).

Melting Point – 79 - 81 ºC

FT-IR (ATR): (vmax/cm-1) 3358 (NH), 2938 (OCH_3), 1718 (C=O), 1688 (C=O, amide).

Experiment 9: Methyl 7-[(4-iodophenyl)carbamoyl]heptanoate [26]

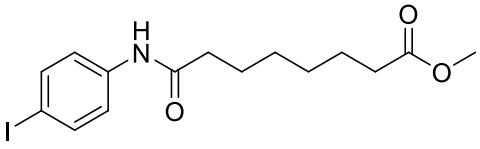

[26]

To a stirred solution of **[2]** (3.72 mmol; 0.700 g) in DMF (3.50 mL), was added 4-iodoaniline (Alfa Aesar) (5.58 mmol; 1.222 g) and EDC (5.58 mmol; 1.069 g). The resulting solution was stirred overnight and the crude purified by recrystallization. This afforded the expected derivative as a purple powder (81%, 1.177 g).

^{1}H NMR (400 MHz, $CDCl_3$) δ 7.61 (d, J = 8.7 Hz, 2H, Ar), 7.34 (s, 1H, NH), 7.31 (d, J = 8.6 Hz, 2H, Ar), 3.67 (s, 3H, OCH_3), 2.32 (dd, J = 15.6, 8.0 Hz, 4H, CH_2-CH_2), 1.78 – 1.57 (m, 4H, CH_2-CH_2), 1.42 – 1.31 (m, 4H, CH_2-CH_2).

^{13}C NMR (101 MHz, $CDCl_3$) δ 174.2 (C=O, quaternary), 171.3 (C=O, quaternary), 137.8 (CH, Ar), 137.8 (C-NH, quaternary), 121.5 (CH, Ar), 87.1 (C-I, quaternary), 51.5 (OCH_3), 37.5 (CH_2), 33.9 (CH_2), 28.67 (CH_2), 28.63 (CH_2), 25.1 (CH_2), 24.6 (CH_2).

Melting Point – 107 - 108 ºC

FT-IR (ATR): (vmax/cm-1) 3367 (NH), 2933 (OCH_3), 1713 (C=O), 1682 (C=O, amide).

Experiment 10: Methyl 7-[(4-bromophenyl)carbamoyl]heptanoate [29]

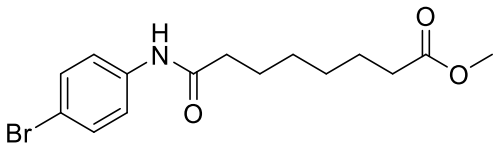

[29]

4-Bromoaniline (SIGMA-ALDRICH) (8.34 mmol; 1.435 g) was added to **[2]** (5.56 mmol; 1 mL) in DMF (5.20 mL), followed by addition of EDC (8.34 mmol; 1.599 g). The final compound was a white powder with 81% yield (1.536 g).

^{1}H NMR (400 MHz, $CDCl_3$) δ 7.42 (s, 4H, Ar), 7.22 (s, 1H, NH), 3.67 (s, 3H, OCH_3), 2.33 (dt, J = 9.3, 7.5 Hz, 4H, CH_2-CH_2), 1.79 – 1.57 (m, 4H, CH_2-CH_2), 1.39 (dd, J = 13.5, 10.0 Hz, 4H, CH_2-CH_2).

^{13}C NMR (101 MHz, $CDCl_3$) δ 174.2 (C=O, quaternary), 171.2 (C=O, quaternary), 137.0 (C-NH, quaternary), 131.9 (CH, Ar), 121.2 (CH, Ar), 116.6 (C-Br, quaternary), 51.5 (OCH_3), 37.5 (CH_2), 33.9 (CH_2), 28.6 (CH_2), 28.6 (CH_2), 25.1 (CH_2), 24.6 (CH_2).

Melting Point – 109 - 111 ºC

FT-IR (ATR): (vmax/cm-1) 3371 (NH), 2941(OCH_3), 1702 (C=O), 1696 (C=O, amide).

Experiment 11: Methyl 7-[(2-bromophenyl)carbamoyl]heptanoate [32]

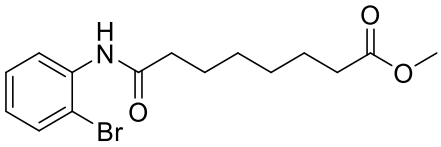

[32]

[2] (5.56 mmol; 1 mL) was mixed with 2-bromofluoroaniline (SIGMA-ALDRICH) (8.34 mmol; 0.94 mL) in DMF (5.20 mL), at RT. EDC (8.34 mmol; 1.599 g) was then added to the solution. The crude was purified by silica flash-column chromatography (7:3 Hex:EtOAc) and the resulting product was a yellow powder (33%, 0.618 g).

^{1}H NMR (400 MHz, $CDCl_3$) δ 8.35 (d, J = 7.8 Hz, 1H, Ar), 7.61 (s, 1H, NH), 7.53 (d, J = 8.1 Hz, 1H, Ar), 7.31 (t, J = 7.8 Hz, 1H, Ar), 6.97 (t, J = 7.7 Hz, 1H, Ar), 3.67 (s, 3H, $OC\underline{H_3}$), 2.37 (dt, J = 43.6, 7.5 Hz, 4H, $C\underline{H_2}$-$C\underline{H_2}$), 1.81 – 1.60 (m, 4H, $C\underline{H_2}$-$C\underline{H_2}$), 1.47 – 1.34 (m, 4H, $C\underline{H_2}$-$C\underline{H_2}$).

^{13}C NMR (101 MHz, $CDCl_3$) δ 174.1 ($\underline{C}$=O, quaternary), 171.1 ($\underline{C}$=O, quaternary), 135.6 ($\underline{C}$-NH, quaternary), 132.1 ($\underline{C}$H, Ar), 128.4 ($\underline{C}$H, Ar), 125.0 ($\underline{C}$H, Ar), 121.9 ($\underline{C}$H, Ar), 113.2 ($\underline{C}$-Br, quaternary), 51.4 ($O\underline{C}H_3$), 37.8 ($\underline{C}H_2$), 33.9 ($\underline{C}H_2$), 28.8 ($\underline{C}H_2$), 28.7 ($\underline{C}H_2$), 25.2 ($\underline{C}H_2$), 24.7 ($\underline{C}H_2$).

Melting Point – 52 - 55 ºC

FT-IR (ATR): (vmax/cm-1) 3271 (NH), 2948 (OCH_3), 1727 (C=O), 1658 (C=O, amide).

<u>Experiment 12:</u> Attempted synthesis of methyl 7-[(3-hydroxyphenyl)carbamoyl]heptanoate [35]

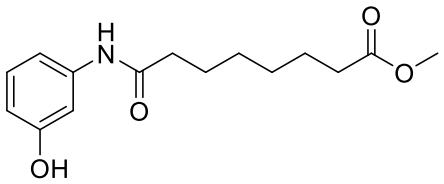

[35]

To a solution of **[23]** (0.34 mmol; 0.100 g) in anhydrous DCM (0.78 mL) at 0 ºC, was added dropwise a solution of boron tribromide (BBr_3, SIGMA-ALDRICH) in DCM (1 M; 0.05 mL). The reaction mixture was warmed to RT and stirred for 15 minutes (min) and then terminated by dropwise addition of DCM (7.81 mL) and water (3.13 mL), with further stirring for 20 min (Zhang et al., 2015). The organic layer was washed with a saturated solution of sodium bicarbonate ($NaHCO_3$, Fisher Scientific), twice with water and dried. After **^{1}H NMR** analysis, in the first attempt it was found that only a small percentage of the starting material has been consumed. By altering the reaction conditions, the result obtained was similar. In one experiment where the reaction was stirred overnight, the NMR spectrum showed that the methyl group attached to the phenol had been cleaved. However, compound [**35]** was not obtained because the ≈ 3.5 ppm peak, characteristic of an ester, was not visible and a deviation occurred in the ppm zone corresponding to the protons of the linker. We conclude that a carboxylic acid was obtained, occurring deprotection of the ester and the methoxide group in the phenol.

Experiment 13: **Methyl 7-[(4-hydroxyphenyl)carbamoyl]heptanoate [36]**

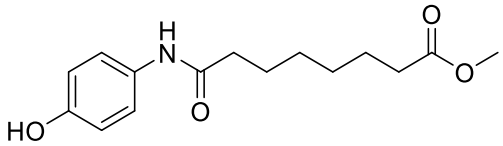

[36]

4-Aminophenol (SIGMA-ALDRICH) (12.51 mmol; 1.364 g) and **[2]** (8.34 mmol; 1.50 mL) were dissolved in DMF (7.90 mL), and then EDC (12.51 mmol; 2.396 g) was added. The solution was stirred overnight. The residue was purified by recrystallization to afford the target compound (white powder, 95%, 2.211 g).

^{1}H NMR (400 MHz, DMSO-d_6) δ 9.57 (s, 1H, OH), 9.13 (s, 1H, NH), 7.34 (d, J = 8.8 Hz, 2H, Ar), 6.66 (d, J = 8.7 Hz, 2H, Ar), 3.57 (s, 3H, OCH_3), 2.25 (dt, J = 26.9, 7.4 Hz, 4H, CH_2-CH_2), 1.53 (dd, J = 12.4, 5.9 Hz, 4H, CH_2-CH_2), 1.28 (m, 4H, CH_2-CH_2).

^{13}C NMR (101 MHz, DMSO-d_6) δ 173.8 (C=O, quaternary), 170.8 (C=O, quaternary), 153.5 (C-OH, quaternary), 131.4 (C-NH, quaternary), 121.2 (CH, Ar), 115.4 (CH, Ar), 51.6 (OCH_3), 36.6 (CH_2), 33.6 (CH_2), 28.7 (CH_2), 28.6 (CH_2), 25.5 (CH_2), 24.7 (CH_2).

Melting Point – 92 - 94 ºC

FT-IR (ATR): (vmax/cm-1) 3351 (NH), 3195, 1436 (OH), 2946 (OCH_3), 1715 (C=O), 1650 (C=O, amide).

Experiment A: **Dibenzyl phosphite [39]**

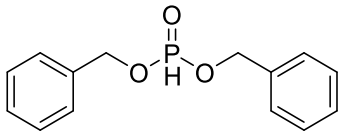

[39]

Using a dropping funnel, a mixture of dimethylaniline (MERCK) (9.99 mmol; 1.27 mL) and benzyl alcohol (BnOH, SIGMA-ALDRICH) (9.99 mmol; 1.04 mL) was slowly added (20 min), with stirring and cooling, to a solution of phosphorus trichloride (MERCK) (5.39 mmol ; 0.47 mL) in toluene (MERCK) (3 mL). After the addition, more BnOH (4.99 mmol; 0.52 mL) was added over a 10 min period. After stirring overnight, water (2 mL) was poured to dissolve the precipitate and the toluene layer was separated and washed successively with water, twice with N-ammonium hydroxide (FLUKA^{TM}) and again with water. The toluene solution was dried with anhydrous sodium sulphate and the solvents removed *in vacuo*; 0.502 g (31%) was collected as colourless viscous oil. The product was pure enough for use

directly in the synthesis of **[40]** (Li and Eakix, 1955). Spectra corresponded to the information provided by SIGMA-ALDRICH on this compound (commercial reference: *D36607 ALDRICH*).

Experiment 13a: Methyl 7-[(4-{[bis(benzyloxy)phosphoryl]oxy}phenyl)carbamoyl]heptanoate [40]

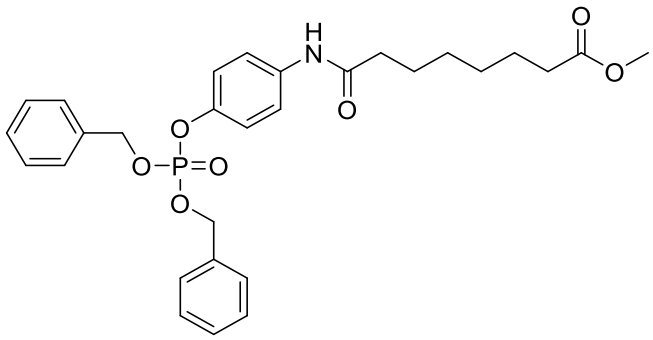

[40]

A multi-necked roundbottom flask fitted with an argon inlet and a magnetic stirrer was charged with **[36]** (2.15 mmol; 0.600 g), and anhydrous acetonitrile (CH_3CN, MERCK) (12 mL). The mixture was stirred to dissolve the phenol and a bath of ice and sodium chloride (NaCl, FLUKA^{TM}) cooled the solution to -10 ºC; then it was added carbon tetrachloride (CCl_4, Riedel-de Haën) (1.06 mL). The mixture was treated with *N*,*N*-diisopropylethylamine (DIPEA, SIGMA-ALDRICH) (4.52 mmol; 0.79 mL) followed by *N*,*N*-dimethylaminopyridine (SIGMA-ALDRICH) (0.22 mmol; 0.026 g), and dropwise addition of **[39]** (3.12 mmol; 0.69 mL), keeping the mixture at or below -10 ºC for a further 70 min, at which point TLC indicated the consumption of the starting materials. The mixture was quenched by the addition of a solution of monopotassium phosphate (KH_2PO_4, Riedel-de Haën) (0.5 M; 3.90 mL), allowed to warm to RT and then extracted with EtOAc three times. The organics phases were washed successively with water and a saturated solution of NaCl, dried and concentrated. The residue was purified by silica flash-chromatography (1:1 Hex:EtOAc), which gave the compound as a yellowish oil (93%, 1.083 g).

^{1}H NMR (400 MHz, DMSO-d_6) δ 9.92 (s, 1H, N<u>H</u>), 7.57 (d, J = 8.5 Hz, 2H, Ar), 7.37 (s, 10H, O-CH_2-P<u>h</u>), 7.11 (d, J = 8.0 Hz, 2H, Ar), 5.15 (d, J = 8.3 Hz, 4H, O-C<u>H$_2$</u>-Ph), 3.58 (s, 3H, OC<u>H$_3$</u>), 2.36 – 2.21 (m, 4H, C<u>H$_2$</u>-C<u>H$_2$</u>), 1.64 – 1.47 (m, 4H, C<u>H$_2$</u>-C<u>H$_2$</u>), 1.29 (s, 4H, C<u>H$_2$</u>-C<u>H$_2$</u>).

^{13}C NMR (101 MHz, DMSO-d_6) δ 173.3 (<u>C</u>=O, quaternary), 171.1 (<u>C</u>=O, quaternary), 145.3 (<u>C</u>-O-P, quaternary), 136.5 (<u>C</u>-NH, quaternary), 128.5 (OCH_2-<u>Ph</u>, Ar, quaternary), 127.9 (OCH_2-<u>Ph</u>, Ar, quaternary), 120.2 (<u>C</u>H, Ar), 69.3 (O-<u>C</u>H_2-Ph, quaternary), 51.1 (O<u>C</u>H_3), 36.2 (<u>C</u>H_2), 33.2 (<u>C</u>H_2), 28.2 (<u>C</u>H_2-<u>C</u>H_2), 24.9 (<u>C</u>H_2), 24.3 (<u>C</u>H_2) .

Melting Point – 92 - 95 ºC

2.1.3 General procedure for hydroxamic acid formation

The corresponding methyl/ethyl esters and $NH_2OH{\cdot}HCl$ (MERCK) were dissolved in anhydrous MeOH, in an ice bath to keep the reaction temperature at 0 ºC. Then a solution of NaOH (PanReac AppliChem) (4M) was added and the mixture stirred for the necessary time, the evolution of the synthesis being monitored by TLC (with the eluent of 1:1 EtOAc:Hex). Water was added and, to remove non-polar impurities, the crude product was washed with ether three times, the layers were separated and the aqueous phases were combined and treated with HCl (10%) until pH 3.5 was reached. The residue present in the aqueous phase was extracted with EtOAc three times; the combined organic phases were washed with a saturated solution of $NaHCO_3$ and dried with $MgSO_4$. The solution was filtred, concentrated *in vacuo* and purified, when needed, by column or preparative thin layer chromatography to get the target compounds (Chen et al., 2011).

Experiment 1.1: (2E) N'-(2-fluorophenyl)-N-hydroxybut-2-enediamide [4]

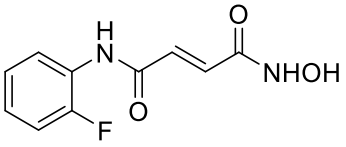

[4]

$NH_2OH{\cdot}HCl$ (2.61 mmol; 0.181 g) was added to a solution of **[3]** (3.2 mmol; 0.776 g) in MeOH (7 mL) at 0 ºC, followed by addition of a solution of NaOH (4 M; 52.22 mmol; 13.10 mL). The mixture was stirred for 35 min, after work-up it afforded an orange powder as final product (17%, 0.126 g).

^{1}H NMR (400 MHz, DMSO-d_6) δ 11.10 (s, 1H, NH), 10.24 (s, 1H, OH), 9.31 (s, 1H, NH), 7.99 (t, J = 8.8 Hz, 1H, Ar), 7.28 (m, 2H, Ar, C<u>H</u>=CH), 7.23 – 7.16 (m, 2H, Ar), 6.84 (d, J = 15.1 Hz, 1H, CH=C<u>H</u>).

^{13}C NMR (101 MHz, DMSO-d_6) δ 163.0 (<u>C</u>=O, quaternary), 161.1 (<u>C</u>=O, quaternary), 155.3 (<u>C</u>-F, quaternary), 152.8 (<u>C</u>-NH, quaternary), 132.1 (<u>C</u>H=CH), 126.3 (<u>C</u>H, Ar), 124.8 (<u>C</u>H, Ar), 124.6 (<u>C</u>H, Ar), 116.1(<u>C</u>H, Ar), 115.9 (CH=<u>C</u>H).

Melting Point – 210 - 212 ºC

FT-IR (ATR): (vmax/cm-1) 3283 (NH), 3067 (OH), 1699 (C=O), 1611 (C=O, amide).

Experiment 2.1: (2E) N'-(2-bromo-4-fluorophenyl)-N-hydroxybut-2-enediamide [6]

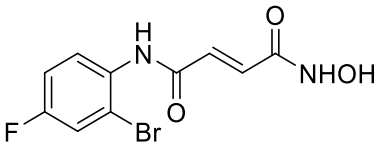

[6]

Compound **[5]** (1.21 mmol; 0.384 g) and $NH_2OH{\cdot}HCl$ (1.21 mmol; 0.088 g) were dissolved in MeOH (2.70 mL) and cooled to 0 ºC. Next, a solution of NaOH (4 M; 9.68 mmol; 2.40 mL) was added. This procedure gave a yellowish powder (34%, 0.124 g).

^{1}H NMR (400 MHz, DMSO-d_6) δ 11.07 (s, 1H, NH), 10.04 (s, 1H, OH), 9.51 (s, 1H, NH), 7.71 – 7.59 (m, 2H, Ar), 7.30 (ddd, J = 8.6, 8.6, 2.9 Hz, 1H, Ar), 7.19 (d, J = 15.2 Hz, 1H, C<u>H</u>=CH), 6.83 (d, J = 15.2 Hz, 1H, CH=C<u>H</u>).

^{13}C NMR (101 MHz, DMSO-d_6) δ 163.1 (<u>C</u>=O, quaternary), 160.9 (<u>C</u>=O, quaternary), 158.6 (<u>C</u>-F, quaternary), 133.0 (<u>C</u>-NH, quaternary), 132.3 (<u>C</u>H=CH), 131.8 (CH=<u>C</u>H), 129.3 (<u>C</u>H, Ar), 120.2 (<u>C</u>H, Ar), 119.4 (<u>C</u>-Br, quaternary), 115.6 (<u>C</u>H, Ar).

Melting Point – 196 - 200 ºC

FT-IR (ATR): (vmax/cm-1) 3299 (NH), 2943 (OH), 1738 (C=O), 1661 (C=O, amide).

Experiment 3.1: (2E) N-hydroxy-N'-(3-methoxyphenyl)but-2-enediamide [9]

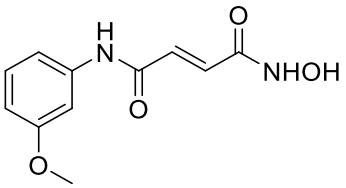

[9]

In a round flask, **[8]** (2.21 mmol; 0.552 g) and MeOH (3.87 mL) were placed in stirring at 0 ºC. $NH_2OH{\cdot}HCl$ (2.21 mmol; 0.153 g) was added, followed by the addition of NaOH (4 M; 17.68 mmol; 4.40 mL). The mixture was stirred for 30 min. This procedure afforded the expected product as an orange solid with 46% of yield (0.241 g).

^{1}H NMR (400 MHz, DMSO-d_6) δ 10.94 (s, 1H, NH), 10.46 (s, 1H, OH), 9.44 (s, 1H, NH), 7.40 – 7.35 (m, 1H, Ar), 7.29 – 7.17 (m, 2 H, Ar), 7.08 (d, J = 15.1 Hz, 1H, C<u>H</u>=CH), 6.81 (d, J = 15.1 Hz, 1H, CH=C<u>H</u>), 6.68 (dd, J = 7.9, 1.2 Hz, 1H, Ar), 3.74 (s, 3H, Ph-OC<u>H</u>$_3$).

^{13}C NMR (101 MHz, DMSO-d_6) δ 162.6 (C=O, quaternary), 160.9 (C=O, quaternary), 159.9 (C-OCH_3, quaternary), 140.3 (C-NH, quaternary), 132.8 (CH=CH), 131.6 (CH=CH), 130.1 (CH, Ar), 112.1 (CH, Ar), 109.6 (CH, Ar), 105.6 (CH, Ar), 55.4 (Ph-OCH_3).

Melting Point – 198 - 203 ºC

FT-IR (ATR): (vmax/cm-1) 3204 (NH), 3074 (OH), 1607 (C=O, amide)**.**

Experiment 4.1: N'-(2-fluorophenyl)-N-hydroxyoctanediamide [12]

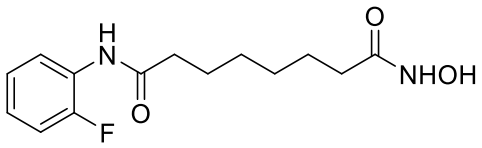

[12]

To a stirred solution of the **[11]** (0.92 mmol; 0.260 g) in MeOH (1.82 mL), was added a solution of NaOH (4 M; 7.36 mmol; 1.90 mL) and $NH_2OH{\cdot}HCl$ (0.92 mmol; 0.064 g). The resulting mixture was stirred for 20 min. This afforded the expected derivative as a white powder (45%, 0.117 g).

^{1}H NMR (400 MHz, DMSO-d_6) δ 10.33 (s, 1H, NH), 9.63 (s, 1H, OH), 8.65 (s, 1H, NH), 7.84 (t, J = 8.7 Hz, 1H, Ar), 7.23 (ddd, J = 7.4, 5.9, 3.1 Hz, 1H, Ar), 7.17 – 7.10 (m, 2H, Ar), 2.36 (t, J = 7.4 Hz, 2H, CH_2), 1.94 (t, J = 7.4 Hz, 2H CH_2), 1.52 (ddd, J = 29.3, 14.2, 7.0 Hz, 4H, CH_2-CH_2), 1.28 (d, J = 3.1 Hz, 4H, CH_2-CH_2).

^{13}C NMR (101 MHz, DMSO-d_6) δ 172.0 (C=O, quaternary), 169.5 (C=O, quaternary), 155.4 (C-F, quaternary), 126.6 (C-NH, quaternary), 125.6 (CH, Ar), 124.9 (CH, Ar), 124.7 (CH, Ar), 115.9 (CH, Ar), 36.1 (CH_2), 32.7 (CH_2), 28.85 (CH_2), 28.81 (CH_2), 25.5 (CH_2-CH_2).

Melting Point – 95 – 97 ºC

FT-IR (ATR): (vmax/cm-1) 3365 (NH), 2934 (OH), 1665 (C=O), 1607 (C=O, amide).

Experiment 5.1: N-hydroxy-N'-(2-iodophenyl)octanediamide [15]

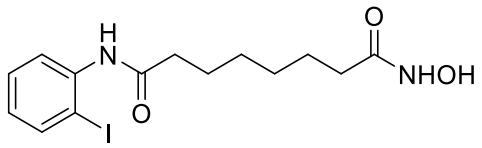

[15]

To a solution of **[14]** (1.05 mmol; 0.407 g) and MeOH (2.80 mL), was added $NH_2OH{\cdot}HCl$ (1.05 mmol; 0.073 g), followed by the solution of NaOH (4 M; 8.40 mmol; 2.10 mL). The mixture was stirred for 20 min. The final compound was obtained as a white powder with 60% of yield (0.245 g).

^{1}H NMR (400 MHz, DMSO-d_6) δ 10.33 (s, 1H, NH), 9.36 (s, 1H, OH), 8.66 (s, 1H, NH), 7.87 (d, J = 7.6 Hz, 1H, Ar), 7.44 – 7.34 (m, 2H, Ar), 7.03 – 6.93 (m, 1H, Ar), 2.32 (t, J = 7.1 Hz, 2H, CH_2), 1.95 (t, J = 7.4 Hz, 2H, CH_2), 1.54 (ddd, J = 21.6, 14.2, 6.9 Hz, 4H, CH_2-CH_2), 1.40 – 1.21 (m, 4H, CH_2-CH_2).

^{13}C NMR (101 MHz, DMSO-d_6) δ 171.6 (C=O, quaternary), 169.5 (C=O, quaternary), 140.1 (C-NH, quaternary), 139.3 (CH, Ar), 129.0 (CH, Ar), 128.0 (CH, Ar), 97.2 (C-I, quaternary), 36.1 (CH_2), 32.7 (CH_2), 28.8 (CH_2-CH_2), 25.57 (CH_2), 25.54 (CH_2).

Melting Point – 126 – 129 ºC

FT-IR (ATR): (vmax/cm-1) 3274 (NH), 2941 (OH), 1658 (C=O), 1620 (C=O, amide).

Experiment 6.1: N'-(4-fluorophenyl)-N-hydroxyoctanediamide [18]

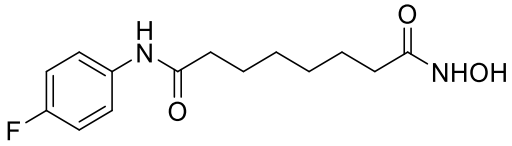

[18]

Compound **[17]** (3.21 mmol; 0.903 g) was mixed with $NH_2OH{\cdot}HCl$ (3.21 mmol; 0.223 g) in MeOH (6.30 mL), cooled to 0 °C. The NaOH solution (4 M; 25.68 mmol; 6.42 mL) was then added to the mixture. The product was obtained as a white powder (38%, 0.341 g).

^{1}H NMR (400 MHz, DMSO-d_6) δ 10.33 (s, 1H, NH), 9.91 (s, 1H, OH), 8.65 (s, 1H, NH), 7.65 – 7.53 (m, 2H, Ar), 7.17 – 7.06 (m, 2H, Ar), 2.28 (t, J = 7.4 Hz, 2H, CH_2), 1.94 (t, J = 7.4 Hz, 2H, CH_2), 1.62 – 1.43 (m, 4H, CH_2-CH_2), 1.33 – 1.22 (m, 4H, CH_2-CH_2).

^{13}C NMR (101 MHz, DMSO-d_6) δ 171.5 (C=O, quaternary), 169.5 (C=O, quaternary), 159.4 (C-F, quaternary), 136.1 (C-NH, quaternary), 121.2 (CH, Ar), 121.1 (CH, Ar), 115.7 (CH, Ar), 115.5 (CH, Ar), 36.7 (CH_2), 32.6 (CH_2), 28.8 (CH_2-CH_2), 25.4 (CH_2-CH_2).

Melting Point – 158 – 162 ºC

FT-IR (ATR): (vmax/cm-1) 3266 (NH), 2932 (OH), 1655 (C=O), 1631 (C=O, amide).

Experiment 7.1: N'-(2-bromo-4-fluorophenyl)-N-hydroxyoctanediamide [21]

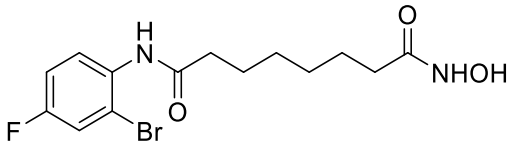

[21]

The compound **[20]** (1.36 mmol; 0.490 g) and $NH_2OH{\cdot}HCl$ (1.36 mmol; 0.095 g) were dissolved in MeOH (3.40 mL), and then NaOH solution (4 M; 10.88 mmol; 2.72 mL) was added. The solution was stirred at 0 ºC for 20 min. After work-up, the target compound was a beige powder (30%, 0.149 g).

^{1}H NMR (400 MHz, DMSO-d_6) δ 10.33 (s, 1H, NH), 9.46 (s, 1H, OH), 8.65 (s, 1H, NH), 7.62 (dd, J = 8.4, 2.8 Hz, 1H, Ar), 7.53 (dd, J = 8.9, 5.8 Hz, 1H, Ar), 7.25 (ddd, J = 8.6, 8.6, 2.9 Hz, 1H, Ar), 2.33 (t, J = 7.3 Hz, 2H, C$\underline{H_2}$), 1.95 (t, J = 7.4 Hz, 2H, C$\underline{H_2}$), 1.53 (ddd, J = 28.7, 14.0, 6.8 Hz, 4H, C$\underline{H_2}$-C$\underline{H_2}$), 1.38 – 1.22 (m, 4H, C$\underline{H_2}$-C$\underline{H_2}$).

^{13}C NMR (101 MHz, DMSO-d_6) δ 171.9 (C$\underline{}$=O, quaternary), 169.5 (C$\underline{}$=O, quaternary), 158.3 (C$\underline{}$-F, quaternary), 133.6 (C$\underline{}$-NH, quaternary), 129.5 (C$\underline{}$H, Ar), 120.0 (C$\underline{}$H, Ar), 119.6 (C$\underline{}$-Br, quaternary), 115.4 (C$\underline{}$H, Ar), 35.9 (C$\underline{H_2}$), 32.7 (C$\underline{H_2}$), 28.8 (C$\underline{H_2}$-C$\underline{H_2}$), 25.5 (C$\underline{H_2}$-C$\underline{H_2}$).

Melting Point – 104 – 108 ºC

FT-IR (ATR): (vmax/cm-1) 3269 (NH), 2936 (OH), 1657 (C=O), 1625 (C=O, amide).

Experiment 8.1: N-hydroxy-N'-(3-methoxyphenyl)octanediamide [24]

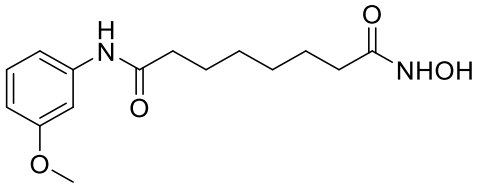

[24]

$NH_2OH{\cdot}HCl$ (3.02 mmol; 0.211 g) was added to a solution of **[23]** (3.02 mmol; 0.885 g) in MeOH (6.20 mL) at 0 ºC. A solution of NaOH (4 M; 24.16 mmol; 6.04 mL) was mixed and the mixture was left to stir for 15 min. The final product was a yellowish powder (30%, 0.268 g).

^{1}H NMR (400 MHz, DMSO-d_6) δ 10.33 (s, 1H, NH), 9.83 (s, 1H, OH), 8.65 (s, 1H, NH), 7.30 (d, J = 2.0 Hz, 1H, Ar), 7.24 – 7.08 (m, 2H, Ar), 6.60 (dd, J = 8.1, 1.6 Hz, 1H, Ar), 3.72 (s, 3H, Ph-OC$\underline{H_3}$), 2.28 (t, J = 7.4 Hz, 2H, C$\underline{H_2}$), 1.94 (t, J = 7.4 Hz, 2H, C$\underline{H_2}$), 1.62 – 1.43 (m, 4H , C$\underline{H_2}$-C$\underline{H_2}$), 1.33 – 1.21 (m, 4H, C$\underline{H_2}$-C$\underline{H_2}$).

^{13}C NMR (101 MHz, DMSO-d_6) δ 171.7 (C=O, quaternary), 169.5 (C=O, quaternary), 159.9 (C- OCH_3, quaternary), 140.9 (C-NH, quaternary), 129.8 (CH, Ar), 111.7 (CH, Ar), 108.8 (CH, Ar), 105.2 (CH, Ar), 55.3 (Ph- OCH_3, quaternary), 36.8 (CH_2), 32.7 (CH_2), 28.8 (CH_2-CH_2), 25.49 (CH_2), 25.43 (CH_2).

Melting Point – 123 - 126 ºC

FT-IR (ATR): (vmax/cm-1) 3271 (NH), 2945 (OH), 1636 (C=O), 1610 (C=O, amide).

Experiment 9.1: N-hydroxy-N'-(4-iodophenyl)octanediamide [27]

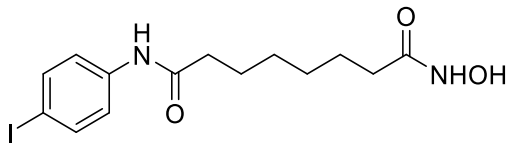

[27]

Compound **[26]** (0.91 mmol; 0.354 g) and $NH_2OH{\cdot}HCl$ (0.91 mmol; 0.063 g) were dissolved in MeOH (2.50 mL) and mixed together with a solution of NaOH (4 M; 7.28 mmol; 1.82 mL). After the reaction and work-up, a lilac powder was obtained (38%, 0.136 g).

^{1}H NMR (400 MHz, DMSO-d_6) δ 10.32 (s, 1H, NH), 9.96 (s, 1H, OH), 8.65 (s, 1H, NH), 7.62 (d, J = 8.7 Hz, 2H, Ar), 7.44 (d, J = 8.7 Hz, 2H, Ar), 2.28 (t, J = 7.4 Hz, 2H, CH_2), 1.94 (t, J = 7.3 Hz, 2H, CH_2), 1.64 – 1.42 (m, 4H, , CH_2-CH_2), 1.27 (d, J = 3.3 Hz, 4H, CH_2-CH_2).

^{13}C NMR (101 MHz, DMSO-d_6) δ 171.8 (C=O, quaternary), 169.5 (C=O, quaternary), 139.6 (C-NH, quaternary), 137.7 (CH, Ar), 121.6 (CH, Ar), 86.6 (C-I, quaternary), 36.8(CH_2), 32.6 (CH_2), 28.8 (CH_2-CH_2), 25.4 (CH_2), 25.3 (CH_2).

Melting Point – 141 - 145 ºC

FT-IR (ATR): (vmax/cm-1) 3282 (NH), 2932 (OH), 1656 (C=O), 1583 (C=O, amide).

Experiment 10.1: N'-(4-bromophenyl)-N-hydroxyoctanediamide [30]

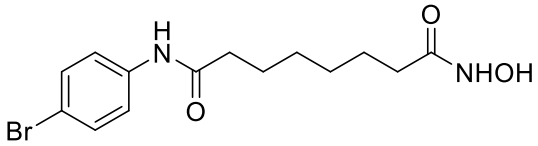

[30]

In a round flask, compound **[29]** (1.27 mmol; 0.435 g) and $NH_2OH{\cdot}HCl$ (1.27 mmol; 0.088 g) were placed in MeOH (3 mL). NaOH solution (4 M; 10.16 mmol; 2.54 mL) was added and the mixture was stirred for 90 min. This procedure afforded the expected product as a beige powder (42%, 0.183 g).

^{1}H NMR (400 MHz, DMSO-d_6) δ 10.33 (s, 1H, NH), 10.00 (s, 1H, OH), 8.66 (s, 1H, NH), 7.57 (d, J = 8.9 Hz, 2H, Ar), 7.46 (d, J = 8.9 Hz, 2H, Ar), 2.29 (t, J = 7.4 Hz, 2H, C$\underline{H_2}$), 1.94 (t, J = 7.4 Hz, 2H, C$\underline{H_2}$), 1.65 – 1.41 (m, 4H, C$\underline{H_2}$-C$\underline{H_2}$), 1.36 – 1.21 (m, 4H, C$\underline{H_2}$-C$\underline{H_2}$).

^{13}C NMR (101 MHz, DMSO-d_6) δ 171.8 ($\underline{C}$=O, quaternary), 169.5 ($\underline{C}$=O, quaternary), 139.1 ($\underline{C}$-NH, quaternary), 131.9 ($\underline{C}$H, Ar), 121.3 ($\underline{C}$H, Ar), 114.8 ($\underline{C}$-Br, quaternary), 36.8 ($\underline{C}H_2$), 32.6 ($\underline{C}H_2$), 28.8 ($\underline{C}H_2$-$\underline{C}H_2$), 25.4 ($\underline{C}H_2$), 25.3 ($\underline{C}H_2$).

Melting Point – 157 – 161 ºC

FT-IR (ATR): (vmax/cm-1) 3299 (NH), 2943 (OH), 1738 (C=O), 1638 (C=O, amide).

<u>Experiment 11.1:</u> N'-(2-bromophenyl)-N-hydroxyoctanediamide [33]

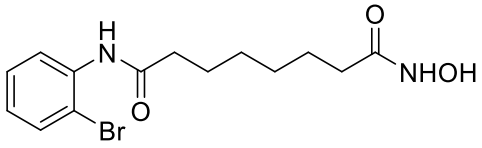

[33]

To a stirred solution of the previous **[32]** (1.75 mmol; 0.598 g) in MeOH (4.10 mL), was added $NH_2OH{\cdot}HCl$ (1.75 mmol; 0.122 g) and a solution of NaOH (4 M; 14 mmol; 3.50 mL). The resulting mixture was stirred for 40 min. After work-up, the expected derivative as a beige powder (39%, 0.234 g).

^{1}H NMR (400 MHz, DMSO-d_6) δ 10.35 (s, 1H, NH), 9.40 (s, 1H, OH), 8.68 (s, 1H, NH), 7.65 (d, J = 7.9 Hz, 1H, Ar), 7.56 (d, J = 7.8 Hz, 1H, Ar), 7.36 (t, J = 7.5 Hz, 1H, Ar), 7.13 (t, J = 7.4 Hz, 1H, Ar), 2.34 (t, J = 6.8 Hz, 2H, C$\underline{H_2}$), 1.95 (t, J = 7.3 Hz, 2H, C$\underline{H_2}$), 1.66 – 1.44 (m, 4H, C$\underline{H_2}$-C$\underline{H_2}$), 1.37 – 1.22 (m, 4H, C$\underline{H_2}$-C$\underline{H_2}$).

^{13}C NMR (101 MHz, DMSO-d_6) δ 171.9 ($\underline{C}$=O, quaternary), 169.6 ($\underline{C}$=O, quaternary), 136.8 ($\underline{C}$-NH, quaternary), 133.0 ($\underline{C}$H, Ar), 128.3 ($\underline{C}$H, Ar), 127.9 ($\underline{C}$H, Ar), 127.4 ($\underline{C}$H, Ar), 118.7 ($\underline{C}$-Br, quaternary), 36.1 ($\underline{C}H_2$), 32.7 ($\underline{C}H_2$), 28.84 ($\underline{C}H_2$), 28.81 ($\underline{C}H_2$), 25.55 ($\underline{C}H_2$), 25.52 ($\underline{C}H_2$).

Melting Point – 104 - 106 ºC

FT-IR (ATR): (vmax/cm-1) 3277(NH), 2906 (OH), 1658 (C=O), 1623 (C=O, amide).

<u>Experiment 13.1:</u> N-hydroxy-N'-(4-hydroxyphenyl)octanediamide [37]

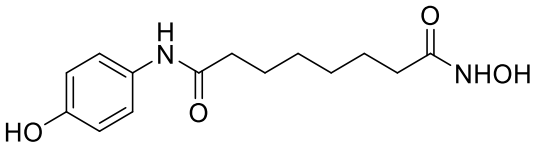

[37]

1,8-Diazabicyclo[5.4.0]undec-7.ene (DBU, SIGMA-ALDRICH) (2.36 mmol; 0.35 mL) was added to a solution of **[36]** (0.788 mmol; 0.220 g) in anhydrous MeOH (0.69 mL). The mixture was stirred at RT and an aqueous solution 50% of NH_2OH (SIGMA-ALDRICH) (7.88 mmol; 0.24 mL) was added. The reaction was stopped with water and the workup, generally similar to the one described on point **2.1.3**, afforded 0.060 mg, 27% as a light brown solid (Beillard et al., 2016).

^{1}H NMR (400 MHz, DMSO-d_6) δ 10.33 (s, 1H, NH), 9.57 (s, 1H, OH), 9.12 (s, 1H, OH), 8.65 (s, 1H, NH), 7.35 (d, J = 8.8 Hz, 2H, Ar), 6.67 (d, J = 8.8 Hz, 2H, Ar), 2.23 (t, J = 7.4 Hz, 2H, CH_2), 1.94 (t, J = 7.4 Hz, 2H, CH_2), 1.61 – 1.42 (m, 4H, CH_2-CH_2), 1.34 – 1.21 (m, 4H, CH_2-CH_2).

^{13}C NMR (101 MHz, DMSO-d_6) δ 170.9 (C=O, quaternary), 169.5 (C=O, quaternary), 153.5 (C-OH, quaternary), 131.5 (C-NH, quaternary), 121.2 (CH, Ar), 115.4 (CH, Ar), 36.6 (CH_2), 32.7 (CH_2), 28.8 (CH_2-CH_2), 25.6 (CH_2), 25.5 (CH_2).

Melting Point – 88 - 90 ºC

FT-IR (ATR): (vmax/cm-1) 3301 (NH), 2938 (OH), 1654 (C=O), 1608 (C=O, amide).

Experiment 13a.1: Dibenzyl 4-[7-(hydroxycarbamoyl)heptanamido]phenyl phosphate [41]

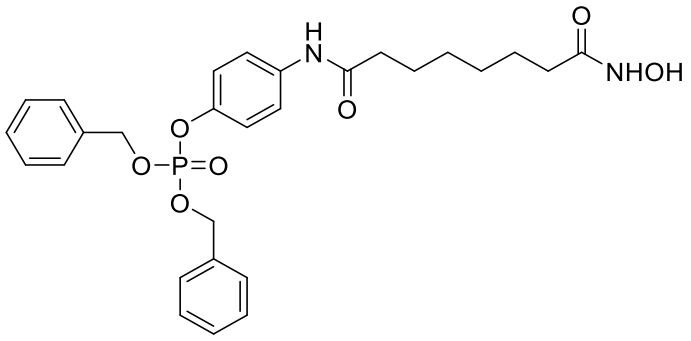

[41]

Compound **[40]** (0.11 mmol; 0.060 g) was mixed with NH2OH·HCl (0.11 mmol; 0.008 g) in MeOH (0.40 mL), cooled to 0 °C and the NaOH solution (4 M; 0.88 mmol; 0.22 mL) was then added. The product was a greenish oil (35%, 0.021 g).

^{1}H NMR (400 MHz, DMSO-d_6) δ 10.33 (s, 1H, NH), 9.92 (s, 1H, OH), 8.65 (d, J = 1.6 Hz, 1H, NH), 7.57 (d, J = 9.0 Hz, 2H, Ar), 7.45 – 7.29 (m, 10H, O-CH_2-Ph), 7.11 (d, J = 8.0 Hz, 2H, Ar), 5.15 (d, J = 8.3 Hz, 4H, O-CH_2-Ph), 2.28 (t, J = 7.4 Hz, 2H, CH_2), 1.94 (t, J = 7.4 Hz, 2H, CH_2), 1.62 – 1.45 (m, 4H, CH_2-CH_2), 1.33 – 1.23 (m, 4H, CH_2-CH_2).

^{13}C NMR (101 MHz, DMSO-d_6) δ 171.6 (C=O, quaternary), 169.5 (C=O, quaternary), 145.8 (C-O-P, quaternary), 137.0 (C-NH, quaternary), 128.9 (OCH_2-Ph, Ar, quaternary), 128.4 (OCH_2-Ph, Ar,

quaternary), 121.2 (CH, Ar), 120.6 (CH -CH, Ar), 69.7 (O-CH_2-Ph, quaternary), 36.7 (CH_2), 33.6 (CH_2), 32.7 (CH_2), 28.8 (CH_2), 25.4 (CH_2), 24.7 (CH_2).

Experiment 13a.1H: {4-[7-(hydroxycarbamoyl)heptanamido]phenoxy}phosphonic acid [42]

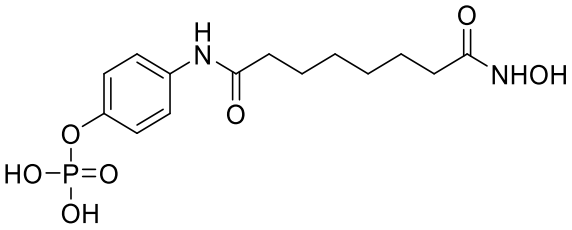

[42]

In a pressure reaction vessel, palladium on carbon (SIGMA-ALDRICH) 10 wt % (0.03 mmol; 0.032 g) and **[41]** (0.30 mmol; 0.162 g) were charged. EtOH (2 mL) was added and the reaction vessel was purged with hydrogen and degassed. The reaction mixture was pressurized at 50 psi for 1 h. The mixture was then filtered through a pad of celite (PanReac AppliChem), rising with MeOH and concentrated. The title compound **[42]** obtained was a rose-coloured compact solid (91%, 0.098 g).

^{1}H NMR (400 MHz, DMSO-d_6) δ 10.33 (s, 1H, NH), 9.82 (s, 1H, OH), 8.66 (s, 1H, NH), 7.43 (dd, J = 63.8, 8.9 Hz, 2H, Ar), 6.87 (dd, J = 159.6, 8.6 Hz, 2H, Ar), 2.27 (t, J = 7.4 Hz, 2H, CH_2), 1.94 (t, J = 7.4 Hz, 2H, CH_2), 1.62 – 1.43 (m, 4H, CH_2-CH_2), 1.35 – 1.20 (m, 4H, CH_2-CH_2).

^{13}C NMR (101 MHz, DMSO-d_6) δ 171.4 (C=O, quaternary), 169.5 (C=O, quaternary), 153.5 (C-O-P, quaternary), 135.5 (C-NH, quaternary), 121.2 (CH, Ar), 120.6 (CH, Ar), 120.5 (CH, Ar), 115.4 (CH, Ar), 36.7 (CH_2), 32.6 (CH_2), 28.8 (CH_2-CH_2), 25.5 (CH_2-CH_2).

Melting Point – 125 – 128 ºC

FT-IR (ATR): (vmax/cm-1) 3299 (NH), 2935 (OH), 1655 (C=O), 1605 (C=O, amide), 1205 (P=O).

2.1.4 General procedure for carboxylic acid formation

The procedure describe by Yamaoka et al., 2011, was adapted. The corresponding methyl/ethyl ester was dissolved in THF (MERCK) and a solution of NAOH (1 M) was added. The mixture stirred at RT for the necessary time, the evolution of the reaction being monitored by TLC. Water was added to quench the reaction and, to remove non-polar impurities, the crude product was washed with ether, three times, the layers were separated and the aqueous phases combined and treated with HCl (10%) until pH 3.5 was reached. The residue was extracted with EtOAc three times; the combined organic phases were dried with anhydrous $MgSO_4$. The mixture was filtred and concentrated *in vacuo*.

Experiment 2.2: (2E)-3-[(2-bromo-4-fluorophenyl)carbamoyl]prop-2-enoic acid [7]

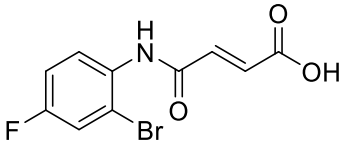

[7]

Compound [**5]** (0.53 mmol; 0.166 g) was dissolved in THF (1 mL), and then a solution of NaOH (1 M; 0.53 mmol; 0.53 mL) was added. The solution was stirred for 45 min. A white powder (90%, 0.136 g) was the target compound.

^{1}H NMR (400 MHz, DMSO-d_6) δ 13.04 (s, 1H, NH), 10.13 (s, 1H, OH), 7.72 – 7.62 (m, 2H, Ar), 7.35 – 7.28 (m, 1H, Ar), 7.26 (d, J = 15.5 Hz, 1H, CH=CH), 6.68 (d, J = 15.5 Hz, 1H, CH=CH).

^{13}C NMR (101 MHz, DMSO-d_6) δ 166.7 (C=O, quaternary), 162.7 (C=O, quaternary), 161.1 (C-F, quaternary), 158.7 (C-Br, quaternary), 136.6 (CH=CH), 132.7 (C-NH, quaternary), 131.9 (CH=CH), 129.2 (CH, Ar), 120.0 (CH, Ar), 115.6 (CH, Ar).

Melting Point – 231 – 232 ºC

FT-IR (ATR): (vmax/cm-1) 3261 (NH), 3050 (OH), 1698 (C=O), 1660 (C=O, amide).

Experiment 3.2: (2E)-3-[(3-methoxyphenyl)carbamoyl]prop-2-enoic acid [10]

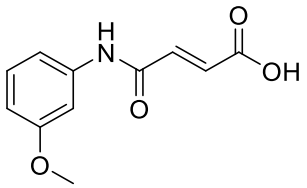

[10]

A solution of NaOH (1 M; 1.33 mmol; 1.33 mL) was added to a solution of **[8]** (1.33 mmol; 0.331 g) in THF (2 mL) at RT. The mixture was left to stir for 55 min and gave a yellow powder (87%, 0.255 g).

^{1}H NMR (400 MHz, DMSO-d_6) δ 13.01 (s, 1H, NH), 10.49 (s, 1H, OH), 7.39 (t, J = 2.1 Hz, 1H, Ar), 7.25 (t, J = 8.1 Hz, 1H, Ar), 7.19 (d, J = 8.5 Hz, 1H, Ar), 7.14 (d, J = 15.4 Hz, 1H, C<u>H</u>=CH), 6.70 (dd, J = 8.1, 1.6 Hz, 1H, Ar), 6.66 (d, J = 15.4 Hz, 1H, CH=C<u>H</u>), 3.75 (s, 3H, Ph-OC<u>H</u>$_3$).

^{13}C NMR (101 MHz, DMSO-d_6) δ 166.3 (<u>C</u>=O, quaternary), 161.6 (<u>C</u>=O, quaternary), 159.5 (<u>C</u>-OCH$_3$, quaternary), 139.7 (<u>C</u>-NH, quaternary), 137.1 (<u>C</u>H=CH), 130.7 (CH=<u>C</u>H), 129.7 (<u>C</u>H, Ar), 111.7 (<u>C</u>H, Ar), 109.5 (<u>C</u>H, Ar), 105.2 (<u>C</u>H, Ar), 55.0 (Ph-O<u>C</u>H$_3$).

Melting Point – 198 – 203 ºC

FT-IR (ATR): (vmax/cm-1) 3292 (NH), 2993 (OH), 1696 (C=O), 1658 (C=O, amide).

<u>Experiment 4.2:</u> 7-[(2-fluorophenyl)carbamoyl]heptanoic acid [13]

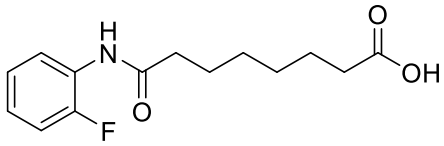

[13]

Compound **[11]** (0.75 mmol; 0.210 g) was dissolved in THF (1.30 mL) and a solution of NaOH (1 M; 0.75 mmol; 0.75 mL) was added and the reaction mixture was stirred for 1.25 h. After work-up, a white powder was obtained as the product (59%, 0.117 g).

^{1}H NMR (400 MHz, DMSO-d_6) δ 11.97 (s, 1H, OH), 9.62 (s, 1H, NH), 7.84 (dd, J = 11.6, 5.8 Hz, 1H, Ar), 7.29 – 7.17 (m, 1H, Ar), 7.17 – 7.02 (m, 2H, Ar), 2.35 (t, J = 7.4 Hz, 2H, C<u>H</u>$_2$), 2.20 (t, J = 7.4 Hz, 2H, C<u>H</u>$_2$), 1.52 (ddd, J = 28.7, 14.2, 7.1 Hz, 4H, C<u>H</u>$_2$-C<u>H</u>$_2$), 1.36 – 1.21 (m, 4H, C<u>H</u>$_2$-C<u>H</u>$_2$).

^{13}C NMR (101 MHz, DMSO-d_6) δ 174.4 (<u>C</u>=O, quaternary), 171.6 (<u>C</u>=O, quaternary), 154.9 (<u>C</u>-F, quaternary), 126.2 (<u>C</u>-NH, quaternary), 125.0 (<u>C</u>H, Ar), 124.4 (<u>C</u>H, Ar), 124.2 (<u>C</u>H, Ar), 115.5 (<u>C</u>H, Ar), 35.7 (<u>C</u>H$_2$), 33.6 (<u>C</u>H$_2$), 28.3 (<u>C</u>H$_2$-<u>C</u>H$_2$), 24.9 (<u>C</u>H$_2$), 24.3 (<u>C</u>H$_2$).

Melting Point – 105 – 108 ºC

FT-IR (ATR): (vmax/cm-1) 3296 (NH), 2938 (OH), 1691 (C=O), 1655 (C=O, amide).

Experiment 5.2: 7-[(2-iodophenyl)carbamoyl]heptanoic acid [16]

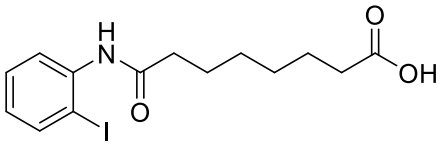

[16]

In a round flask, **[14]** (0.45 mmol; 0.174 g) and THF (1.60 mL) were placed under stirring. A solution of NaOH (1 M; 0.45 mmol; 0.68 mL) was added and the reaction stopped after 5 h. This procedure afforded the expected product as a yellowish powder with 83% of yield (0.139 g).

^{1}H NMR (400 MHz, DMSO-d_6) δ 11.98 (s, 1H, NH), 9.35 (s, 1H, OH), 7.87 (d, J = 7.6 Hz, 1H, Ar), 7.51 – 7.26 (m, 2H, Ar), 7.03 – 6.88 (m, 1H, Ar), 2.31 (t, J = 6.9 Hz, 2H, CH_2), 2.20 (t, J = 7.4 Hz, 2H, CH_2), 1.66 – 1.44 (m, 4H, CH_2-CH_2), 1.42 – 1.20 (m, 4H, CH_2-CH_2).

^{13}C NMR (101 MHz, DMSO-d_6) δ 174.5 (C=O, quaternary), 171.2 (C=O, quaternary), 139.6 (C-NH, quaternary), 138.8 (CH, Ar), 128.6 (CH, Ar), 127.5 (CH, Ar), 96.7 (C-I, quaternary), 35.6 (CH_2), 33.6 (CH_2), 28.3 (CH_2-CH_2), 25.0 (CH_2), 24.4 (CH_2).

Melting Point – 117 – 121 ºC

FT-IR (ATR): (vmax/cm-1) 3282 (NH), 2940 (OH), 1693 (C=O), 1659 (C=O, amide).

Experiment 6.2: 7-[(4-fluorophenyl)carbamoyl]heptanoic acid [19]

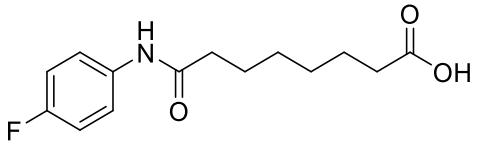

[19]

To a solution of compound **[17]** (1.09 mmol; 0.308 g) in THF (1.90 mL), was added a solution of NaOH (1 M; 1.09 mmol; 1.10 mL). The resulting mixture was stirred for 85 min. The expected derivative was obtained as a white powder with 57% of yield (0.168 g).

^{1}H NMR (400 MHz, DMSO-d_6) δ 11.99 (s, 1H, NH), 9.90 (s, 1H, OH), 7.60 (dd, J = 8.9, 5.1 Hz, 2H, Ar), 7.12 (t, J = 8.9 Hz, 2H, Ar), 2.28 (t, J = 7.4 Hz, 2H, CH_2), 2.20 (t, J = 7.3 Hz, 2H, CH_2), 1.64 – 1.43 (m, 4H, CH_2-CH_2), 1.39 – 1.21 (m, 4H, CH_2-CH_2).

^{13}C NMR (101 MHz, DMSO-d_6) δ 174.4 (C=O, quaternary), 171.0 (C=O, quaternary), 158.9 (C-F, quaternary), 135.7 (C-NH, quaternary), 120.7 (CH, Ar), 115.2 (CH, Ar), 36.2 (CH_2), 33.6 (CH_2), 28.3 (CH_2), 28.3 (CH_2), 24.9 (CH_2), 24.3 (CH_2).

Melting Point – 115 – 118 ºC

FT-IR (ATR): (vmax/cm-1) 3302 (NH), 2934 (OH), 1689 (C=O), 1656 (C=O, amide).

Experiment 7.2: 7-[(2-bromo-4-fluorophenyl)carbamoyl]heptanoic acid [22]

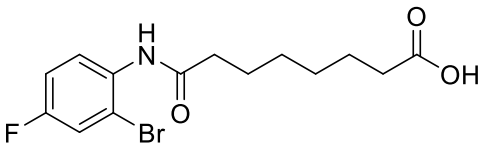

[22]

Compound **[20]** (0.99 mmol; 0.358 g) was dissolved in THF (3.20 mL) and a solution of NaOH (1 M; 0.99 mmol; 1.5 mL) was added. The mixture was stirred for 2 h. The final compound was a withe powder with 49% of yield (0.168 g).

^{1}H NMR (400 MHz, DMSO-d_6) δ 11.99 (s, 1H, NH), 9.46 (s, 1H, OH), 7.62 (dd, J = 8.4, 2.9 Hz, 1H, Ar), 7.53 (dd, J = 8.9, 5.8 Hz, 1H, Ar), 7.25 (td, J = 8.6, 2.9 Hz, 1H, Ar), 2.33 (t, J = 7.3 Hz, 2H, CH_2), 2.20 (t, J = 7.3 Hz, 2H, CH_2), 1.65 – 1.43 (m, 4H, CH_2-CH_2), 1.39 – 1.23 (m, 4H, CH_2-CH_2).

^{13}C NMR (101 MHz, DMSO-d_6) δ 174.4 (C=O, quaternary), 171.5 (C=O, quaternary), 160.3 (C-F, quaternary), 157.9 (C-Br, quaternary), 133.1 (C-NH, quaternary), 129.1 (CH, Ar), 119.5 (CH, Ar), 115.0 (CH, Ar), 35.5 (CH_2), 33.6 (CH_2), 28.2 (CH_2-CH_2), 25.0 (CH_2), 24.3 (CH_2).

Melting Point – 114 – 117 ºC

FT-IR (ATR): (vmax/cm-1) 3280 (NH), 2940 (OH), 1692 (C=O), 1659 (C=O, amide).

Experiment 8.2: 7-[(3-methoxyphenyl)carbamoyl]heptanoic acid [25]

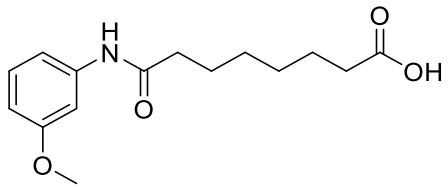

[25]

A solution of NaOH (1 M; 1.68 mmol; 1.7 mL) was mixed with **[23]** (1.29 mmol; 0.378 g) in THF (2.95 mL). The reaction was stopped after 2.5 h and the product was a white powder (82%, 0.295).

^{1}H NMR (400 MHz, DMSO-d_6) δ 11.98 (s, 1H, NH), 9.83 (s, 1H, OH), 7.31 (t, J = 2.0 Hz, 1H, Ar), 7.18 (t, J = 8.1 Hz, 1H, Ar), 7.11 (d, J = 8.4 Hz, 1H, Ar), 6.60 (dd, J = 8.1, 1.6 Hz, 1H, Ar), 3.72 (s, 3H, Ph-OC$\underline{H}_3$), 2.28 (t, J = 7.4 Hz, 2H, C$\underline{H}_2$), 2.20 (t, J = 7.3 Hz, 2H, C$\underline{H}_2$), 1.62 – 1.46 (m, 4H, C$\underline{H}_2$-C$\underline{H}_2$), 1.29 (dd, J = 8.7, 5.4 Hz, 4H, C$\underline{H}_2$-C$\underline{H}_2$).

^{13}C NMR (101 MHz, DMSO-d_6) δ 174.4 (C=O, quaternary), 171.2 (C=O, quaternary), 159.4 (C-O-CH_3, quaternary), 140.5 (C-NH quaternary), 129.4 (CH, Ar), 111.2 (CH, Ar), 108.3 (CH, Ar), 104.7 (CH, Ar), 54.9 (Ph-OCH_3), 36.4 (CH_2), 33.6 (CH_2), 28.3 (CH_2), 28.3 (CH_2), 24.9 (CH_2), 24.3 (CH_2).

Melting Point – 85 – 87 ºC

FT-IR (ATR): (vmax/cm-1) 3300 (NH), 2932 (OH), 1688 (C=O), 1660 (C=O, amide).

Experiment 9.2: 7-[(4-iodophenyl)carbamoyl]heptanoic acid [28]

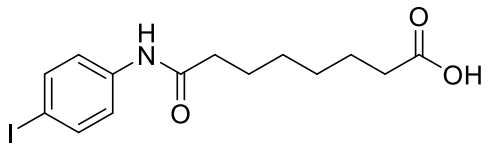

[28]

Compound **[26]** (0.83 mmol; 0.325 g) was dissolved in THF (2.95 mL) and a solution of NaOH (1 M; 1.25 mmol; 1.25 mL) was added, the mixture was stirred for 2.75 h. A lilac powder was obtained, being the target compound (95%, 0.297 g).

^{1}H NMR (400 MHz, DMSO-d_6) δ 11.98 (s, 1H, OH), 9.96 (s, 1H, NH), 7.62 (d, J = 8.8 Hz, 2H, Ar), 7.43 (d, J = 8.8 Hz, 2H, Ar), 2.29 (t, J = 7.4 Hz, 2H, C$\underline{H}_2$), 2.20 (t, J = 7.3 Hz, 2H, C$\underline{H}_2$), 1.61 – 1.45 (m, 4H, C$\underline{H}_2$-C$\underline{H}_2$), 1.29 (dd, J = 8.7, 5.4 Hz, 4H, C$\underline{H}_2$-C$\underline{H}_2$).

^{13}C NMR (101 MHz, DMSO-d_6) δ 174.4 (C=O, quaternary), 171.4 (C=O, quaternary), 139.1 (C-NH, quaternary), 137.2 (CH, Ar), 121.2 (CH, Ar), 86.2 (C-I, quaternary), 36.3 (CH_2), 33.6 (CH_2), 28.3 (CH_2-CH_2), 24.8 (CH_2), 24.3 (CH_2).

Melting Point – 177 – 180 ºC

FT-IR (ATR): (vmax/cm-1) 3297 (NH), 2934 (OH), 1688 (C=O), 1658 (C=O, amide).

Experiment 10.2: 7-[(4-bromophenyl)carbamoyl]heptanoic acid [31]

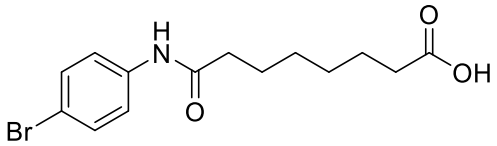

[31]

A solution of NaOH (1 M; 1.71 mmol; 1.70 mL) was added to **[29]** (1.14 mmol; 0.390 g) in THF (3.50 mL) at RT. The mixture was stirred for 3.5 hours (h), giving 92% of a white powder (0.345 g).

^{1}H NMR (400 MHz, DMSO-d_6) δ 11.98 (s, 1H, NH), 9.99 (s, 1H, OH), 7.57 (d, J = 8.9 Hz, 2H, Ar), 7.46 (d, J = 8.9 Hz, 2H, Ar), 2.29 (t, J = 7.4 Hz, 2H, C$\underline{H}_2$), 2.20 (t, J = 7.3 Hz, 2H, C$\underline{H}_2$), 1.64 – 1.43 (m, 4H, C$\underline{H}_2$-C$\underline{H}_2$), 1.35 – 1.23 (m, 4H, C$\underline{H}_2$-C$\underline{H}_2$).

^{13}C NMR (101 MHz, DMSO-d_6) δ 174.4 (C=O, quaternary), 171.4 (C=O, quaternary), 138.6 (C-NH, quaternary), 131.4 (CH, Ar), 120.9 (CH, Ar), 114.4 (C-Br, quaternary), 36.3 ($\underline{C}H_2$), 33.6 ($\underline{C}H_2$), 28.3 ($\underline{C}H_2$-$\underline{C}H_2$), 24.8 ($\underline{C}H_2$), 24.3 ($\underline{C}H_2$).

Melting Point – 158 – 161 ºC

FT-IR (ATR): (vmax/cm-1) 3296 (NH), 2852 (OH), 1688 (C=O), 1656 (C=O, amide).

Experiment 11.2: 7-[(2-bromophenyl)carbamoyl]heptanoic acid [34]

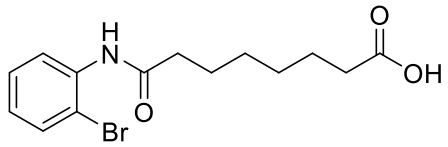

[34]

Compound **[32]** (1.34 mmol; 0.457 g) and THF (4.10 mL) were dissolved in a solution of NaOH (1 M; 2.01 mmol; 2 mL) and stirred for 4.5 h. A yellow powder was obtained as the product (93%, 0.409 g).

^{1}H NMR (400 MHz, DMSO-d_6) δ 9.39 (s, 1H, OH), 7.64 (d, J = 7.8 Hz, 1H, Ar), 7.55 (d, J = 7.8 Hz, 1H, Ar), 7.35 (t, J = 7.4 Hz, 1H, Ar), 7.12 (t, J = 7.3 Hz, 1H, Ar), 2.34 (t, J = 6.8 Hz, 2H, C$\underline{H}_2$), 2.20 (t, J = 7.3 Hz, 2H, C$\underline{H}_2$), 1.64 – 1.44 (m, 4H, C$\underline{H}_2$-C$\underline{H}_2$), 1.38 – 1.19 (m, 4H, C$\underline{H}_2$-C$\underline{H}_2$).

^{13}C NMR (101 MHz, DMSO-d_6) δ 174.5 (C=O, quaternary), 171.5 (C=O, quaternary), 136.4 (C-NH, quaternary), 132.6 (CH, Ar), 127.9 (CH, Ar), 127.5 (CH, Ar), 127.0 (CH, Ar), 118.2 (C-Br, quaternary), 35.6 ($\underline{C}H_2$), 33.7 ($\underline{C}H_2$), 28.3 ($\underline{C}H_2$-$\underline{C}H_2$), 25.1 ($\underline{C}H_2$), 24.4 ($\underline{C}H_2$).

Melting Point – 105 – 107 ºC

FT-IR (ATR): (vmax/cm-1) 3262 (NH), 2856 (OH), 1690 (C=O), 1662 (C=O, amide).

Experiment 13.2: 7-[(4-hydroxyphenyl)carbamoyl]heptanoic acid [38]

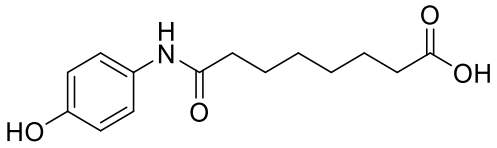

[38]

In a flask, to a solution of **[36]** (0.72 mmol; 0.200 g) and THF (2.65 mL), a solution of NaOH (1 M; 1.58 mmol; 1.60 mL) was added at RT. The mixture was placed under stirring overnight. This procedure afforded the expected product as a brown solid (93%, 0.173 g).

^{1}H NMR (400 MHz, DMSO-d_6) δ 11.97 (s, 1H, NH), 9.57 (s, 1H, OH), 9.11 (s, 1H,OH), 7.35 (d, J = 8.8 Hz, 2H, Ar), 6.67 (d, J = 8.8 Hz, 2H, Ar), 2.21 (dt, J = 11.9, 7.4 Hz, 4H, C$\underline{H_2}$-C$\underline{H_2}$), 1.61 – 1.45 (m, 4H, C$\underline{H_2}$-C$\underline{H_2}$), 1.35 – 1.24 (m, 4H, C$\underline{H_2}$-C$\underline{H_2}$).

^{13}C NMR (101 MHz, DMSO-d_6) δ 174.9 (<u>C</u>=O, quaternary), 170.9 (<u>C</u>=O, quaternary), 153.5 (<u>C</u>-OH, quaternary), 131.5 (<u>C</u>-NH, quaternary), 121.2 (<u>C</u>H Ar), 115.4 (<u>C</u>H, Ar), 36.6 (<u>C</u>H_2), 34.0 (<u>C</u>H_2), 28.8 (<u>C</u>H_2), 28.7 (<u>C</u>H_2), 25.5 (<u>C</u>H_2), 24.8 (<u>C</u>H_2).

Melting Point – 142 – 149 ºC

FT-IR (ATR): (vmax/cm-1) 3303 (NH), 2864 (OH), 1689 (C=O), 1657 (C=O, amide).

Experiment 13a.2: 7-[(4-{[bis(benzyloxy)phosphoryl]oxy}phenyl)carbamoyl]heptanoic acid [43]

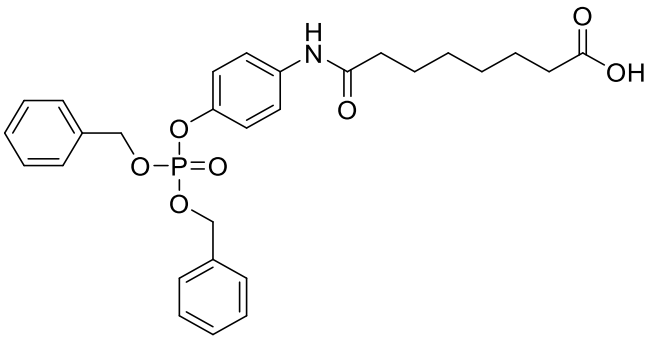

[43]

To a stirred solution of **[40]** (0.73 mmol; 0.395 g) in THF (4.75 mL), was added a solution of NaOH (1 M; 1.46 mmol; 1.46 mL) and the reaction mixture stirred overnight. This afforded the expected derivative as a brown oil (83%, 0.310 g).

^{1}H NMR (400 MHz, DMSO-d_6) δ 12.04 (s, 1H, NH), 9.94 (s, 1H, OH), 7.57 (d, J = 8.9 Hz, 2H, Ar), 7.42 – 7.30 (m, 10H, O-CH_2-Ph), 7.10 (d, J = 8.4 Hz, 2H, Ar), 5.14 (d, J = 8.3 Hz, 4H, O-CH_2-Ph), 2.28 (t, J = 7.4 Hz, 2H, CH_2), 2.20 (t, J = 7.3 Hz, 2H, CH_2), 1.62 – 1.45 (m, 4H, CH_2-CH_2), 1.33 – 1.26 (m, 4H, CH_2-CH_2).

^{13}C NMR (101 MHz, DMSO-d_6) δ 174.5, (C=O, quaternary), 171.2 (C=O, quaternary), 145.3 (C-O-P, quaternary), 136.5 (C-NH, quaternary), 128.5 (OCH_2-Ph, Ar, quaternary), 128.0 (OCH_2-Ph, Ar, quaternary), 120.3 (CH, Ar), 120.2 (CH, Ar), 69.4 (O-CH_2-Ph, quaternary), 36.3 (CH_2), 33.6 (CH_2), 28.3 (CH_2 -CH_2), 25.0 (CH_2), 24.4 (CH_2).

Experiment 13a.2H: 7-{[4-(phosphonooxy)phenyl]carbamoyl}heptanoic acid [44]

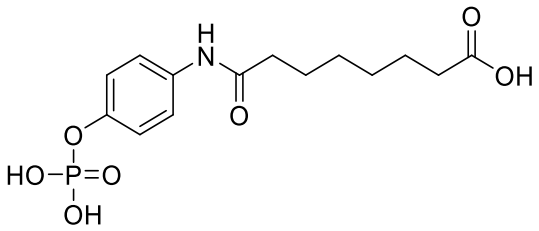

[44]

In a pressure reaction vessel, palladium on carbon, 10 wt % (0.058 mmol; 0.062 g) and **[43]** (0.58 mmol; 0.306 g) were charged. EtOH (3 mL) was added and the reaction vessel was purged with hydrogen and degassed. The reaction mixture was pressurized at 50 psi for 1 h. The mixture was then filtered through a pad of celite, rinsing with MeOH and concentrated. The title compound obtained was a greyish solid. (99%, 0.198 g).

^{1}H NMR (400 MHz, DMSO-d_6) δ 9.83 (s, 1H, OH), 9.57 (s, 1H, NH), 7.43 (dd, J = 68.7, 8.7 Hz, 2H, Ar), 6.87 (dd, J = 161.7, 8.7 Hz, 2H, Ar), 3.58 (s, 2H, HO-P-OH), 2.25 (ddd, J = 17.6, 15.9, 7.4 Hz, 4H, CH_2-CH_2), 1.63 – 1.49 (m, 4H, CH_2-CH_2), 1.36 – 1.21 (m, 4H, CH_2-CH_2).

^{13}C NMR (101 MHz, DMSO-d_6) δ 173.8 (C=O, quaternary), 171.4 (C=O, quaternary), 153.5 (C-O-P, quaternary), 135.7 (C-NH, quaternary), 121.2 (CH, Ar), 120.5 (CH, Ar), 115.4 (CH, Ar), 36.6 (CH_2), 33.6 (CH_2), 28.7 (CH_2), 28.6 (CH_2), 25.4 (CH_2), 24.7 (CH_2).

Melting Point – 124 – 127 ºC

FT-IR (ATR): (vmax/cm-1) 3338 (NH), 2944 (OH), 1715 (C=O), 1653 (C=O, amide), 1189 (P=O).

2.2 Plant Material

2.2.1 BY2 cell transformation

Transgenic suspension cell cultures of *Nicotina tabacum* L. cv. BY2 expressing a human recombinant protein (lipocalin-type Prostaglandin D synthase, L-PGDS) were formerly obtained by *Agrobacterium tumefaciens* mediated transformation with pTRA-BT-AH plasmid (Figure 2-1) and were already available in the laboratory, labelled as BTAH line 4.

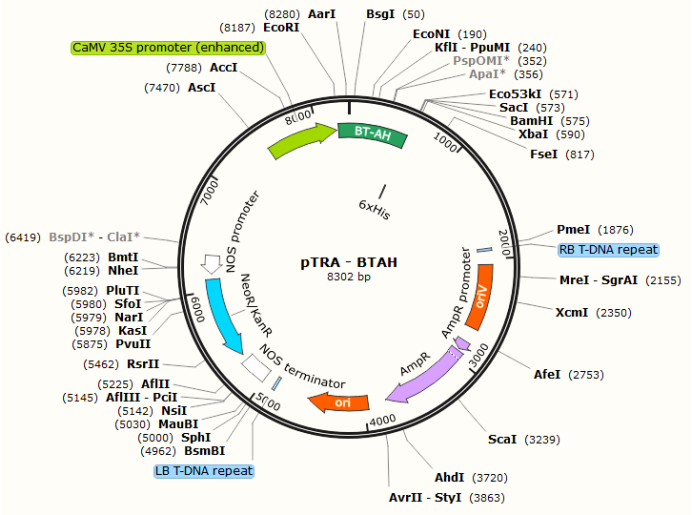

Figure 2-1- *Representation of pTRA-BT-AH (L-PGDS) plasmid.*

The T-DNA (transfer DNA) region included in the plasmid contains the cDNA (complementary DNA) that codifies for L-PGDS controlled by the 35SS constitutive promoter. Upstream of the cDNA is an untranslated region CHS that stabilizes mRNA (messenger RNA) and a plant-optimised murine signal peptide (LPH) which guides the protein to the secretory pathway. Downstream of the L-PGDS gene is a His6 (C-terminal fusion tag containing six histidine residues) for protein purification and a terminator sequence (35ST). The transgene cassette is flanked by MARs (Matrix Attachment Regions) that prevent phenomena of gene silencing and stabilize transgene expression. This T-DNA region is delimited by the right border (RB), and the left border (LB). Next to the LB, as can be seen in Figure 2.2, is the kanamycin resistance cassette with the gene nptII under the control of the Pnos promoter and the NosT terminator.

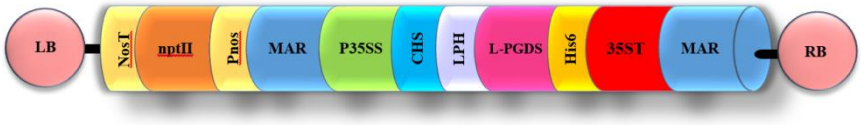

Figure 2-2- *Schematic representation of the L-PGDS T-DNA region.*

2.2.2 Maintenance of BY2 cell suspension cultures

A plant cell suspension culture of BTHA4 was maintained by adding 4% of inoculum to 50 mL of fresh Murashige & Skoog (MS) culture medium (sub-section **6.2** in chapter **6**). Erlenmeyer flasks were incubated on an orbital shaker (Gerhardt) at constant temperature (28 ºC) and rotation (120 rpm) in the dark. Subculture was carried out every ten days.

2.2.3 Characterization of BTAH4 growth curve

Growth curves were determined by the analysis of dry weight of cells per volume of cell suspension culture. For seven-day growth curve, three erlenmeyers containing BY2 cell suspension culture for each point of the curve were prepared, as described previously in section **2.1.2**. Triplicate samples for control cultures were collected on day 0, 2, 4, 7 and, for BY2 cell cultures incubated with an HDACi on day 2, triplicate samples were collected on day 4 and 7. Four replicates were used to determine a 14-day growth curve. Vacuum filtration allowed the separation of cells from the culture medium using a kitasato, büchner funnel and pre-weighed filter paper (VWR®). The plant cell culture was filtered; the collected culture medium was stored at -20 ºC and the filter paper containing the cells was placed in an oven at 60 ºC for 48 h, for weighing of dry mass.

In parallel, cell counting was performed as explained next, in order to determine cell viability along culture growth. This methodology is very simple and essentially requires a haemocytometer (Hirschmann™), represented in Figure 2-3.

Figure 2-3- *An "H" shaped haemocytometer with two counting chambers, each with a grid engraved (4x4 squares) and each square with a 4x4 pattern.*

After cleaning the haemocytometer with EtOH, the cell suspension to be applied in each counting chamber is prepared by adding 0.4% Trypan Blue into the sample (1:1) (sub-section **6.2** in chapter **6**). This dye selectively penetrates the membrane of the dead cells, thus allowing to distinguish the viable cells from the dead ones which turn blue. The process of counting is done by using a microscope (Leica DMRB) and, subsequently, the cellular viability in the sample is determined by applying the following equation (Strober, 2001):

$$\text{Viable cells (\%)} = \frac{\text{number of viable cells per mL of aliquot}}{\text{total number of cells per mL of aliquot}} \text{ x } 100$$

2.2.4 Nuclei extraction

BY2 cell suspension culture, described in sub-section **2.2.2**, was filtered and the filtered cells were transferred to a falcon tube, with the aid of a frozen spatula, and stored at – 80 ºC. Cells were grinded with liquid nitrogen in a mortar and homogenized with buffer NE1, described in sub-section **6.2**. Then, the cells were filtered through a series of filters (150, 100, 50, and 30 µm pore size), nuclei were pelleted by centrifugation (Eppendorf, Centrifuge 5415 D) (4000 g for 5 min) and washed in buffer NE1 without Triton X-100. Another centrifugation was performed, and then the pellet was resuspended in buffer NE2 (described in sub-section **6.2)** and kept on ice. The solution was sonicated for 30 seconds at 4 ºC, kept on ice for another 30 min and, only then, centrifuged for 10 min (15000 g). The pellet was discarded and the supernatant stored at - 80 °C.

2.2.5 Molecular modelling using AutoDockTools

In order to carry out this experiment, it was necessary to verify the sequence similarity between HDACs of different organisms. For this purpose, the Basic Local Alignment Search Tool (BLAST) was used and a blastp was made from the predicted sequence of *Nicotiana tabacum* histone deacetylase 6 against *Arabidopsis thaliana* histone deacetylase 6, *Saccharomyces cerevisiae* histone deacetylase RPD3 and *Homo sapiens* histone deacetylase 1.

Next, it was necessary to identify an appropriate homologue protein structure available in Protein Data Bank (PDB) similar to the target sequence to be modelled. The target sequence, *Nicotiana tabacum* histone deacetylase 6, was submitted to blastp against all sequences present in the PDB.

2.2.5.1 Ligands preparation

The structure of the synthesised compounds was processed with AutoDockTools to add Gasteiger-Marsili charges and hydrogen atoms, as well as to define the number of torsion angles.

2.2.5.2 4LXZ_A preparation

B and C chains, PG4 and NHE residues and sodium ion were removed from the structure, since they are not relevant for this analysis. SAHA ligand was also removed, due to the fact that the protein active site must be free during the docking calculations. AutoDockTools was used to add hydrogen atoms,

remove water molecules, assign Gasteiger charges and merge non-polar hydrogens. Zinc ion was manually assigned +2.0 charge.

2.2.5.3 Docking parameters

After 4LXZ_A and ligand preparation, a grid map describing potential affinity maps was calculated. The docking grid box was defined to be centered on the ligand and sized to extend 60 Å from any ligand atom, with a distance of 0.3 Å between grid points. The interaction of the active site zinc with the ligands could not be appropriately modelled using the default parameters, since this interaction is not a typical non-covalent interaction. Therefore, the parameters of this interaction were changed. Note that, to do this thoroughly, it would be necessary to use a larger training set with known experimental binding affinities. However, this approach would be too complex to be implemented in this project. Thus, the objective of this work was to try to reproduce the binding pose of SAHA, which has been determined in a human HDAC by X-ray crystallography. In spite of the fact that this approach could lead to some inaccuracies in terms of the absolute binding free energies, it should not affect the relative values of different ligands, since the same parameters were used for all the ligands. Then, the autodock input file and parameters were prepared.

This protocol was based on Morris and Huey, 2009, Santos-Martins et al. and 2014 Yan et al., 2016.

2.2.6 Analysis of HDAC inhibition

The Epigenase^{TM} HDAC Activity / Inhibition Assay kit (colourimetric) allowed the measurement of the activity of HDACi. An acetylated histone HDAC substrate, coated onto the microplate wells, binds to active HDACs and the acetyl group is removed. HDAC substrate and assay buffer were incubated for 90 min with or without of 10 µM of each inhibitor in a microplate. Deacetylated products are formed and they are recognized by specific antibodies. The capture antibody was incubated for 1 h followed by incubation with the detection antibody for 30 min. Then, the developer and stop solutions were mixed in each well. The amount of deacetylated products is proportional to the enzyme activity and it can be colourimetrically measured by spectrophotometry. This assay followed the manufacturer's instructions (EPIGENTEK).

2.2.7 Histone extraction

For days 2, 4, 7, 11 and 14 of the growth curve, the plant cell culture was filtered and the filtered cells were transferred to a falcon tube, with the aid of a frozen spatula, and stored at – 80 ºC. Cells were grinded with liquid nitrogen, in a mortar, and homogenized with buffer HE1 (5 mL of buffer per g of cell

powder), described in sub-section **6.2**. The cells were filtered through a nylon mesh and a series of filters (300, 180, 150 and 30 µm pore size) (PanReac AppliChem). The solution was centrifuged at 15000 g for 15 min and the pellet was washed in buffer HE2, described in sub-section **6.2**. After another centrifugation, 16100 g for 5 min, the pellet was homogenized in 1 mL of buffer HE3, described in sub-section **6.2**, and 1 mL of a solution of sulfuric acid (0.4 M) and incubated on ice for 45 min. Then, the sample was centrifuged once more (10000 g for 10 min), the supernatant stored and the pellet resuspended in 1 mL of sulfuric acid for another 45 min. After centrifugation, this supernatant was stored separately from the previous one. The proteins present in the supernatants were precipitated in 5 volumes of EtOH at -20 ºC. 48 h later, the supernatants were centrifuged at 12000 g for 10 min, the pellet washed with EtOH (80%), centrifuged once more and left to dry. The pellet was resuspended in sample buffer (100 µL), described in sub-section **6.2**, boiled at 100 ºC for 10 min in a dry bath and stored at – 20 ºC until further use.

2.3 Protein Analysis

2.3.1 Bradford protein assay

The Bradford Assay is an accurate and simple method for determining the concentration of proteins present in the culture medium, describe in sub-section **2.2.3**, using Coomassie Brilliant Blue G-250 dye. This assay followed the manufacturer's instructions (Quick Start™ Bradford Protein Assay, BIO-RAD). In a 96 well plate, 40 µL of Bradford reagent plus 160 µL of culture medium sample were homogenized. Three replicates for each samples were made; for each time point, were collect three samples. Samples from day 11 and 14 were diluted in distilled water (1:1) prior to mixing with the Bradford reagent. The standard curve was established using bovine serum albumin (BSA) as standard protein in the following concentrations: 10 µg/mL, 20 µg/mL, 40 µg/mL and 60 µg/mL. A spin down of the culture medium was done for each sample to ensure that precipitation in the culture medium did not interfere with the assay.

2.3.2 Sample preparation for SDS – PAGE

Each sample of culture medium (400 µL) was precipitated in EtOH (1600 µL) overnight at – 20 ºC and then centrifuged at 16100 g for 10 min, the supernatant was discarded and the pellet dried. After the EtOH was completely dried, the pellet ressuspended in 1 x sample buffer (sub-section **6.2**), leading to a 2.5 fold concentration, and boiled at 100 ºC for 10 min in a dry bath. A spin down was done for each sample before use.

2.3.3 Sodium dodecyl sulfate – polyacrylamide gel electrophoresis (SDS-PAGE) Preparation

The SDS-PAGE gel was assembled in a Mini-PROTEAN Tetra Cell Casting Module Electrophoresis system (BIO-RAD) (Figure 2-4).

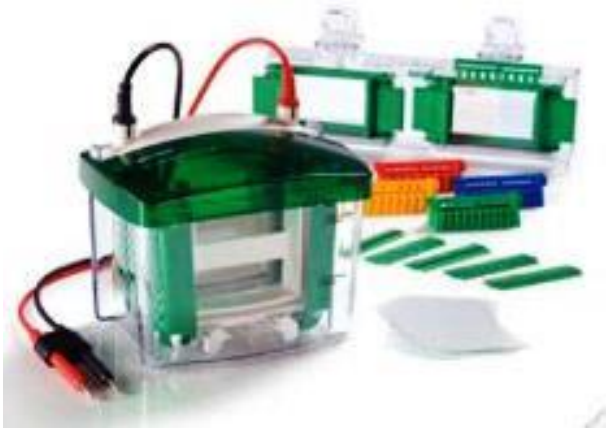

Figure 2-4 – *Mini-PROTEAN tetra cell component.*

First, the resolving gel with 12.5% acrylamide or 15% acrylamide (Table 2.1) was prepared by mixing the components, in the same order in which they appear in the table. The gel mix was pipetted between the plates (1 mm), filled with isopropanol for bubbles removal and, once the gel was polymerized (≈ 45 min), the top of the gel was washed with water. While the excess of water was blotted off with a filter paper, the stacking gel was prepared (Table 2.1), added to the gel cassette and the combs were placed between the glasses, avoiding air bubbles.

Table 2-1- *Preparation of resolving and stacking gels.*

Components	Resolving gel (mL) (12.5% acrylamide)	Resolving gel (mL) (15% acrylamide)	Stacking gel (mL)
Total volume	8.875	10.010	6.160
Water	2.820	2.983	3.980
Stacking gel buffer stock (sub-section **6.2**)	-	-	1.250
Resolving gel buffer stock (sub-section **6.2**)	1.250	1.250	-
10% SDS	0.100	0.100	0.050
Acrylamide:Bisacrylamide (30 : 0.8) (NZYtech)	4.200	5.000	0.625
1.5% Ammonium persulphate (APS, MERCK)	0.500	0.667	0.250
TEMED (SIGMA-ALDRICH)	0.005	0.010	0.005

Once the gel was polymerized, the electrophoresis apparatus was assembled and the running buffer added to the tank, covering the electrodes. The marker NZYColour Protein Marker II (NZYTech) (3 µL) was loaded, followed by the samples (20 µL each) and sample buffer (sub-section **6.2**) in the empty wells. A 180 V and 30 mA (15 mA per gel) electric field was applied for 90 to 120 min. One gel was coloured with BlueSafe (NZYTech) overnight and further washed with water, and the other gel was used for protein transfer.

2.3.4 Protein transfer from SDS-PAGE gel to nitrocellulose membrane

This technique is based on a semi-dry transfer method where the SDS-PAGE gel, filter paper (3 mm, GE Healthcare Life Sciences) and a nitrocellulose membrane (0.2 µm pore, GE Healthcare Life Sciences) were immersed in protein transfer buffer (sub-section **6.2**). Three sheets of the filter paper were placed, then the nitrocellulose membrane, then the gel and finally another three pieces of filter paper, in a Trans-Blot SD Semi-dry Transfer Cell (BIO-RAD), an electric field of 200 mA and 16 V was applied to the apparatus for 25 min.

2.4 Recombinant L-PGDS immunodetection

The nitrocellulose membrane, after transfer, was placed in a blocking solution [5% of skimmed milk powder (Nestlé) and 3% of BSA (SIGMA-ALDRICH) in 10 mL of Phosphate-buffered saline with tween-20 (PBS-T)] for at least 1 h with gentle shaking, washed 3 x 5 min with PBS-T and incubated with α-L-PGDS primary antibody (Abcam, ab61866) (diluted to a ratio of 1: 500 in PBS-T) for 1 h at room temperature and then stored at 4 ºC, shaking, overnight. The next day, the membrane was washed 3 x 5 min with PBS-T (sub-section **6.2**), incubated in anti-rabbit secondary antibody coupled to HRP (SIGMA-ALDRICH, A3687) (diluted to a ratio of 1: 4000 in PBS-T) for 2 h at room temperature and then washed with PBS-T, 3 x 5 min. The membrane was placed on a mica plastic sheet, the detection solution Amersham Enhanced Chemiluminescence Prime Western Blotting Detection Reagent (GE Healthcare) spread on it and the proteins detected by chemiluminescence using a ChemiDoc XRS+ (BIO-RAD).

2.5 Analysis of Histone H3 acetylation levels

Immunodetection of acetylated histones followed the method described above with slight changes. Total protein extracts were resolved in a 15% SDS-PAGE gel and proteins were transferred to a nitrocellulose membrane for 20 min. The nitrocellulose membrane was placed in a blocking solution (5% of BSA in 10 mL of PBS-T) for 2 h, washed 3 x 10 min with PBS-T and incubated, overnight and morning, with anti-acetyl-histone H3 primary antibody (06-599, Merck Millipore) (1:5000 PBS-T) at 4 ºC. The membrane was washed 3 x 10 min with PBS-T, incubated in anti-rabbit coupled to HRP

secondary antibody (SIGMA-ALDRICH, A3687; diluted to a ratio of 1: 4000 in PBS-T) for 2 h and then washed again 3 x 10 min, with PBS-T. The membrane was placed on a mica plastic sheet, the SuperSignal™ West Femto Maximum Sensitivity Substrate detection solution spread on it and the proteins detected by chemiluminescence by ChemiDoc XRS+. After detection, the membrane was stripped 5 x 20 min with PBS-T and incubated, overnight and morning, with anti-histone H3 primary antibody (07- 340 690, Merck Millipore) (1:25000 in PBS-T) at 4 ºC. The membrane was washed 3 x 10 min with PBS-T, incubated in anti-rabbit coupled to HRP secondary antibody (SIGMA-ALDRICH, A3687) for 2 h and then washed again with 3 x 10 min, with PBS-T. The membrane was placed on a mica plastic sheet, the detection solution Amersham Enhanced Chemiluminescence Prime Western Blotting Detection Reagent spread on it and the proteins detected by chemiluminescence by ChemiDoc XRS+ (BIO-RAD).

3 RESULTS AND DISCUSSION

3.1 Synthesis of HDACis

Overall, twenty five compounds, thirteen hydroxamic acids and twelve carboxylic acids, were successfully synthesised, as outlined in Table 3-1.

A subfamily of these compounds was synthesised with a 4-carbon linker and a *trans* double bond, similar to the commercial HDACi, Belinostat represented in Figure 3-1. Three anilines derivates were used to obtain different capping groups and assembled to mono-ethyl fumarate, in order to obtain Belinostat analogues. Substituents were introduced in the *ortho*, *meta* and *para* position. Taking into account the structure of SAHA (Figure 3-1), the remaining compounds were synthesised from an 8-carbon linker (starting from suberic acid monomethyl ester), different anilines and further converted into hydroxamic and carboxylic acids. SAHA is another commercial inhibitor that has shown promising results because of its capability to inhibit all mammalian HDAC in classes I and II that are metal dependent (reviewed in Marks, 2007).

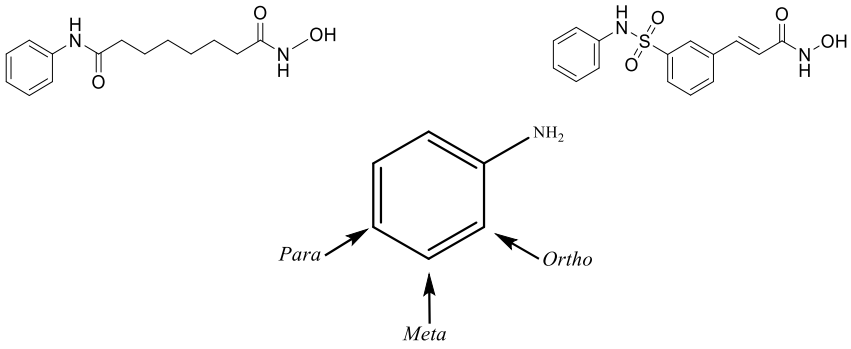

Figure 3-1- *Structural representation of the commercial HDACis SAHA (left) and Belinostat (right). Structural representation of an aniline (down) with the possibility of introducing a substituent in the second (ortho), third (meta) or fourth carbon (para) of the aromatic ring.*

Table 3-1- *Structure, IUPAC name and yield of all synthesised compounds, intermediates and final products.*

Compound	Number	Name	Yield (%)	Exp.
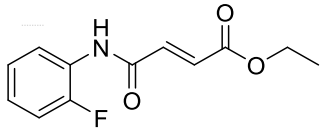	**3**	Ethyl (2E)-3-[(2-fluorophenyl)carbamoyl]prop-2- enoate	83	1
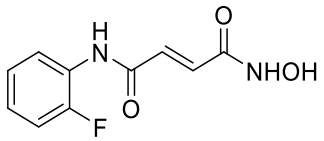	**4**	(2E)-N'-(2-fluorophenyl)-N-hydroxybut-2-enediamide	17	1.1
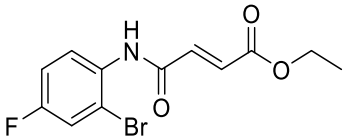	**5**	Ethyl (2E) -3- [(2-bromo-4-fluorophenyl)carbamoyl] prop-2-enoate	63	2
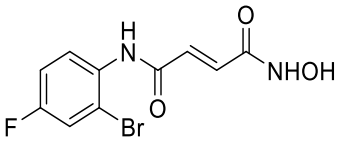	**6**	(2E)-N'-(2-bromo-4-fluorophenyl)-N-hydroxybut-2-enediamide	34	2.1
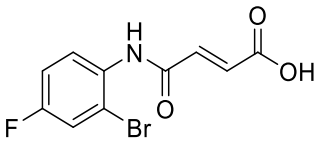	**7**	(2E)-3-[(2-bromo-4-fluorophenyl)carbamoyl]prop-2-enoic acid	90	2.2
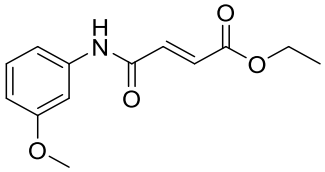	**8**	ethyl (2E)-3-[(3-methoxyphenyl)carbamoyl]prop-2-enoate	79	3
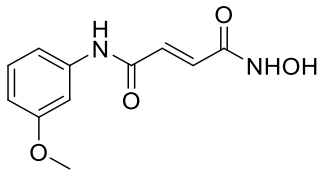	**9**	(2E)-N-hydroxy-N'-(3-methoxyphenyl)but-2-enediamide	46	3.1
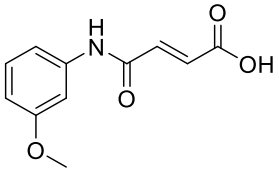	**10**	(2E)-3-[(3-methoxyphenyl)carbamoyl]prop-2-enoic acid	87	3.2
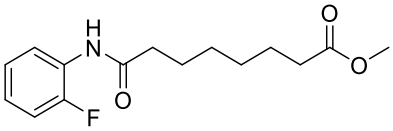	**11**	Methyl 7-[(2-fluorophenyl)carbamoyl]heptanoate	54	4
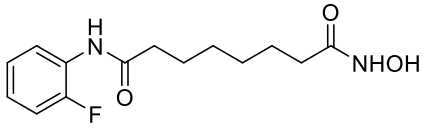	**12**	N'-(2-fluorophenyl)-N-hydroxyoctanediamide	45	4.1

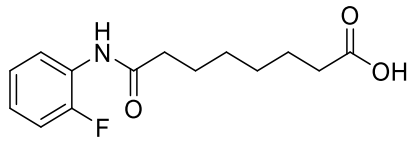	**13**	7-[(2-fluorophenyl)carbamoyl]heptanoic acid	59	4.2
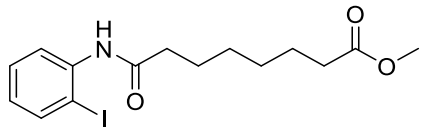	**14**	methyl 7-[(2-iodophenyl)carbamoyl]heptanoate	30	5
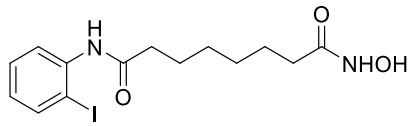	**15**	N-hydroxy-N'-(2-iodophenyl)octanediamide	60	5.1
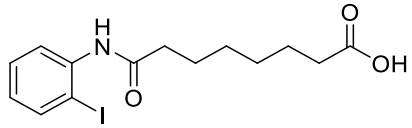	**16**	7-[(2-iodophenyl)carbamoyl]heptanoic acid	83	5.2
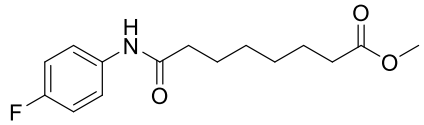	**17**	Methyl 7-[(4-fluorophenyl)carbamoyl]heptanoate	87	6
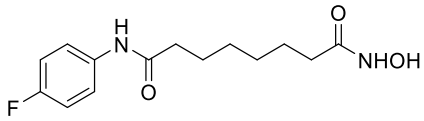	**18**	N'-(4-fluorophenyl)-N-hydroxyoctanediamide	38	6.1
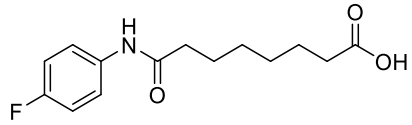	**19**	7-[(4-fluorophenyl)carbamoyl]heptanoic acid	57	6.2
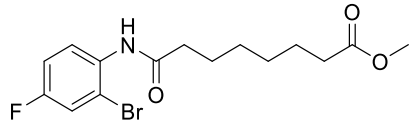	**20**	Methyl 7-[(2-bromo-4-fluorophenyl)carbamoyl]heptanoate	46	7
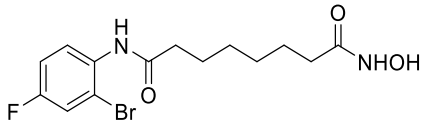	**21**	N'-(2-bromo-4-fluorophenyl)-N-hydroxyoctanediamide	30	7.1
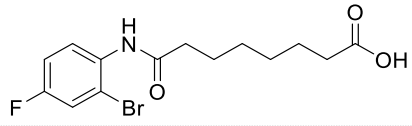	**22**	7-[(2-bromo-4-fluorophenyl)carbamoyl]heptanoic acid	49	7.2
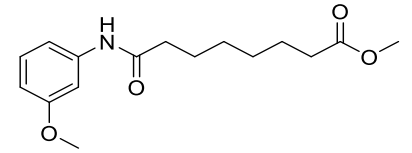	**23**	Methyl 7-[(3-methoxyphenyl)carbamoyl]heptanoate	87	8
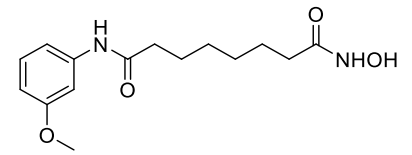	**24**	N-hydroxy-N'-(3-methoxyphenyl)octanediamide	30	8.1

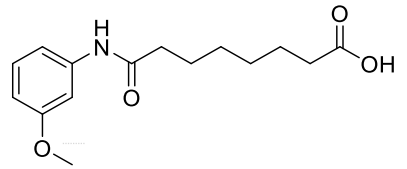	**25**	7-[(3-methoxyphenyl)carbamoyl]heptanoic acid	82	8.2
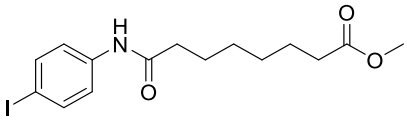	**26**	Methyl 7-[(4-iodophenyl)carbamoyl]heptanoate	81	9
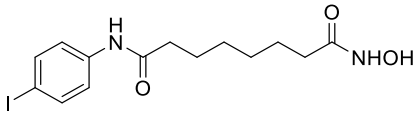	**27**	N-hydroxy-N'-(4-iodophenyl)octanediamide	38	9.1
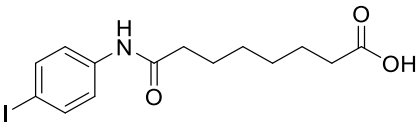	**28**	7-[(4-iodophenyl)carbamoyl]heptanoic acid	95	9.2
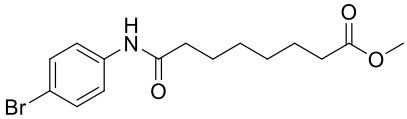	**29**	Methyl 7-[(4-bromophenyl)carbamoyl]heptanoate	81	10
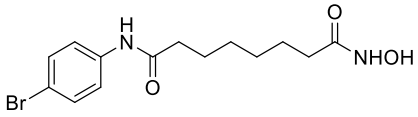	**30**	N'-(4-bromophenyl)-N-hydroxyoctanediamide	42	10.1
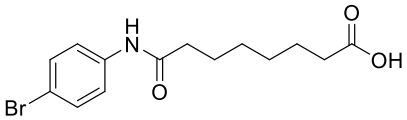	**31**	7-[(4-bromophenyl)carbamoyl]heptanoic acid	92	10.2
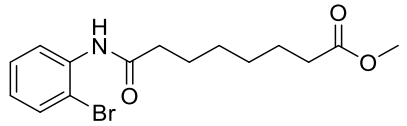	**32**	Methyl 7-[(2-bromophenyl)carbamoyl]heptanoate	33	11
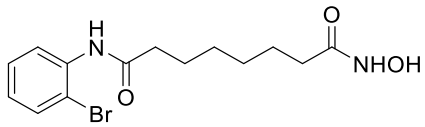	**33**	N'-(2-bromophenyl)-N-hydroxyoctanediamide	39	11.1
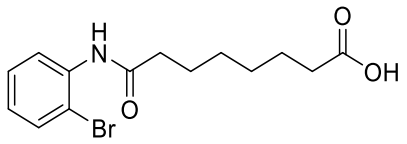	**34**	7-[(2-bromophenyl)carbamoyl]heptanoic acid	93	11.2
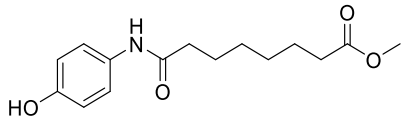	**36**	Methyl 7-[(4-hydroxyphenyl)carbamoyl] heptanoate	95	13
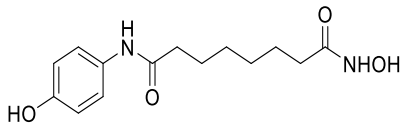	**37**	N-hydroxy-N'-(4-hydroxyphenyl)octanediamide	27	13.1

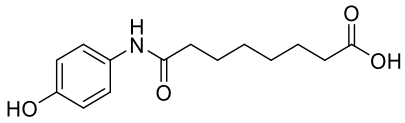	**38**	7-[(4-hydroxyphenyl) carbamoyl]heptanoic acid	93	13.2
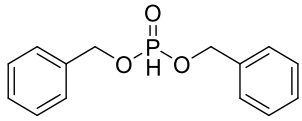	**39**	Dibenzyl phosphite	31	A
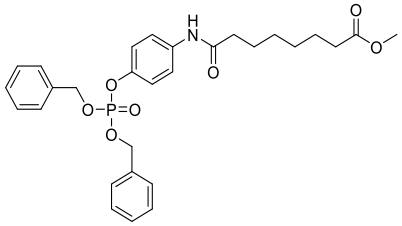	**40**	Methyl 7-[(4-{[bis(benzyloxy)phosphoryl]oxy}phenyl)carbamoyl]heptanoate	93	13.a
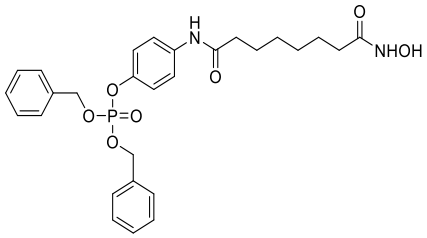	**41**	Dibenzyl 4-[7-(hydroxycarbamoyl)heptanamido] phenyl phosphate	35	13.a1
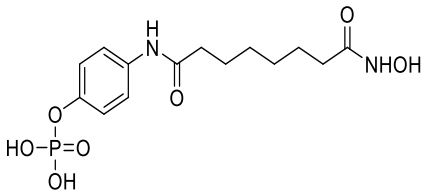	**42**	{4-[7-(hydroxycarbamoyl)heptanamido] phenoxy}phosphonic acid	91	13.a1H
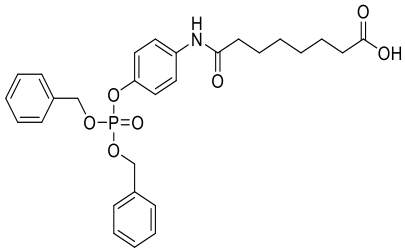	**43**	7-[(4-{[bis(benzyloxy)phosphoryl]oxy}phenyl)carbamoyl]heptanoic acid	83	13.a2
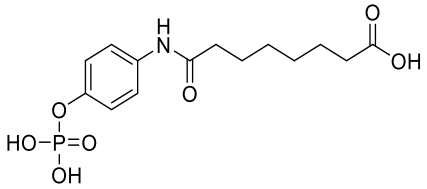	**44**	7-{[4-(phosphonooxy)phenyl]carbamoyl}heptanoic acid	99	13.a2H

3.1.1 Amide formation

The intermediates (1st step reaction) are organized and identified in Table 3-2 and Table 3-3; these compounds were generally obtained in good yields, between 33% and 95%. Further product was collected

when the mother waters, from the first recrystallization, were submitted to another recrystallization; however, this was usually accompanied by impurities.

Table 3-2- *General route for amide synthesis using mono-ethyl fumarate as starting material and different anilines.*

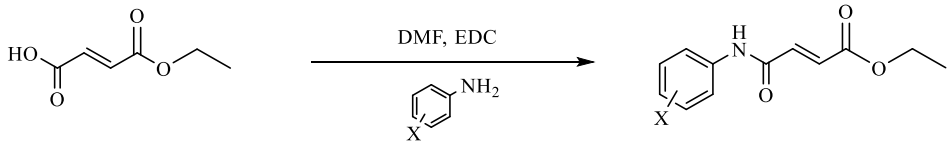

Starting material	X	Compound	Page
1	2-Fluoro*	**3**	18
	2-Bromo-4-fluoro*	**5**	19
	3-Methoxy*	**8**	20

**phenyl amide*

Table 3-3- *General route for amide synthesis using suberic acid monomethyl ester as starting material and different anilines.*

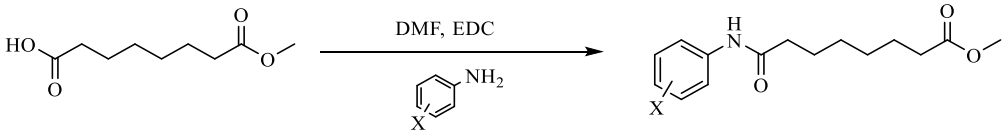

Starting material	X	Compound	Page
2	2-Fluoro*	**11**	20
	2-Iodo*	**14**	21
	4-Fluoro*	**17**	21
	2-Bromo-4-Fluoro*	**20**	22
	3-Methoxy*	**23**	23
	4-Iodo*	**26**	23
	4-Bromo*	**29**	24
	2-Bromo*	**32**	24
	4-Hydroxy*	**36**	26

**phenyl amide*

Only one synthetic step failed, which was the demethylation of compound **23** to give the compound **35**. On the first attempt, ^{1}H NMR confirmed that the product was formed along with a small quantity of starting material, **23**; however, this amount was minimal and the purification process would not be cost-effective. In subsequent attempts, the reaction time was increased and/or the reaction

temperature was decreased to -78 ° C, with a dry ice bath and acetone. The NMR spectra revealed that the starting compound, **23**, has not been consumed in its entirety (≈ 50%), being present in the ^{1}H-NMR as well as more impurities appeared in the ppm range corresponding to the aromatic hydrogens. Again, because of the low amount of crude and the amount of impurities being greater than the amount of the suspected product, purification would not be cost-effective. In the last attempt, the dicarboxylic acid was obtained because of the deprotection of both methoxide and methyl ester groups present in the compound **23**. Therefore this synthetic route, outlined in Table 3-4, was abandoned.

Table 3-4– *The synthetic route to compound **35** production, involving demethylation of compound **23**.*

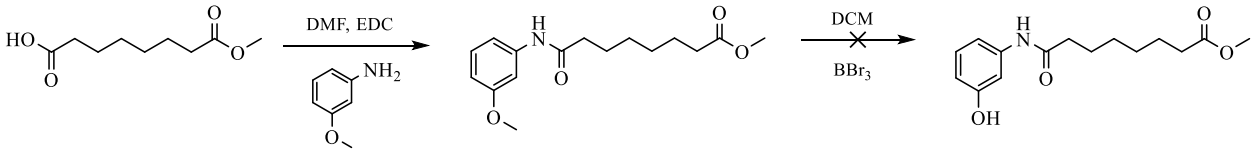

η = 85%

2 **23** **35**

3.1.2 Synthesis of carboxylic acid compounds

Depending on the aniline used or the amount of starting material, some reactions to produce carboxylic acids took longer to be complete or required the addition of more solvent. The compound **22**, containing 2-bromo-4-fluorophenyl amide, was obtained in the lower yield (49%) and the compound **28**, with 4-iodophenyl amide as capping group, was synthesised in the higher yield, of 95%. All the carboxylic acids synthesised are represented in Table 3-5 and Table 3-6.

Table 3-5- *Synthesis of carboxylic acid derivatives from compounds present in Table 3-2.*

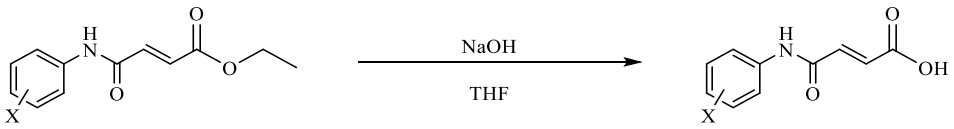

Intermediate	X	Compound	Page
5	2-Bromo-4-fluoro*	**7**	37
8	3-Methoxy*	**10**	38

**phenyl amide*

Table 3-6- *Synthesis of carboxylic acid derivatives from compounds present in Table 3-3.*

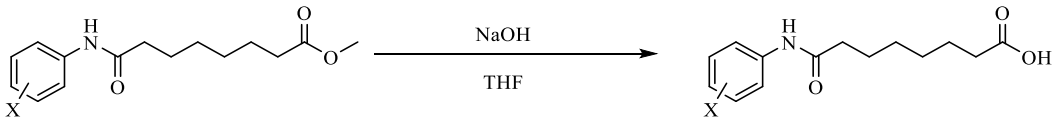

Intermediate	X	Compound	Page
11	2-Fluoro*	**13**	38
14	2-Iodo*	**16**	39
17	4-Fluoro*	**19**	39
20	2-Bromo-4-fluoro*	**22**	40
23	3-Methoxy*	**25**	40
26	4-Iodo*	**28**	41
29	4-Bromo*	**31**	42
32	2-Bromo*	**34**	42
36	4-Hydroxy*	**38**	43

**phenyl amide*

3.1.3 Synthesis of hydroxamic acid compounds

The reaction where hydroxamic acids were formed is described in Table 3-7 and Table 3-8.

Table 3-7- *Synthesis of hydroxamic acid derivatives from intermediate compounds present in Table 3-2.*

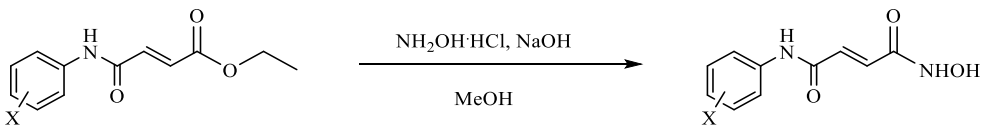

Intermediate	X	Compound	Page
3	2-Fluoro*	**4**	28
5	2-Bromo-4-fluoro*	**6**	29
8	3-Methoxy*	**9**	29

**phenyl amide*

Table 3-8- *Synthesis of hydroxamic acid derivatives from intermediate compounds present in Table 3-3.*

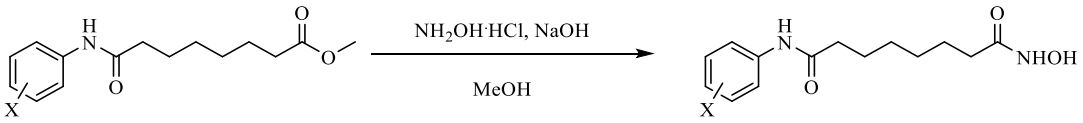

Intermediate	X	Compound	Page
11	2-Fluoro*	**12**	30
14	2-Iodo*	**15**	30
17	4-Fluoro*	**18**	31
20	2-Bromo-4-fluoro*	**21**	32
23	3-Methoxy*	**24**	32
26	4-Iodo*	**27**	33
29	4-Bromo*	**30**	33
32	2-Bromo*	**33**	34

**phenyl amide*

Overall, this synthetic step gave lower yields compared with the other steps. Compound **4** was obtained in the lower yield (17%) and the compound **15** was synthesised in the higher yield, of 60%. These low yields were not overcome by the increase in $NH_2OH{\cdot}HCl$ or the reaction time. The formation of hydroxamic acid from the methyl/ethyl ester precursor was accompanied by the formation of a nearly equal quantity of the carboxylic acid impurity, a by-product in this case. When NaOH is used as a base, it can hydrolyse the ester group to form a carboxylic acid that is removed when carrying out a $NaHCO_3$ wash; ^{1}H-NMR analysis of the aqueous phase, resulting from the bicarbonate wash, revealed the presence of the compound in the form of carboxylic acid. A partial advantage of this method is its simplicity, mild reaction conditions and it does not require chromatographic purification.

A new protocol has been tried in order to achieve higher yields (Table 3-9). After reading Beillard et al., 2016, DBU was employed as a nucleophilic base to increase the ratio of hydroxamic acid product over carboxylic acid impurities. Although it was only applied once, to compound **37**, the yield was not as expected (27%); so it is necessary to repeat these processes and, if possible, optimise the quantities of reagents/solvents used or alter the extraction process.

Table 3-9- *Application of DBU-based protocol for the synthesis of compound **37**, a hydroxamic acid.*

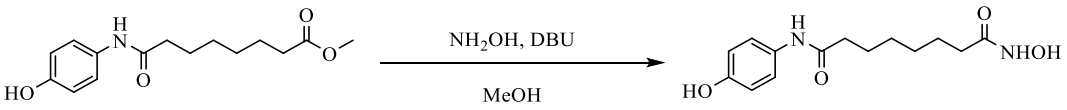

η = 95% **36** η = 27% **37**

Phosphorylation is an important regulatory mechanism of proteins and consists of the addition of a phosphate group to a protein. This addition may cause changes in the protein conformations, which may affect ligand binding to the protein (Deprez et al., 2002). HDAC enzymes are regulated by phosphorylation; so dephosphorylation of these enzymes results in an increase of the HDAC activity (Lusser et al, 2001) . However, it may happen that in some proteins the phosphate group itself belongs to the structure that the binding sites of certain proteins recognize. This type of compounds may influence the levels of acetylation and/or phosphorylation of a protein, which could lead to changes in transcription. As this structure is new, nothing is known regarding its activity.

After synthesising a variety of compounds by applying different synthetic methods, two new compounds were synthesised, compound **42** and compound **44**, applying all the knowledge gained. These compounds are structurally more complex, their synthetic route, shown in the Table 3-10, encompasses different mechanisms and different reactants to obtain the final product.

Table 3-10- *New synthesis of phosphate-derived compound **42** and compound **44**, a hydroxamic and carboxylic acid, respectively.*

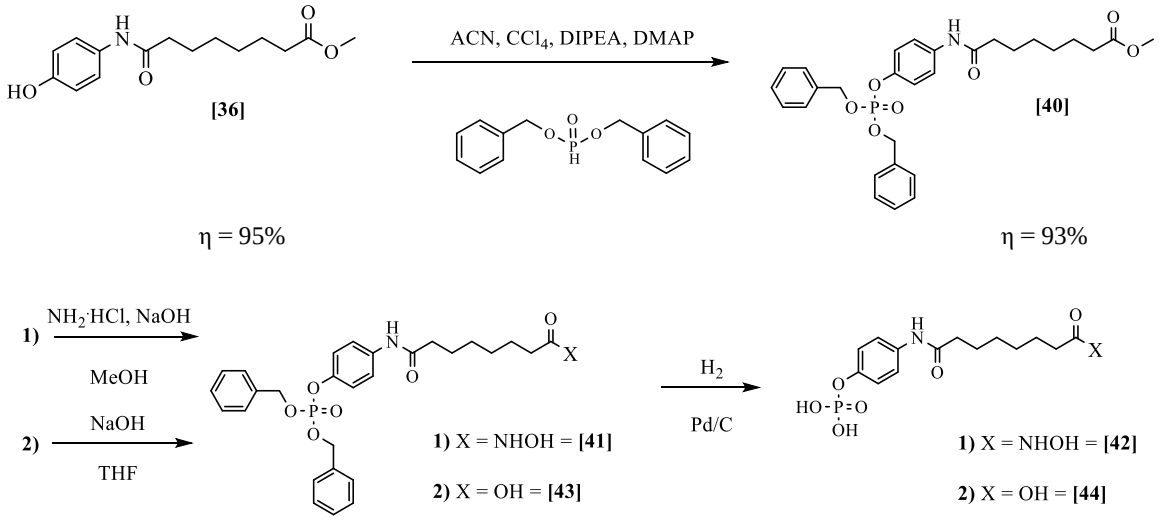

For the first step of the synthesis, which is characterized by the phosphorylation of a phenol, all reagents or solvents were previously distilled, except for dibenzylphosphite (compound **39**). These distillations are summarized in section **6.1**. The reactant **39** was produced in the laboratory and its synthesis optimised, using toluene instead of benzene as the solvent and by making slow extractions, with more solvent, in order to break the emulsion and the product remains in the organic phase. This reactant was chosen because the benzyl groups are easily removed by hydrogenolysis (Silverberg et al., 1996). The following step was the synthesis of hydroxamic acid **41** and carboxylic acid **43** from this ester using the standard methods outlined in this section. After that, it was necessary to deprotect the hydroxyl groups. Hydrogenation using palladium on carbon and EtOH provided a fast and simple removal of O-benzyl groups from the acid derivatives, to obtain the final compounds **42** and **44**.

Amongst hydroxamic acids and carboxylic acids with the same aniline derivative, the only structural difference is the metal binding moiety, the first being composed of two more atoms, one nitrogen and one hydrogen. In ^{1}H spectra, the simplest way to distinguish them is to observe the shift of the peaks related to protons in the linker, the ones closer to the carbonyl groups.

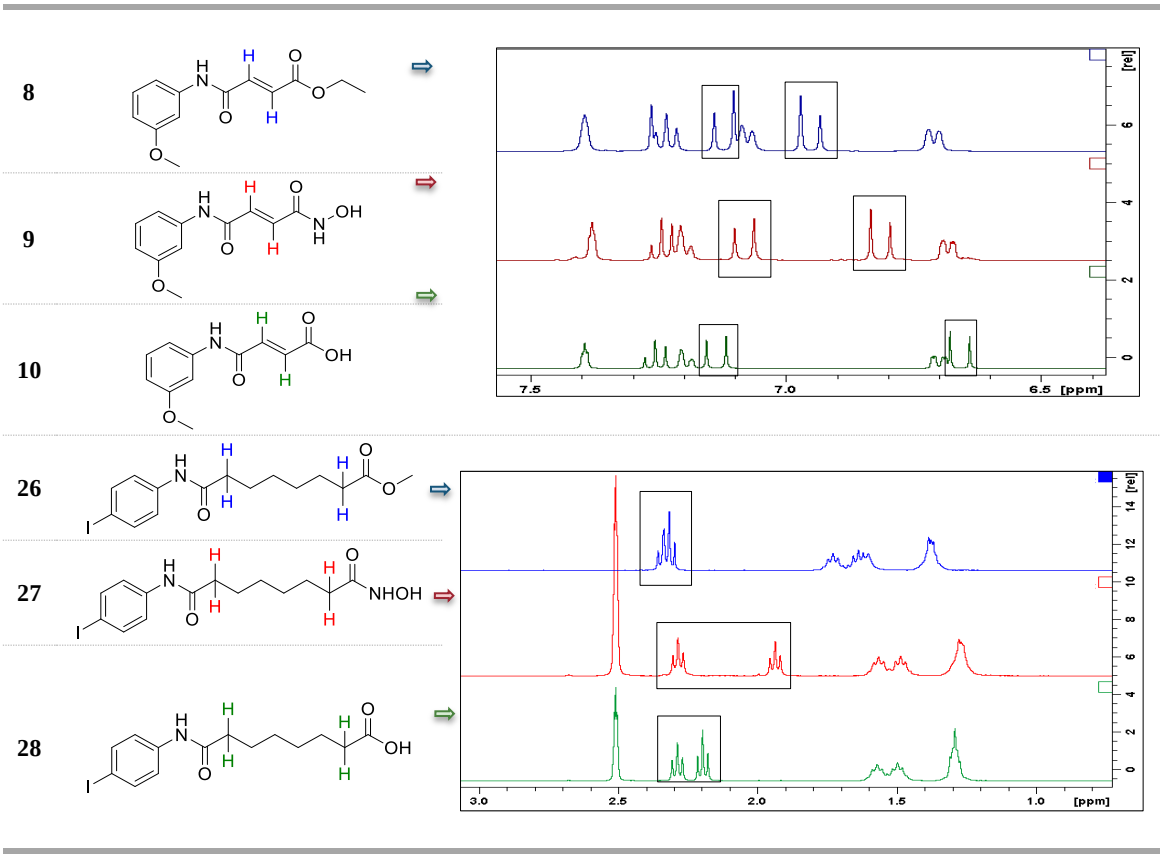

Figure 3-2- *^{1}H-NMR spectra of compounds **8**, **9**, **10**, **26**, **27** and **28** and their respective structure. Black squares represent the zone of the chemical shift, with reference to the spectra of intermediate compounds, **8** and **26.***

After analysis of Figure 3-2, it can be concluded that the existing protons closer to the carbonyl groups undergo a chemical shift (ppm), depending on whether the compound is an ester, a hydroxamic acid or a carboxylic acid, and it is possible to confirm the metal binding moiety of each compound.

Every compound structure was confirmed by NMR spectroscopy and stored at -20 ºC before performing the biological assays. Further characterization of the compounds was performed: the melting points of all solid compounds were determined, and the FT-IR spectra too. The final compounds were obtained in the 60 mg - 460 mg range.

All compounds to be tested, including the commercial compound SAHA, were dissolved in DMSO at a concentration of 100 mM and stored at – 20 ºC.

3.2 Theoretical prediction of the optimal conformation and relative orientation between HDAC and the ligands

The interaction of all synthesised compounds (ligands), described in sub-section **2.1.3** and **2.1.4,** with an HDAC was tested by performing docking calculations, explained in sub-section **2.2.5**. Firstly, an HDAC structure available in the PDB database was selected with support of BLAST, as explained in Material and Methods. The ideal was to identify the structure which had the highest percentage identity to the *Nicotiana tabacum* histone deacetylase 6 and a structure with appropriate ligand or cofactors. Since there is no crystallographic structure of *Nicotiana tabacum* available in the PDB, it was verified whether there would be significant differences between HDACs of different organisms.

The results obtained with BLAST are shown in Table 3-11, comparing the sequence of *Nicotiana tabacum* with *Arabidopsis thaliana*, *Homo sapiens* and *Saccharomyces cerevisiae* sequences. These results indicate that there is high degree of homology between organisms (identity values between 59 and 78%).

Table 3-11- *Description of the amino acid sequences of* Arabidopsis thaliana, Homo sapiens *and* Saccharomyces cerevisiae *producing significant alignments in comparison with* Nicotiana tabacum *amino acid sequence.*

Description	Max score	Total score	Query cover	E value	Ident	Accession
histone deacetylase 6 [Arabidopsis thaliana]	740	740	97%	0.0	78%	NP_201116.1
histone deacetylase 1 [Homo sapiens]	576	576	81%	0.0	66%	NP_004955.2
RPD3 [Saccharomyces cerevisiae]	513	513	84%	0.0	59%	AAB20328.1

Blastp was used to compare the amino acid sequence of *Nicotiana tabacum* histone deacetylase 6 with the sequences of HDACs already available in the PDB. The Human Hdac2 In Complex With Saha (4LXZ_A) structure was selected for the molecular docking experiment, among the structures shown in Table 3-12. This structure has 78% of query cover and 67% of identity, indicating that 67% of the same residues were in the same position in an alignment.

Table 3-12- *Sequences available in PDB producing significant alignments in comparison with* Nicotiana tabacum *histone deacetylase 6 sequence.*

Description	Max score	Total score	Query cover	E value	Ident	Accessior
Chain B, The Structure Of Hdac1 In Complex With The Dimeric Elm2-sant Domain Of Mta1 From The Nurd Complex	576	576	81%	0.0	66%	4BKX_B
Chain B, Hdac1:mta1 In Complex With Inositol-6-phosphate And A Novel Peptide Inhibitor Based On Histone H4	564	564	79%	0.0	66%	5ICN_B
Chain A, Structure Of Human Hdac2 In Complex With Saha (vorinostat)	543	543	78%	0.0	67%	4LXZ_A
Chain A, Hdac2 With Ligand Brd4884	541	541	78%	0.0	67%	5IWG_A
Chain A, Hdac2 With Ligand Brd7232	541	541	78%	0.0	67%	5IX0_A
Chain A, Crystal Structure Of Human Hdac2 Complexed With An N-(2-Amin Benzamide	539	539	77%	0.0	67%	3MAX_A

Molecular docking gave the preferential binding mode of the ligands (grouped in clusters) and estimated the binding free energy (BFE). The lowest binding free energy value corresponds to the best binding mode for each ligand. In order to predict which compounds were more efficient in inhibiting the enzyme activity, the preferred binding mode of each ligand was selected and their BFE compared (Figure 3-3).

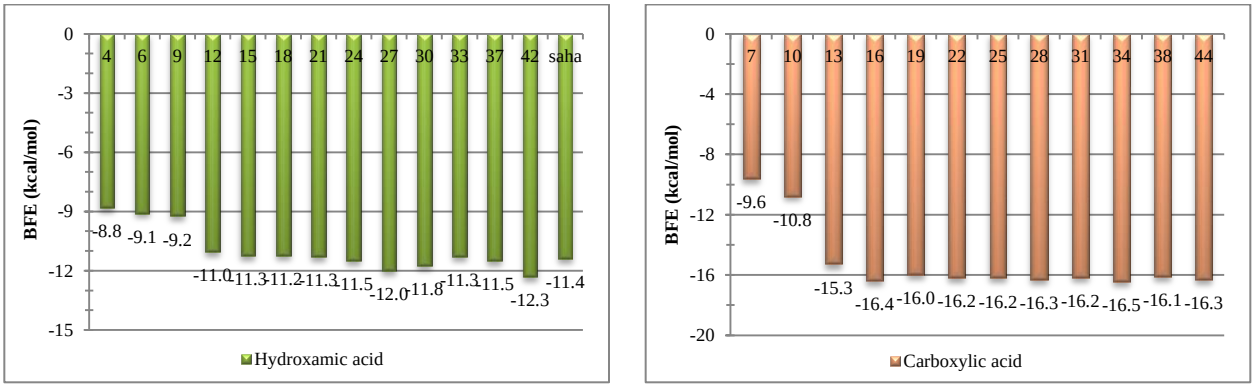

Figure 3-3- *Clustering histogram of all docking solutions, as a function of BFE, for all the synthesised hydroxamic compounds (left) and carboxylic compounds (right).*

It was not very useful to compare the corresponding values for hydroxamic and carboxylic acids, since this comparison may be affected by the parameters used for the interaction with zinc ion. Thus, it was decided to compare the BFE values within each group separately. When analysing the histogram on the left in Figure 3-3, compounds **4**, **6** and **9** with the smaller linker show lower BFE values compared with the remaining compounds which have an 8-carbon linker. However, there is no significant difference in the BFE values to establish which compound would be better as HDACi, based only on this parameter. Compounds **42** and **27**, with phosphate and iodine in the aromatic ring, respectively, were the compounds with the best conformation docked in the HDAC, with the highest BFE values, -12.3 and -12 kcal/mol, respectively.

Similar results were obtained for the carboxylic acid ligands (Figure 3-3, right histogram). The best conformation for compound **34** was obtained with the highest BFE value, -16.5 kcal/mol. This compound has a capping group consisting of an aromatic ring with a bromine substituent. Compound **16**, which has an iodine substituent in the aromatic ring, had a BFE value of -16.4 kcal/mol. Both these compounds have an 8-carbon linker. The best conformations of compounds **7** and **10**, with a 4-carbon linker, were obtained with BFE values of -9.6 and -10.8 kcal/mol, respectively.

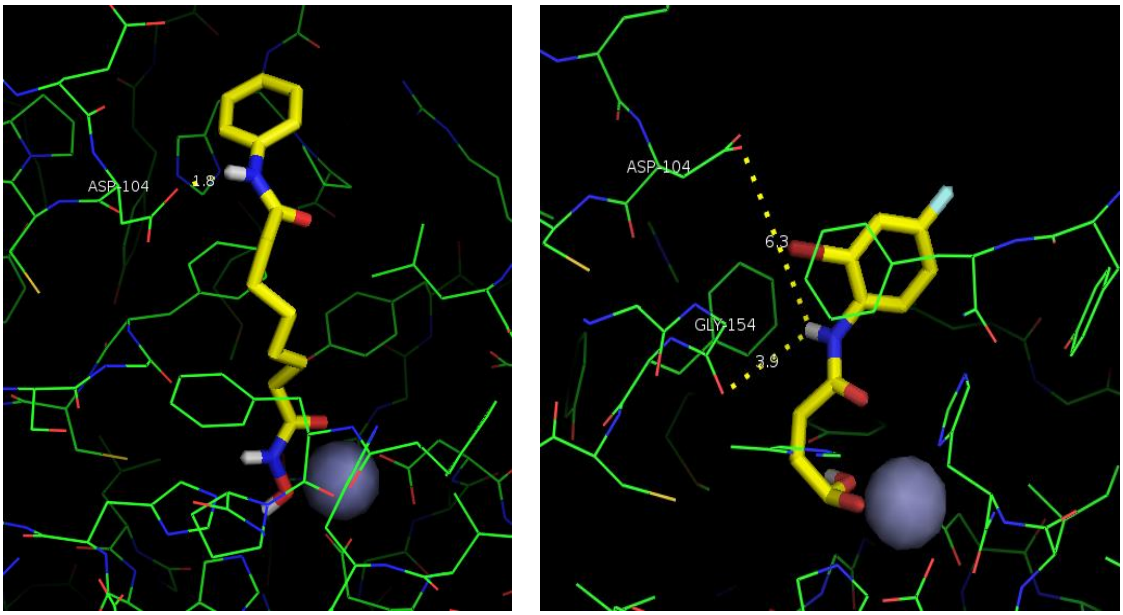

Figure 3-4- *Predicted binding of SAHA (left) and compound **6** (right) to Hdac2. The elements are represented by red – oxygen, blue – nitrogen, white -hydrogen, yellow – carbon, light blue – fluorine, brown – bromine, grey solid sphere - zinc.*

Next, a visual analysis of the conformation with lower BFE value of each compound was done. The main goal of this method was to try to understand the influence of the substituents in the capping group and the size of the linker. As shown in Figure 3-4, the 8-carbon linker from SAHA allows a hydrogen bond to occur with the ASP104 residue of Hdac2, while compound **6**, with a smaller linker, is spaced apart from the residues to form that hydrogen bond. Regarding to the capping group, the results displayed in Figure 3-5 allowed the evaluation of the difference caused by substituents in the aromatic ring. SAHA, which does not have substituents on the aromatic ring, was compared with compounds **12** and **6**, which have a fluorine and a fluorine and a bromine substituents, respectively. There is a change in how the ligands are positioned in the active site. These halogens are bulkier, taking up more space at the entrance of the active site, which can confer them an improvement as HDACi. Also, the ligands are exposed to the solvent and the hydrophilic substituents may help to stabilize the interaction with water.

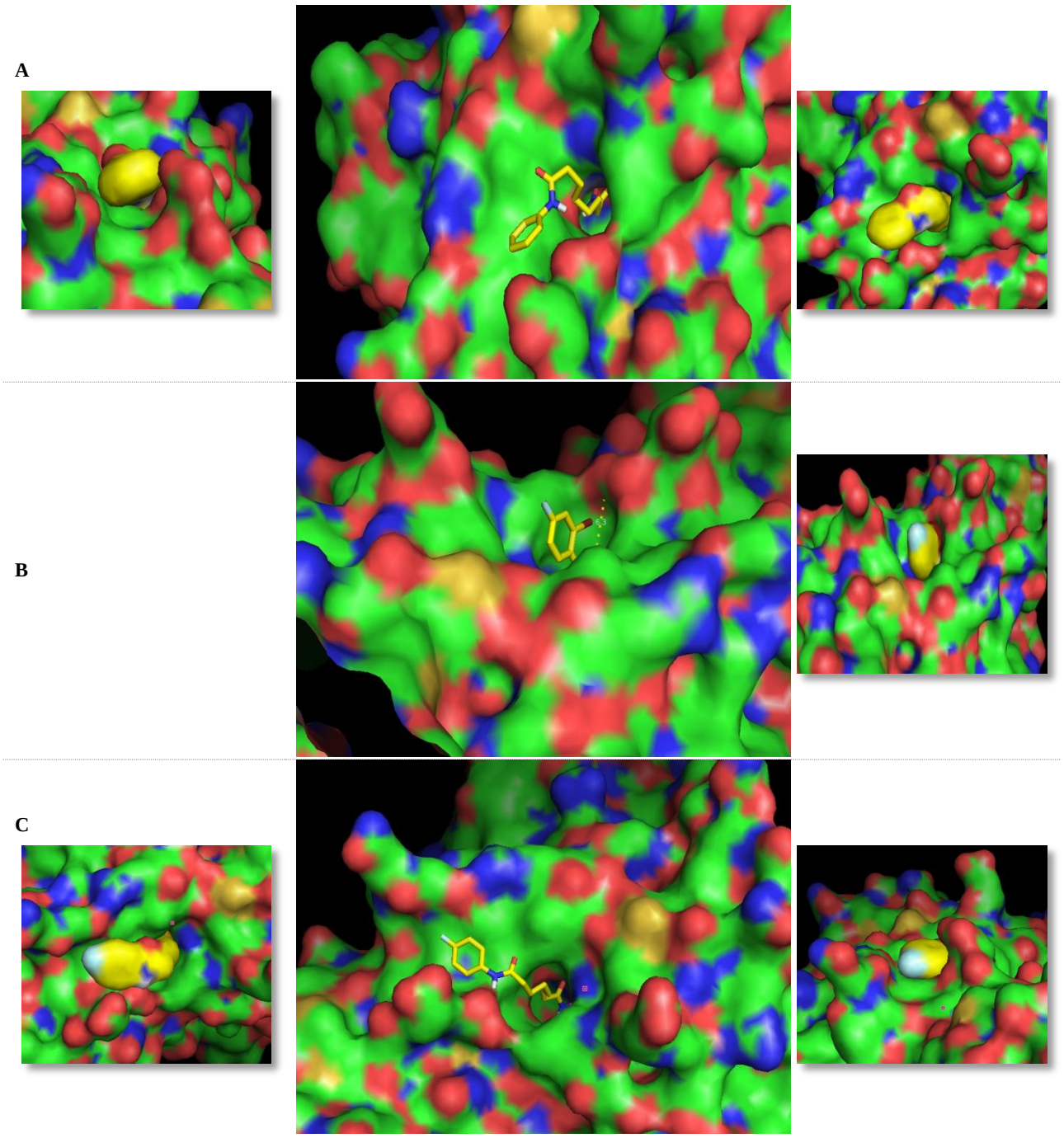

Figure 3-5- *Molecular docking results of Hdac2 crystal structure with docked SAHA (A), compound* ***6*** *(B), compound* ***12*** *(C) into catalytic site. The elements are represented by red – oxygen, blue – nitrogen, white -hydrogen, yellow – carbon, light blue – fluorine, brown – bromine.*

With this study, it was intended to restrict the number of compounds synthesised to be tested. Previous work realized at the Plant Cell Biology laboratory consisted in the analysis of some analogues of the compounds previously synthesised. Since analogues with bromine or iodine at the *para* position of the

aromatic ring had already been tested *in vivo*, compounds with the best BFE value and with different capping groups were chosen for the following experiments. Furthermore, the compounds with methoxide group in the *meta* position and bromine and fluorine in the *ortho* and *para* positions of the aromatic ring, respectively, but with the smaller linker, were chosen. This selection served to understand how the chain size of the compounds influences their activity.

3.3 HDACi evaluation as enhancers of protein production

3.3.1 *In vitro* screening of compounds as potential HDAC inhibitors

The synthesised compounds compiled in Table 3-1, analogues of commercial HDACis, were tested *in vivo*. However, these assays in BY2 cell suspension cultures are time consuming, so a prior *in vitro* test for screening which inhibitors have to be tested was carried out. Since it was not possible to test all the synthesised compounds, the compounds that were previously tested in the Plant Cell Biology laboratory were not chosen for the following assay, and the remaining compounds were selected based on three criteria: (1) compounds with the smaller unsaturated linker and with the linker with 8 carbons; (2) compounds with different aromatic group substituents and (3) hydroxamic and carboxylic acid compounds with the same capping group. This selection was also assisted by the molecular docking analysis described in section **3.2.** SAHA was the commercial FDA-approved HDACi chosen as a reference for this work. It has been proven to inhibit two classes of HDACs, as previously mentioned, acting as a pan-inhibitor (Bieliauskas and Pflum, 2008; Marks, 2007). Besides, due to its inhibitory potential, SAHA was tested in *Medicago truncatula* and results positively demonstrate its function as SMEs (Santos et al., 2017, submitted).

For this purpose, the Epigenase^{TM} HDAC Activity/Inhibition Direct Assay Kit (see sub-section **2.2.6** for more information), was used to measure the activity/inhibition of total HDAC enzyme using nuclear extracts from BY2 cell suspension cultures. After colour change in the microplate wells of the kit, the absorbance was read at 450 and 655 nm and the data obtained were inserted into the following formulas A, B and C:

A - $\text{Deacetylated product (ng)} = \frac{\text{(Sample OD-Blank OD)}}{\text{Slope}}$

B - $\text{HDAC Activity (ng/min/mg)} = \frac{\text{Deacetylated product (ng)}}{\text{(Protein amount (µg)x min)}} \times 100$

C- $\text{Inhibition (\%)} = \left(1 - \frac{\text{Inhibitor sample OD - Blank OD}}{\text{No Inhibitor sample OD - Blank OD}}\right) \times 100$

The results of this experiment with the chosen synthesised compounds, **6**, **7**, **9**, **10**, **12**, **13**, **15**, **16**, **18**, **19**, **33**, **34**, **37**, **38**, **42** and **44**, were plotted as shown in Figure 3-6. The ability of each compound to inhibit HDAC was measured, Figure 3-6 (C). This inhibition caused a decrease in the activity of HDAC which produced a smaller amount of deacetylated products. This amount is proportional to the enzyme activity and was colourimetrically measured in a spectrophotometer.

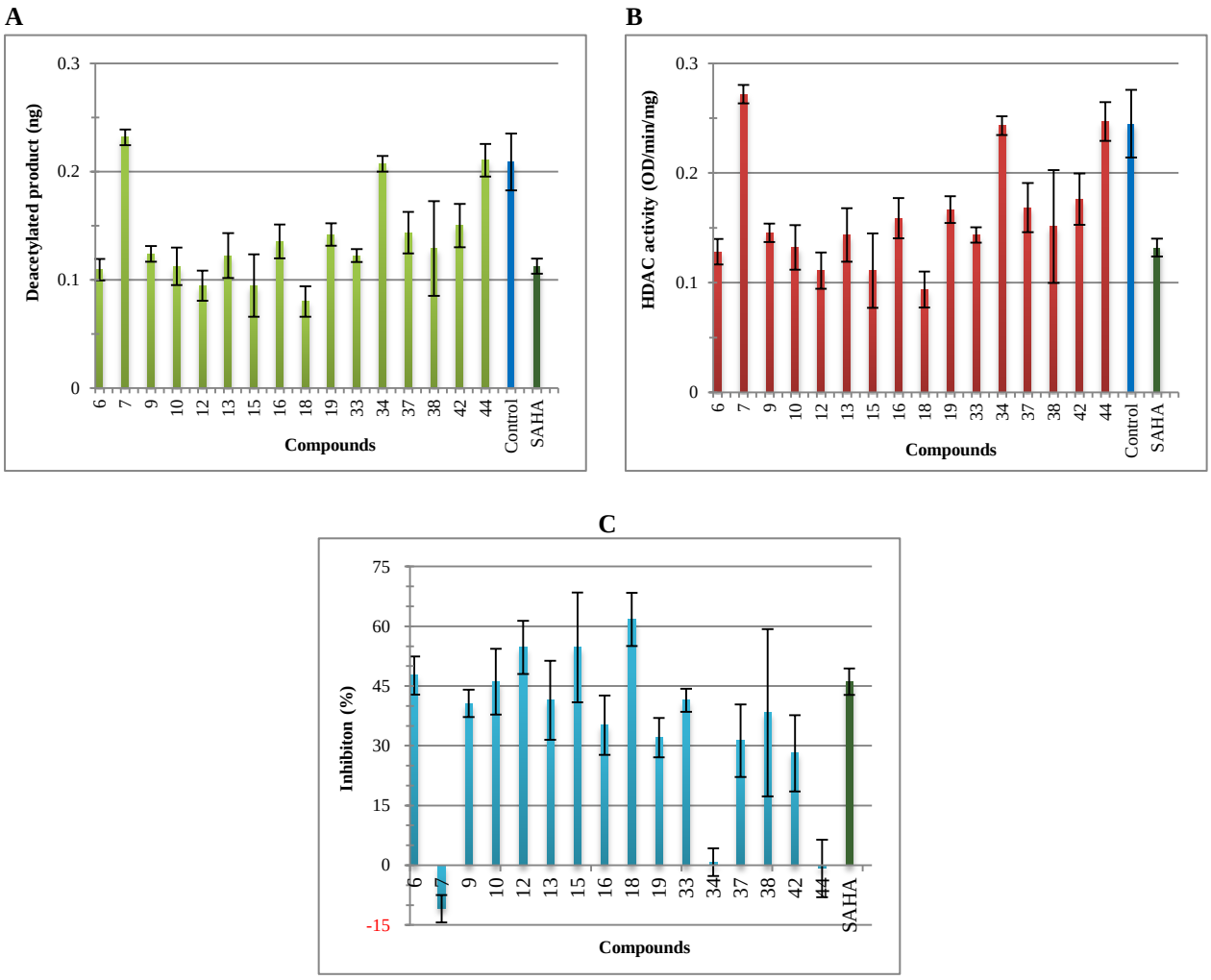

Figure 3-6- *Measurement of the amount of deacetylated product (A), activity (B) and inhibition (c) of total HDAC enzyme for each synthesised compound. Error bars represent the standard deviation of three technical replicates*

Considering the values obtained in each graph coupled with the standard deviation, compounds **6**, **10**, **12**, **15** and **18** showed higher or similar inhibition (C) values and lower or similar HDAC activity values (B) compared to SAHA. Control samples that were not incubated with any inhibitor had a higher HDAC activity, which led to a larger production of deacetylated products. The compounds selected for further testing are structurally represented in Figure 3-7.

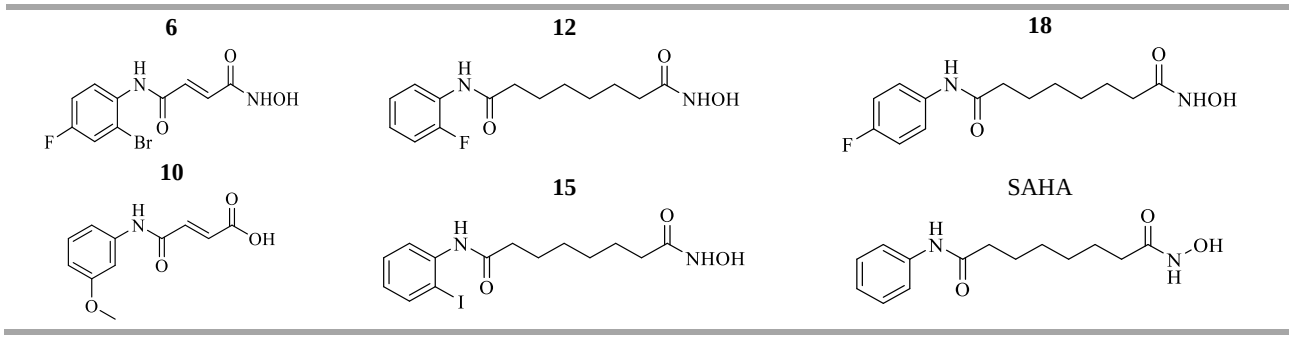

Figure 3-7- *Chemical structure of the synthesised compounds chosen after analysis of the results obtained in the kit Epigenase.*

3.3.2 *In vivo* testing of compounds 6, 10, 12, 15, 18 and SAHA

To assess the effect of these inhibitors, three 7-day growth curves of BY2 cell suspension cultures expressing L-PDGS were performed with three biological replicates, as explained in Material and Methods (section **2.2.3**). Cells and culture medium were collected on days 0, 2, 4 and 7. The effect caused by the addition of the synthesised inhibitors on day 2 was tested, with a final concentration of 10 µM. This concentration was determined in work previously performed in the Plant Cell Biology laboratory and showed not to be toxic to BY2 cells. A cell culture without inhibitors was monitored as a control, for each curve. Dry weight *vs* time graphs were built, as shown in Figure 3-8 (A-C).

To quantify the total soluble protein in BY2 cultures, a Bradford assay was carried out using BSA for a standard curve. Culture medium collected at each point of the curve, in the presence and absence of inhibitor. Three replicates were used for each time point.

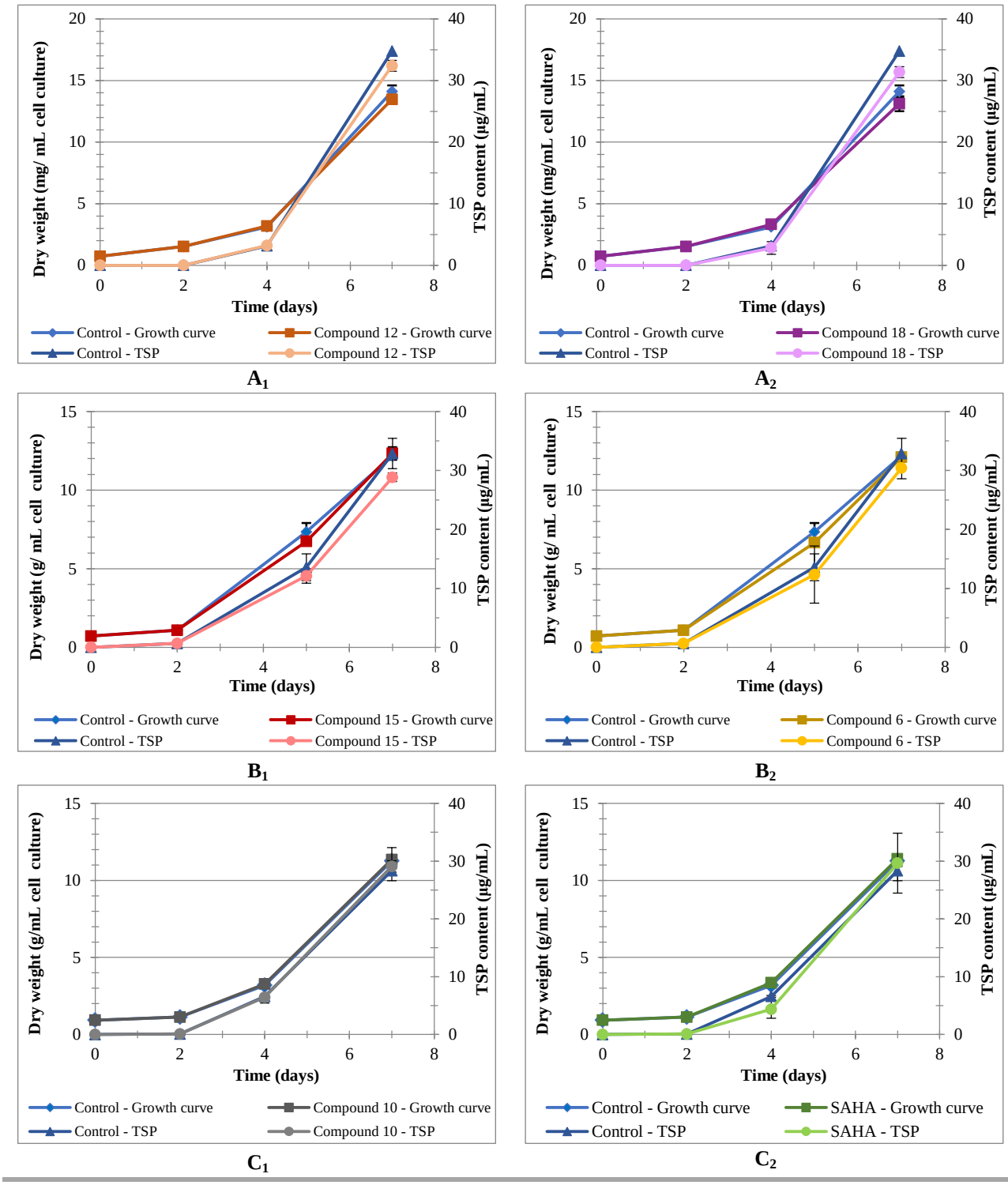

Figure 3-8- *Results obtained for the assays with 10 µM of each inhibitor and respective control. Growth curve and total soluble protein (TSP) of BY2 cultures expressing L-PDGS:* ***A_1/A_2-*** *control culture and cultures with compound* ***12*** *and* ***18***; ***B_1/B_2-*** *control culture and cultures with compound* ***15*** *and* ***6***; ***C_1/C_2*** *- control culture and cultures with compound* ***10*** *and SAHA. Error bars represent the standard deviation of three biological replicates.*

Figure 3-8 shows that the growth curves of all cell cultures had a similar behaviour. Comparing with the control samples, the addition of each inhibitor did not affect or delay cell growth, within each assay. As demonstrated in Figure 3-8, the curve of TSP had equal behaviour to the respective growth curve, i.e., as cell growth occurs, the amount of protein produced and secreted into the medium also increases. The TSP on day 7, for the three growth curves, was obtained within the range of 28 and 35 µg/mL.

To determine the relative amount of L-PGDS present in the culture medium, samples were resolved by SDS-PAGE. The presence of recombinant L-PGDS in the medium was confirmed by western blotting. For each point collected on each growth curve and analysed by Bradford assay, the sample which had the highest TSP values and a low standard deviation was chosen to be analysed by SDS-PAGE, as explained in Material and Methods, sub-section **2.3.2** and **2.3.3**.

The results obtained in the three assays can be found in Figures 3-9, 3-10 and 3-11. L-PGDS production varied depending on the compound added to the cell suspension cultures. This difference is noticeable in the size and density of the band present in the western blots presented below. The band appeared to have 26 kDa, which corresponds to the L-PDGS predicted molecular weight described in the literature. A marker NZYColour Protein Marker II was used. Relative quantification of recombinant L-PGDS was performed using FIJI software based on the relative density of the bands.

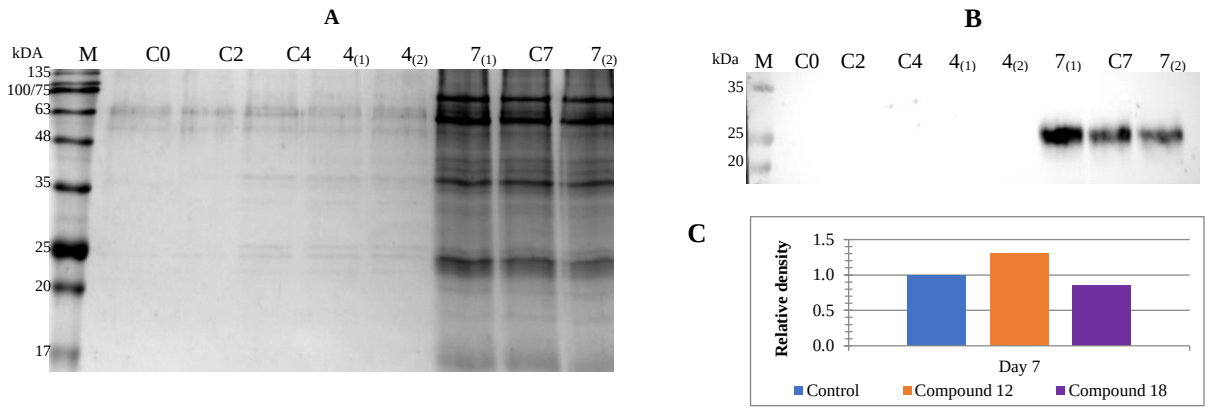

***Figure 3-9**- SDS-PAGE **(A)** and western blot **(B)** analysis of L-PGDS levels in BY2 cell culture. Culture medium was collected on day 0, 2, 4 and 7, before (C0, C2, C4, C7) and after treatment with 10 µM of compound **12** ($5_{(1)}$, $7_{(1)}$) and compound **18** ($4_{(2)}$, $7_{(2)}$). Graph **C** represents the relative density between compound and control in this screening.*

The scheme above (Figure 3-9) represents the analysis of L-PGDS levels from samples collected in growth curve A (Figure 3-8). The accumulation of L-PGDS was observed seven days after addition of compound **12** and compound **18**, which were added on day 2. Compared to the control samples, the

protein expression had a 1.3-fold increase in the presence of compound **12**. L-PGDS production decreased in the presence of compound **18**.

As explained in the previous experiment, Figure 3-10 shows the analysis of L-PGDS levels from samples collected in growth curve B (Figure 3-8). By analysing the western blot quantification, accumulation of L-PGDS was observed in higher amount in control samples, instead of the samples with compounds **15** and **6**. The L-PGDS levels were lower in the growth curve samples where compounds **15** and **6** were added on day 2.

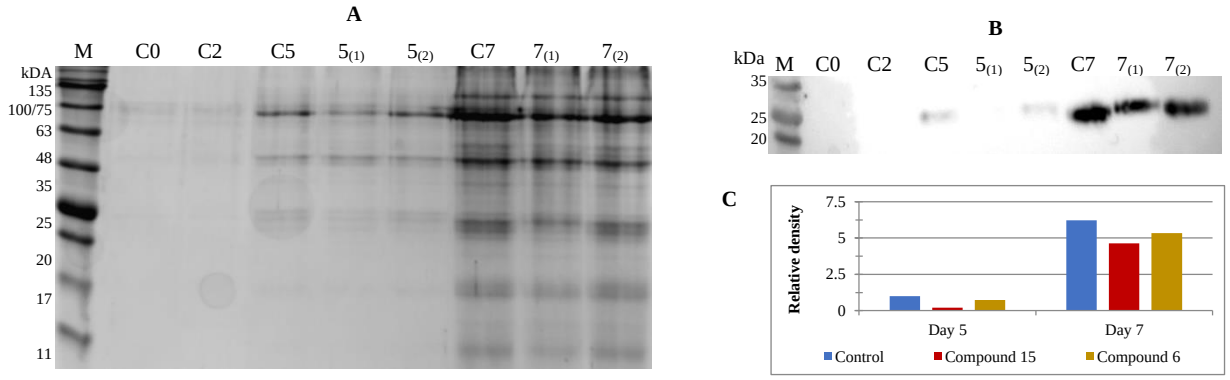

Figure 3-10- *SDS-PAGE **(A)** and western blot **(B)** analysis of L-PGDS levels in BY2 cell culture. Culture medium was collected on day 0, 2, 5 and 7, before (C0, C2, C5, C7) and after treatment with 10 µM of compound **15** ($5_{(1)}$, $7_{(1)}$) and compound **6** ($5_{(2)}$, $7_{(2)}$). Graph **C** represents the relative density between compound and control in this screening.*

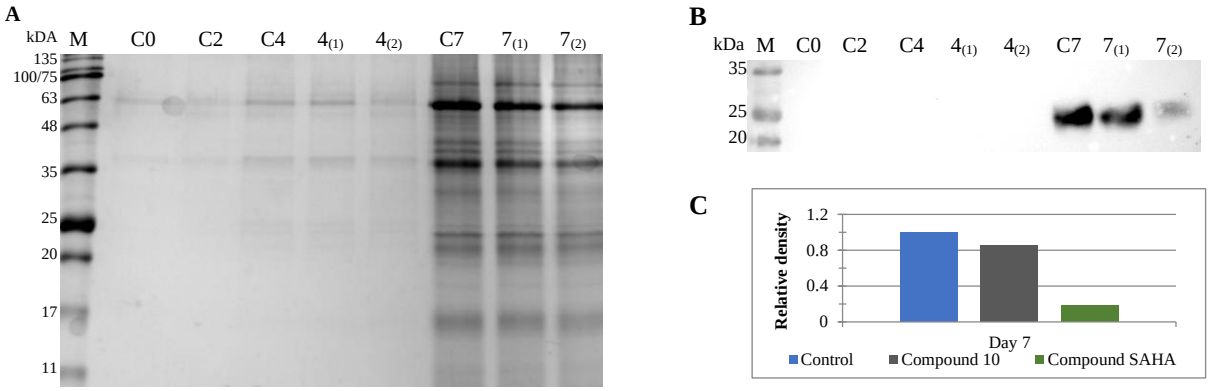

Figure 3-11- *SDS-PAGE **(A)** and western blot **(B)** analysis of L-PGDS levels in BY2 cell culture. Culture medium was collected on day 0, 2, 4 and 7, before (C0, C2, C4, C7) and after treatment with 10 µM of compound **10** ($4_{(1)}$, $7_{(1)}$) and SAHA ($4_{(2)}$, $7_{(2)}$). Graph **C** represents the relative density between compound and control in this screening.*

The third growth curve to be analysed (C, Figure 3-8) was composed by control samples and samples treated with compound **10** and commercial SAHA, represented in Figure 3-11. The addition of

compound **10** on day 2 had no effect towards increasing recombinant L-PGDS production, since the values obtained were similar to the control. However, the addition of SAHA caused a decrease of approximately 80% in the production of L-PGDS, in comparison to the control.

In order to simplify the observation of the effects of each of the inhibitors on the BY2 cultures, the samples corresponding to day 7 of the three western blot assays, represented above, were reanalysed by western blot, in a single experiment (Figure 3-12).

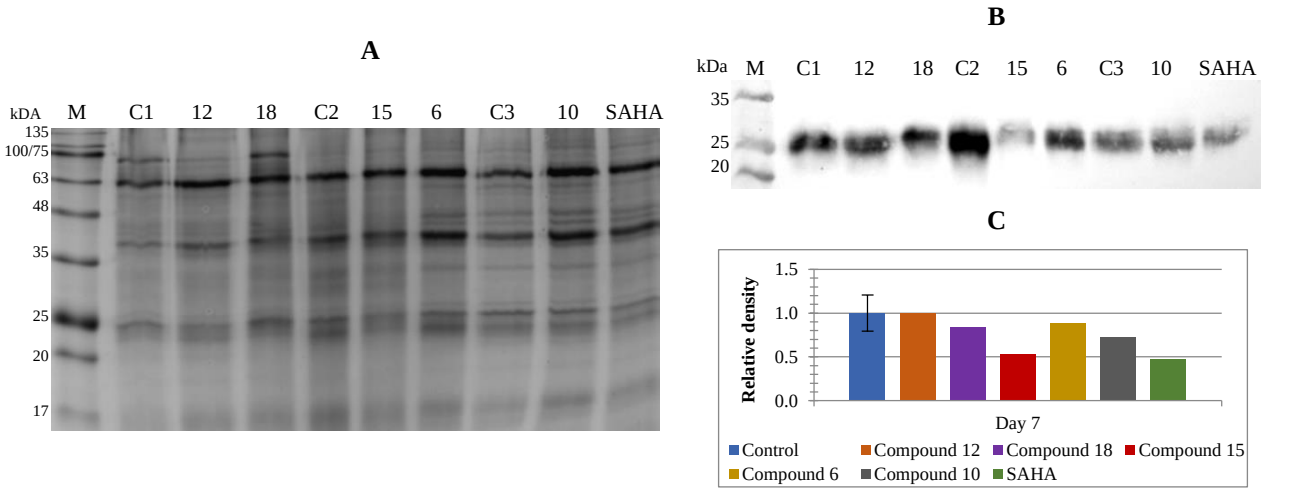

Figure 3-12- *SDS-PAGE **(A)** analysis for each inhibitor and respective control on day 7, stained with Blue safe and western blot detecting L-PGDS **(B)**: lanes C1, C2 and C3 correspond to control culture for each assay (day 7); the remaining lanes correspond to compounds **12**, **18**, **15**, **6** , **10** and SAHA. Graphisc **C** represents the relative density between compound and control samples.*

C2 from the second assay (assay represented in Figure 3-10) showed the strongest band density, followed by the sample with compound **12** and C1 (assay represented in Figure 3-9). Other samples showed similar band density, whereas samples with compound **15** and SAHA had very low band density. These bands regarding to L-PGDS protein were also quantified by FIJI software, by dividing the absolute density of the samples band by the absolute density of the control bands. Graph C in Figure 3-12 shows the ratio of L-PGDS concentration between control sample and samples treated with the respective inhibitor. The control sample in graph C is represented by the mean of C1, C2 and C3, with the respective standard deviation.

Combining the results obtained in sub-section **3.3.1** with the results obtained with these three screenings, the chosen compounds to undergo further biological tests were compound **12** and **6**.

3.3.3 Evaluation of the effect caused by compound 12

3.3.3.1 Analysis of cell viability and L-PGDS production

The possible toxic effect of compound **12** in BY2 cell culture expressing recombinant L-PGDS was evaluated by its impact on cell viability. The assay was run for 14 days, consisting of three biological replicates for the growth curve and four biological replicates for the TSP quantification. Collection of the culture medium and cells dry weights occurred on days 0, 2, 4, 7, 11 and 14. The results obtained are shown in Figure 3-13.

A

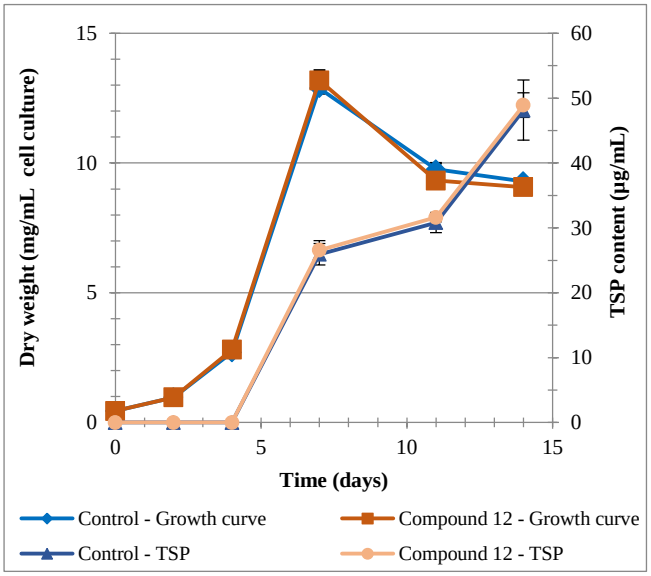

B

Cell viability (%)	Days					
	0	**2**	**4**	**7**	**11**	**14**
Control	87	87	94	94	87	79
Compound 12	-	-	88	91	88	81

Figure 3-13- (A) *- Growth curve and total soluble protein (TSP) of BY2 cultures expressing L-PDGS with and without inhibitor* ***12****. Error bars represent the standard deviation of three and four biological replicates, respectively.* ***(B) -*** *Measurement of cell viability along the growth curve in the presence or absence of compound* ***12****.*

The growth curve represented in graph A, Figure 3-13, had the expected behaviour, the exponential phase started on day 4 and reached its maximum before day 11. Cell viability followed the behaviour of the growth curve. The similarity between control cultures and the cultures where compound **12** was added on day 2, allowed us to conclude that this compound was not toxic to BY2 cells, since the difference between cell viability was less than 10%.

Although the amount of viable cells decreased on day 11 and 14, the production of proteins, Figure 3-13 (B), increased until day 14. When analysing the western blot (Figure 3-14, C_2), the presence of L-PGDS, with molecular weight close to 26 kDa in the culture medium of BY2 suspension cells was

verified. An accumulation of L-PGDS was observed over time. On day 7 there was a slight difference in L-PGDS expression between the cultures incubated with and without compound **12** on day 2. In the control culture, a higher production of the recombinant protein was observed on day 7. When compared to the control culture, protein expression increased 1.1-fold on day 11 and 1.3-fold on day 14, in the presence of compound **12**. This information corresponds to the data obtained in the initial screening.

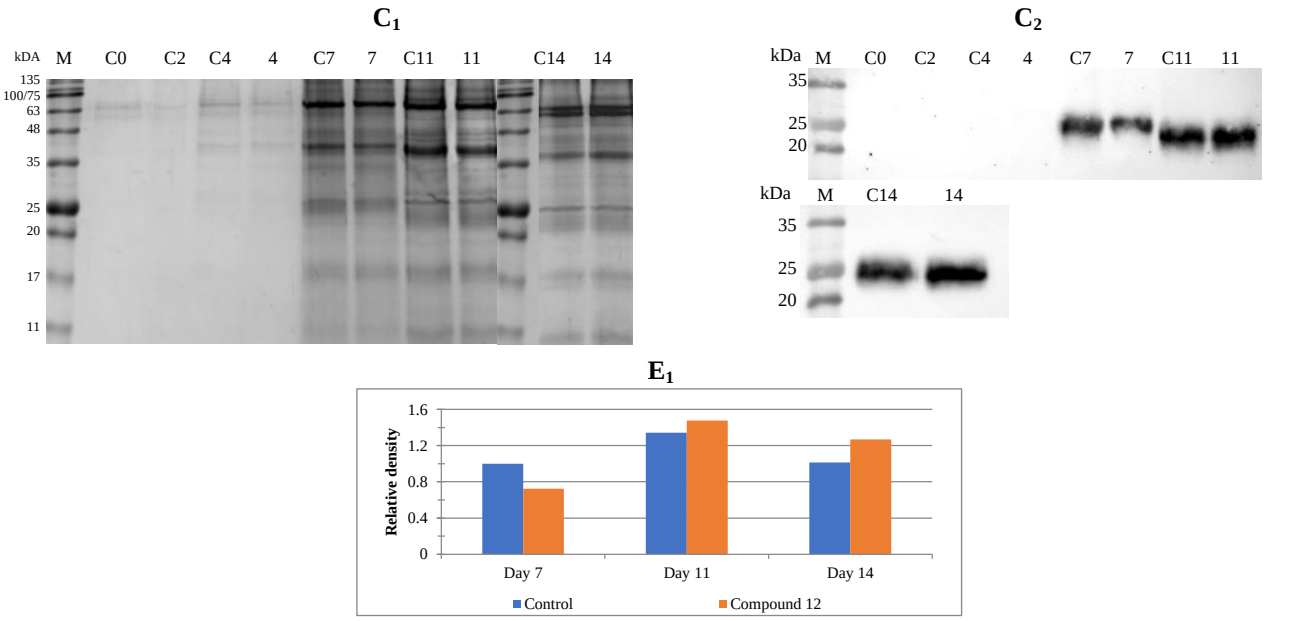

Figure 3-14- *Analysis of BY2 culture medium by SDS-PAGE* ***(C1)****, stained with Blue safe, and western blot detecting L-PGDS* ***(C2)*** *for days 0, 2, 4, 7, 11 and 14: lanes C0, C2, C4, C7, C11 and C14 correspond to control cultures and lanes 4, 7, 11 and 14 correspond to cultures with 10 µM of compound* ***12****. Graph* ***(E1)*** *shows the relative density between L-PGDS concentration.*

3.3.3.2 Analysis of acetylation levels in the presence of compound 12

Studies reveal that histone H3 is the most extensively acetylated histone in plants (Lusser et al., 2001). To test the efficacy of the synthesised compounds, the histone H3 acetylation levels were measured along the curve, in the absence or presence of inhibitor **12**. Histones were extracted from the samples collected along the growth curve after compound **12** addition on day 2, more details in section **2.2.7** and **2.5**. Each sample was analysed by SDS-PAGE (D_1) and western blot (D_2 and D_3), using a 15% of SDS-PAGE gel, Figure 3-15. A band with approximately 17 kDa was observed which is in accordance with the expected molecular weight for histone H3. This band was observed in the western blot (D_2) for the

detection of histone H3 acetylation levels as in the western blot (D_3) for detection of total histone H3 amount.

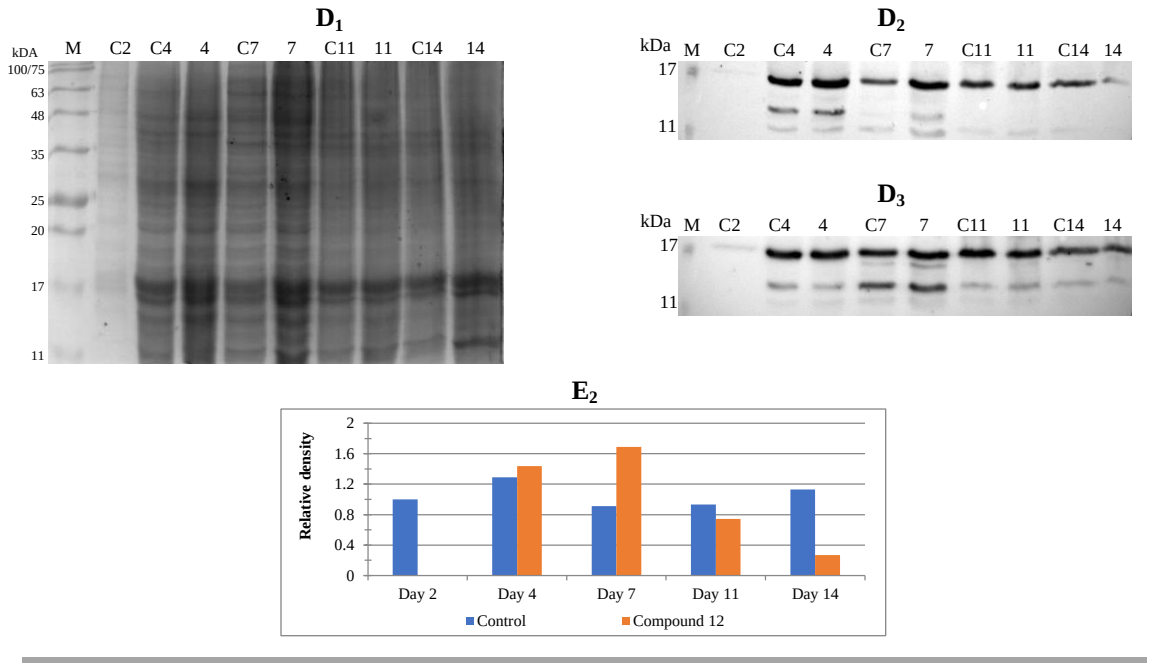

Figure 3-15- *The resulting extracts from histone extraction were analysed by SDS-PAGE* ***(D_1)*** *and western blotting: detection of acetyl-Histone H3* ***(D_2)*** *and Histone H3* ***(D3)****. Sample loading: lanes C2 (20 µL), C4-C11 (10 µL) and C14 (15 µL) corresponding to control cultures and lanes 4-11 (10 µL) and 14 (15 µL) corresponding to cultures with 10 µM of compound* ***12****. Graph* ***(E_2)*** *shows the relative density between Histone H3 acetylation.*

The bands were additionally quantified by FIJI software and the histone H3 acetylation levels were normalized to histone H3 protein levels (E_2). The relative density corresponds to the ratio of acetylation level of histone H3 and the total amount of histone H, for control samples and samples treated with compound **12**. This ratio was lower on days 4 and 7 in control cultures. It means that the compound **12** worked as HDACi, leading to an increase in histone H3 acetylation levels, 1.1 and 1.9-fold, respectively. However, on days 11 and 14, the ratio was higher on control cultures, meaning that the compound **12** did not affect the levels of acetylation. One of the hypothesis relays on the fact that compound **12** could be metabolized by the cells over time. Without inhibition, HDACs become active again, decreasing the levels of acetylation. In order to be able to continue increasing the acetylation levels, it would be necessary to add more compound **12**.

The analysis of histone H3 acetylation levels confirms that compound **12** could inhibit HDAC activity and this inhibition led to the accumulation of acetyl groups in histone H3 lysines on days 4 and 7. However, when the acetylation levels of the sample with compound **12** were lower, the amount of L-PGDS expressed in the culture medium of those samples was higher. Although the histones were less

acetylated at the end of the growth curve, the L-PGDS continues to be produced and accumulated in the culture medium.

3.3.4 Evaluation of the effect caused by SAHA

3.3.4.1 Analysis of cell viability and L-PGDS production

In sub-section **3.3.2** it was concluded that SAHA did not function as enhancer of L-PGDS production. Nonetheless, since SAHA is a commercial HDACi which is known to increase the level of histone acetylation, its inhibitory effect was tested on BY2 cells.

This experiment followed the same protocol as for compound **12**. The cell growth was followed for 14 days, consisting of three biological replicates for growth curve and four biological replicates for TSP quantification. The culture medium and cell dry weights were collected on days 0, 2, 4, 7, 11 and 14. The results obtained are shown in Figure 3-16. The growth curve represented in graph A, Figure 3-16, had the expected behaviour, the exponential phase starts from day 4 and reaches its maximum before day 11. Cell viability followed the behaviour of the growth curve. The similarity between control cultures and cultures where SAHA was added on day 2, allowed us to conclude that this compound was not toxic to BY2 cells, since the difference between cell viability was less than 5%.

A

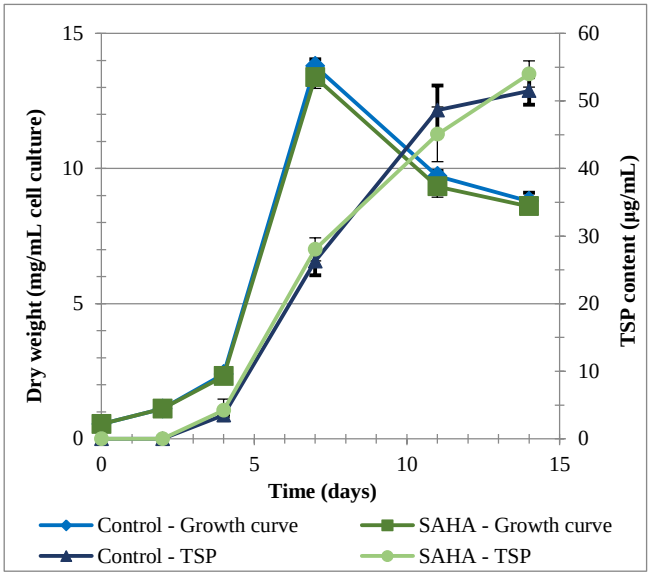

B

Cell viability (%)	Days					
	0	**2**	**4**	**7**	**11**	**14**
Control	90	89	89	90	86	86
SAHA	-	-	92	93	89	88

Figure 3-16- (A) - *Growth curve and total soluble protein (TSP) of BY2 cultures expressing L-PDGS with and without inhibitor SAHA addition. Error bars represent the standard deviation of three and four biological replicates, respectively.* ***(B) -*** *Measurement of cell viability along the growth curve in the presence or absence of SAHA.*

From the analysis of the western blot in Figure 3-17, C_2, the presence of L-PGDS, with molecular weight close to 26 kDa in the culture medium of BY2 suspension cells, was verified. An accumulation of L-PGDS was observed over time, decreasing on day 14.

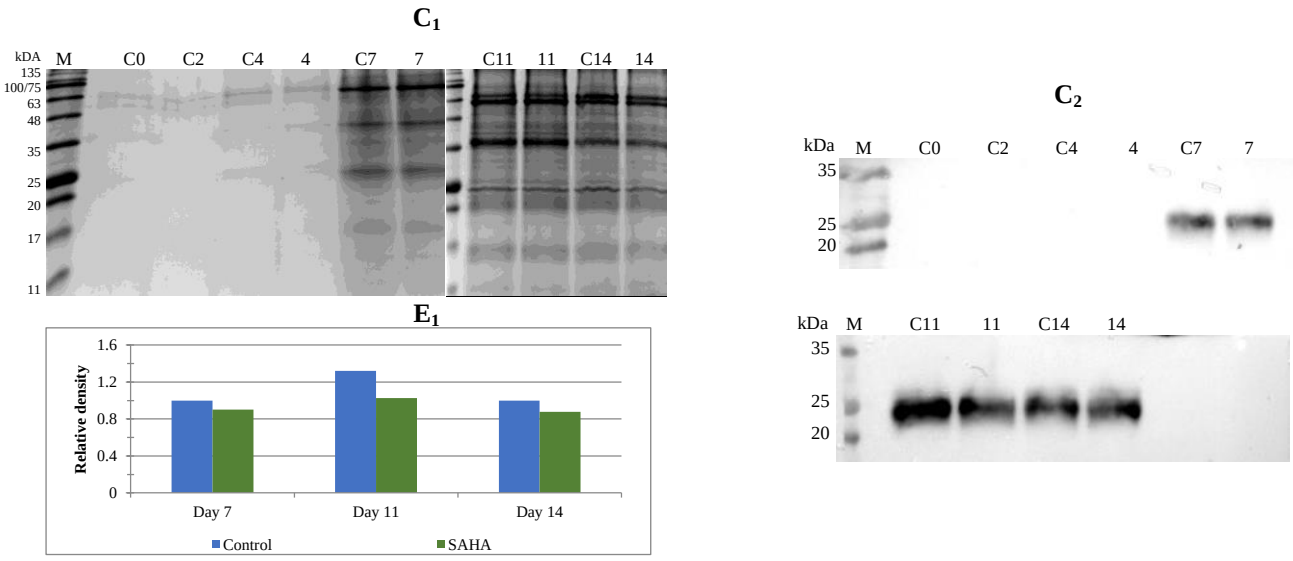

Figure 3-17- *Analysis of BY2 culture medium by SDS-PAGE* ***(C_1)****, stained with Blue safe, and western blot detecting L-PGDS* ***(C_2)*** *for days 0, 2, 4, 7, 11 and 14: lanes C0, C2, C4, C7, C11 and C14 correspond to control cultures and lanes 4, 7, 11 and 14 correspond to cultures with 10 µM SAHA. Graph* ***(E_1)*** *shows the relative density between L-PGDS concentration.*

In the control culture, a higher production of the recombinant protein occurred along the growth. Relative density results (E_1) allowed us to conclude that SAHA did not increase the production of L-PGDS, in none of the analysed samples. This information corresponds to the data obtained in the initial screening.

3.3.4.2 Analysis of acetylation levels in the presence of SAHA

Histone H3 acetylation levels were measured when SAHA was added. Histones were extracted from the samples collected along the growth curve, described in section **2.2.7** and **2.5**. Each sample was analysed by SDS-PAGE (D_1) and western blot (D_2 and D_3), using a 15% SDS-PAGE gel (Figure 3-18). There was a band with approximately 17 kDa corresponding to histone H3. This band was observed in the western blot (D_2) for the detection of histone H3 acetylation levels as in the western blot (D_3) for detection of total histone H3 amount.

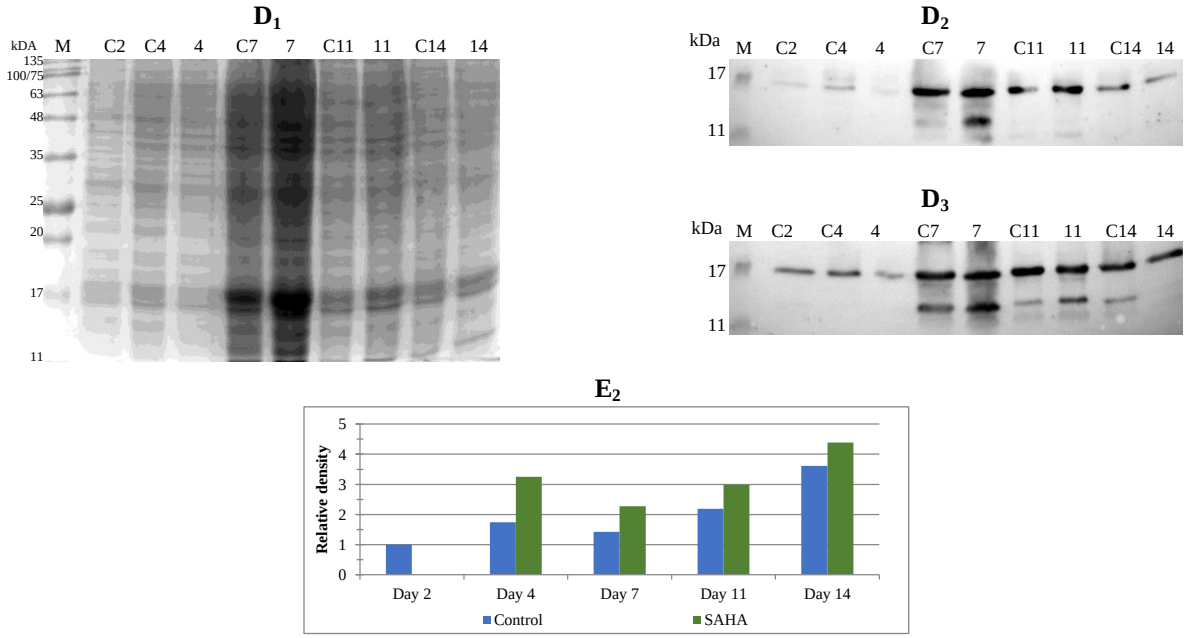

Figure 3-18- *The resulting extracts from histone extraction were analysed by SDS-PAGE* ***(D_1)*** *and western blotting: detection of acetyl-Histone H3* ***(D_2)*** *and Histone H3* ***(D3)****. Sample loading: lanes C2 (20 µL), C4-C11 (10 µL) and C14 (15 µL) corresponding to control cultures and lanes 4-11 (10 µL) and 14 (15 µL) corresponding to cultures with 10 µM of SAHA. Graph* ***(E_2)*** *shows the relative density between Histone H3 acetylation.*

The bands were additionally quantified by FIJI software and the results are presented after normalization (Figure 3-18, E_2). This ratio was lower in control cultures, it means that SAHA worked as HDACi, leading an increase of histone H3 acetylation levels on the analysed days. In this case, inhibition of HDACs occurred, since the levels of acetylated H3 in SAHA samples was higher than the control, with an increase of 1.9, 1.6, 1.4 and 1.2-fold on days 4, 7, 11 and 14, respectively. However, the increase of L-PGDS production did not occur. Although an increase in transcription may occur, it may not affect directly the production of the recombinant L-PGDS. On the other hand, the inhibitory potential of this compound may affect other mechanisms rather than acetylation, which may affect protein production.

These results indicate that a small modification in the structure of the compounds can influence their activity, by comparing the results obtained with SAHA and compound **12**. The addition of an electronegative element in compound **12**, fluorine at the *ortho* position, caused alterations in acetylation that caused an increase in the production of L-PGDS. This assay should be repeated in order to understand the effects of SAHA in BY2 cell cultures. Another possibility would be to investigate the expression of the L-PGDS gene to try to find out why there is no increase in the L-PGDS production.

3.3.5 Evaluation of the effect caused by compound 6

3.3.5.1 Analysis of cell viability and L-PGDS production

A

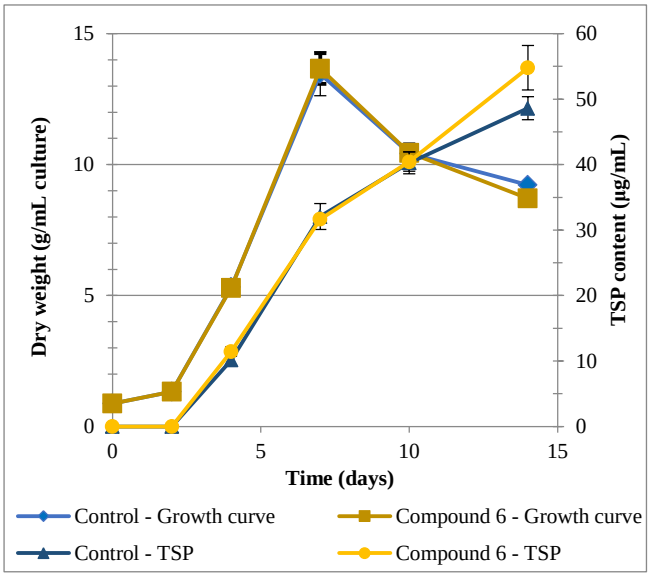

B

Cell viability (%)	Days					
	0	**2**	**4**	**7**	**10**	**14**
Control	89	89	90	89	89	89
Compound 6	-	-	93	90	92	88

Figure 3-19- (A) *- Growth curve and total soluble protein (TSP) of BY2 cultures expressing L-PDGS with and without inhibitor 6 addition. Error bars represent the standard deviation of three and four biological replicates, respectively.* ***(B)*** *– Measurement of cell viability along the growth curve in the presence or absence of compound* ***6****.*

Culture medium and cell dry weights were collected on days 0, 2, 4, 7, 10 and 14. The results obtained are shown in Figure 3-19. The growth curve represented in graph A, Figure 3-19, had the expected behaviour, the exponential phase starts from day 4 and reaches its maximum before day 10. Cell viability followed the behaviour of the growth curve and, the similarity between control cultures and cultures where compound **6** was added on day 2, allowed us to conclude that this compound was not toxic to BY2 cells, since the difference between cell viability was less than 5%.

The results obtained from the western blot analysis (Figure 3-20, C_2), confirmed the presence of L-PGDS, with molecular weight close to 26 kDa. An accumulation of L-PGDS was observed over time, decreasing on day 14.

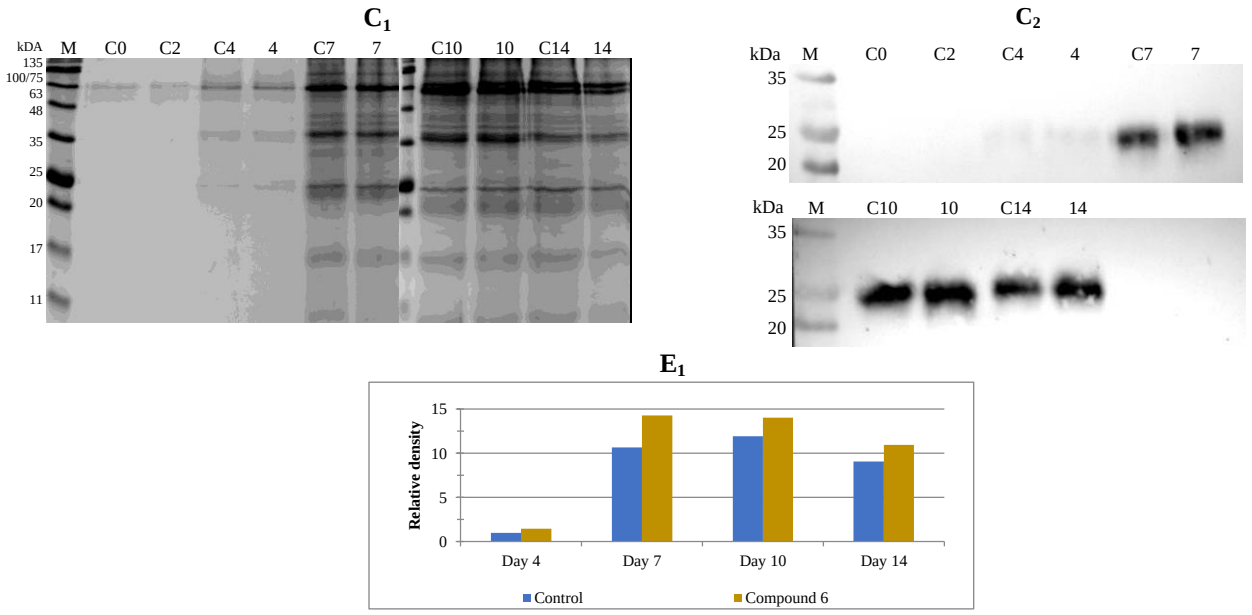

Figure 3-20- *Analysis of BY2 culture medium by SDS-PAGE* ***(C1)****, stained with Blue safe, and western blot detecting L-PGDS* ***(C2)*** *for days 0, 2, 4, 7, 11 and 10 : lanes C0, C2, C4, C7, C10 and C14 correspond to control cultures and lanes 4, 7, 10 and 14 correspond to cultures with 10 µM compound* ***6****. Graph* ***(E1)*** *shows the relative density between L-PGDS concentration.*

Along with the relative density (E_1), it was found that the compound **6** increased 1.4 and 1.3-fold the production of L-PGDS relative to the control culture, on day 4 and 7, respectively. On days 11 and 14, a higher production of L-PDGS in samples treated with compound **6** was also observed comparing to their controls, with an increase of 1.2-fold. This result was contradictory to the data obtained in the initial screening (section **3.3.2**, Figures 3-10 and 3-12). In that screening, the difference of L-PGDS levels between control cultures and the cultures with compound **6** was minimal. The variation observed in this assay was due to the use of biological replicates, which reflects intrinsic variations between samples. It is necessary to analyse more than one biological replicate to correctly assess the significance of results.

3.3.5.2 Analysis of acetylation levels in the presence of compound 6

Histone H3 acetylation levels were measured when the compound **6** was added. Histones were extracted from the samples collected along the curve, as described in section **2.2.7** and **2.5**. Each sample was analysed by SDS-PAGE (D_1) and western blot (D_2 and D_3), using a 15% SDS-PAGE gel (Figure 3-21).

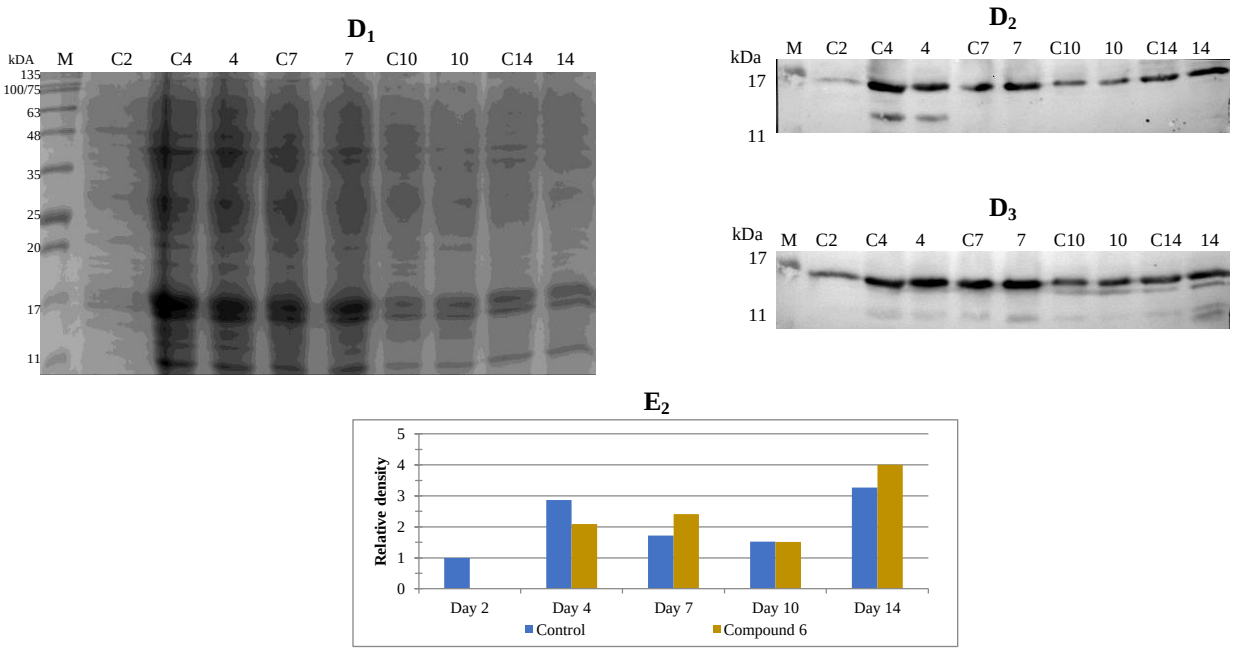

Figure 3-21- *The resulting extracts from histone extraction were analysed by SDS-PAGE* ***(D_1)*** *and western blotting: detection of acetyl-Histone H3* ***(D_2)*** *and Histone H3* ***(D3)****. Sample loading: lanes C2 (20 µL), C4-C10 (10 µL) and C14 (15 µL) corresponding to control cultures and lanes 4-10 (10 µL) and 14 (15 µL) corresponding to cultures with 10 µM of compound* ***6****. Graph* ***(E_2)*** *shows the relative density between Histone H3 acetylation.*

The band with approximately 17 kDa corresponded to histone H3. This band was observed in the western blot (D_2) detecting histone H3 acetylation levels as in the western blot (D_3) detecting histone H3 protein levels. The bands were also quantified by FIJI software and the results are presented after normalization (Figure 3-21, E_2). This ratio was lower on day 4 for control cultures but higher or equal to samples treated with compound **6** on days 7, 10 and 14, with 1.4, 1 and a 1.2-fold increase in acetylation levels, respectively.

Having two electronegative atoms in the aromatic ring, fluorine (*para*) and bromine (*ortho*), different stereoelectronic effects are expected that might affect the interaction of the compound with the enzyme. The linker is shorter, which has to be considered as well. This chemical structure may influence the mode of attachment to the active site, leading to different levels of binding stability. Even though the increase in acetylation levels was not constant, this compound is still very promising, both as inhibitor and as protein production enhancer. Similar to compound **12**, it has a fluorine in the capping group that seems to positively affect the L-PGDS production. It is necessary to repeat the assay to understand the effects of compound **6** in L-PGDS production and histone acetylation levels, or if it aids protein production by other mechanisms.

4 CONCLUSIONS

This master project aimed at producing a small library of hydroxamic and carboxylic acids and their corresponding esters. A total of 40 compounds were prepared and evaluated on *Nicotiana tabacum* BY2 cell suspension cultures, as potential enhancers of L-PGDS production. Six synthetic routes, each one with different conditions and starting materials, were performed in order to obtain these compounds. Even though the methodology used was not new, this allowed the efficient and rapid synthesis of a wide range of new compounds, which were fully characterized by NMR and FT-IR. The design of HDACi was quite challenging due to incomplete structural information of HDACs, especially regarding its isoforms.

Docking experiments were performed to describe the interaction between the metal binding moiety and the zinc ion present in the HDAC active site. It was a helpful methodology to understand how the capping group interacts with the surrounding residues in the entrance of the active site. This experiment allowed the visualisation of the best conformation for each ligand inside the HDAC active site. The molecular docking study in the human Hdac2 active site indicated an acceptable binding mode of the synthesised hydroxamic and carboxylic acids. The BFE values obtained were in the range of -8.8 kcal/mol and -16.5 kcal/mol. The ligands were differently positioned in the active site when a halogen was present in the capping group. These halogens take up more space at the entrance of the active site, possibly stabilizing the compound. This may positively influence the inhibitory potential of the compounds.

N. tabacum BY2 cell culture was used in this study since it is easily transformed, simple to manipulate and has a fast growth. A cell line expressing a human recombinant protein was used in this study, in order to test whether the addition of HDACi to the culture medium would cause an increase in the product yield. Inhibition of HDAC caused by the binding of the synthesised inhibitors to the HDAC active site, results in the accumulation of acetylated histones and other proteins. Acetylation of histone tails induces transcriptional activation through the opening of chromatin.

The toxicity of the synthesised HDACi, with a final concentration of 10 µM, was evaluated by their impact on cell viability. All compounds tested did not demonstrate toxicity towards the cells. When comparing the results obtained by SDS-PAGE electrophoresis and western blotting, compound **12** proved to be a good inducer of L-PGDS production. It has a fluorine substituent in the *ortho* position on the phenyl ring and an 8-carbon linker. On days 11 and 14, the L-PGDS expression had a 1.1 and 1.3-fold increase, respectively. Positive results were also obtained with the addition of compound **6**, with a 6-carbon linker, a fluorine substituent in the *ortho* and a bromine in the *para* position. The production of L-PGDS increased 1.3-fold on day 7 and 1.2-fold on days 10 and 14. Since electronegativity is a relative measure of the pulling force that an atom exerts, these electronegative halogens might aid the stabilization

of the compounds in the active site of an HDAC. However, a steric effect must also be considered, as the position of the halogen on the aromatic ring also influences the activity of the compounds. In contrast, SAHA did not lead to an improvement of L-PGDS production. The difference between SAHA and compound **12** is in the capping group. SAHA has no substitution on the phenyl ring. Compound **6**, besides the halogen substitution on the aromatic ring, has a shorter and rigid linker, due to the presence of the double bond, so different interactions occur at the binding site. SAHA may be involved in other cellular processes that may affect protein production.

Gene regulation is influenced by an intricate interrelation of HAT and HDAC activity. When the activity of the HDAC is low, hyperacetylation of histones can occur, thereby affecting gene expression. This interferes with the packing of chromatin, having a positive effect on gene transcription. The inhibition of HDAC activity resulted in different acetylation levels, which were measured by immunodetection with specific antibodies. The histone acetylation levels obtained were higher in SAHA treated samples comparing to control samples, for each day analysed. Compounds **12** and **6** also caused an increase in acetylation levels, but this increase was not as regular as it was in the presence of SAHA, which may be due to the use of only one replicate in this assay. Combining the information obtained from the assays, there must be other variants or mechanisms that influence the protein production, since the production of L-PGDS was not proportional to the acetylation caused by the presence of an HDACi.

Preliminary conclusions regarding the synthesised compounds reveal that substitution in the *ortho* position of the phenyl ring may be an important feature for HDAC inhibition and protein production. With the results obtained, it was confirmed that structural features other than the metal binding moiety of the synthesised compounds were important for HDAC inhibition, since not all hydroxamic acid compounds tested acted as protein enhancers or HDACis. Additionally, the geometry of the double bond can change the spatial arrangement of the molecule, influencing the biological activity of the analogues. Some reports suggest that modifications in the metal binding moiety are eliciting isoform selectivity. So, analogues with a carboxylic acid in that domain were synthesised and tested. However, carboxylic acid compounds did not appear to have an impact on the inhibition of HDACs. Subtle differences in HDAC catalytic site, depending on the isoform, may be the reason that there is no decrease in HDAC activity. In order to establish a detailed structure-function relationship, including the influence of the nature of the substituent, the position and number of these substituents at the aromatic ring, the size and rigidity of the linker, and the nature of the metal binding moiety, the other compounds of the library should be tested as well.

The project development is still very preliminary. In future work, several modifications should be tested to complete the information collected in this work. Perhaps, the design of an inhibitor with an aromatic group in the linker region could possibly result in discrimination among the HDACs isoforms. For this, it would be necessary to evaluate if the interaction of this group with residues in the hydrophobic

channel would be favourable or not. On the other hand, the design of the capping group with bulky groups could allow us to understand the behaviour and influence of this domain in the entrance of the active site of an HDAC. Every assay performed must be repeated, with biological and technical replicates to confidently assert that the results are accurate. Also, the growth curves with an HDACi addition should be built with more points per curve, i.e., collecting samples on day 0, 2, 4, 6, 8, 10, 12, 14 for example. Prior to implementation in large-scale or further testing, toxicity, cost and environmental impact should be rigorously evaluated and optimised.

Although the work is not yet completed, it was possible to draw some conclusions. New compounds were successfully synthesised by applying slightly more advanced chemical methodologies. This research has given an insight into the capability of some compounds to be a good fit in the HDAC catalytic site, verified by its inhibitory capacity. Two of the synthesised compounds significantly increased L-PGDS production. These compounds proved to be better enhancers than the commercial compound SAHA. This discovery will enable the design and synthesis of new analogues, taking into account the structural particularities of these two compounds. It was an extensive process that went through several steps: the synthesis of each compound, the computational prediction of the interaction between each compound and an HDAC, *in vitro* testing and, finally, *in vivo* experiments using BY2 cell suspension cultures. This multidisciplinary project was composed of three fields with different theoretical knowledge and different practical methodologies, allowing a more widespread learning.

5 BIBLIOGRAPHY

Abranches, R.; Marcel, S.; Arcalis, E.; Altmann, F.; Fevereiro, P.; Stoger, E. Plants as Bioreactors: A Comparative Study Suggests That Medicago Truncatula Is a Promising Production System. *J. Biotechnol.* **2005**, *120* (1), 121–134.

Allen, M. J.; Boyce, J. P.; Trentalange, M. T.; Treiber, D. L.; Rasmussen, B.; Tillotson, B.; Davis, R.; Reddy, P. Identification of Novel Small Molecule Enhancers of Protein Production by Cultured Mammalian Cells. **2008**, *100* (6), 1193–1204.

Aoki, S.; Ito, M. Molecular Phylogeny of Nicotiana (Solanaceae) Based on the Nucleotide Sequence of the matK Gene. *Plant Biol.* **2000**, *2* (3), 316–324.

Backliwal, G.; Hildinger, M.; Kuettel, I.; Delegrange, F.; Hacker, D. L.; Wurm, F. M. Valproic Acid: A Viable Alternative to Sodium Butyrate for Enhancing Protein Expression in Mammalian Cell Cultures. *Biotechnol. Bioeng.* **2008**, *101* (1), 182–189.

Barta, A.; Sommergruber, K.; Thompson, D.; Hartmuth, K.; Matzke, M. A.; Matzke, A. J. M . The expression of a nopaline synthase - human growth hormone chimaeric gene in transformed tobacco and sunflower callus tissue. *Plant Molecular Biology*. **1986**, (6) 347-357 .

Beillard, A.; Bhurruth-Alcor, Y.; Bouix-Peter, C.; Bouquet, K.; Chambon, S.; Clary, L.; Harris, C. S.; Millois, C.; Mouis, G.; Ouvry, G.; Pierre, R. A Facile and Rapid Preparation of Hydroxamic Acids by Hydroxylaminolysis Using DBU as Base. *Tetrahedron Lett.* **2016**, *57* (20), 2165–2170.

Bieliauskas, A. V.; Pflum, M. K. H. Isoform-Selective Histone Deacetylase Inhibitors. *Chem. Soc. Rev.* **2008**, *37* (7), 1402.

Boehm, R. Bioproduction of Therapeutic Proteins in the 21st Century and the Role of Plants and Plant Cells as Production Platforms. *Ann. N. Y. Acad. Sci.* **2007**, *1102*, 121–134.

Buyel, J. F. Process Development Strategies in Plant Molecular Farming. *Curr Pharm Biotechnol.* **2015**, *16* (11), 966–982.

Castilho, A.; Steinkellner, H. Glyco-Engineering in Plants to Produce Human-like N-Glycan Structures. *Biotechnol. J.* **2012**, *7* (9), 1088–1098.

Chen, X.; Wang, L.; Du, Y.; Wu, Y.; Jia, X.; Yang, Y.; Hong, B. Design, Synthesis and Biological Evaluation of Hydroxamic Acid Derivatives as Potential High Density Lipoprotein (HDL) Receptor CLA-1 up-Regulating Agents. *Molecules* **2011**, *16* (11), 9178–9193.

Chuang, D. M.; Leng, Y.; Marinova, Z.; Kim, H. J.; Chiu, C. T. Multiple Roles of HDAC Inhibitors in Neurodegenerative Conditions. *Trends Neurosci.* **2009**, *32* (11), 591–601.

Deprez, P.; Mandine, E.; Gofflo, D.; Meunier, S.; Lesuisse, D. Small Ligands Interacting with the Phosphotyrosine Binding Pocket of the Src SH2 Protein. *Bioorganic Med. Chem. Lett.* **2002**, *12* (9), 1295–1298.

Dietz, K. C.; Casaccia, P. HDAC Inhibitors and Neurodegeneration: At the Edge between Protection and Damage. *Pharmacol. Res.* **2010**, *62* (1), 11–17.

Fischer, R.; Stoger, E.; Schillberg, S.; Christou, P.; Twyman, R. M. Plant-Based Production of Biopharmaceuticals. *Curr. Opin. Plant Biol.* **2004**, *7* (2), 152–158.

Fischer, R.; Vasilev, N.; Twyman, R. M.; Schillberg, S. High-Value Products from Plants: The Challenges of Process Optimization. *Curr. Opin. Biotechnol.* **2015**, *32*, 156–162.

Gediya, L. K.; Chopra, P.; Purushottamachar, P.; Maheshwari, N.; Njar, V. C. O. A New Simple and High-Yield Synthesis of Suberoylanilide Hydroxamic Acid and Its Inhibitory Effect Alone or in Combination with Retinoids on Proliferation of Human Prostate Cancer Cells. *J. Med. Chem.* **2005**, *48* (15), 5047–5051.

Gomord, V.; Fitchette, A. C.; Menu-Bouaouiche, L.; Saint-Jore-Dupas, C.; Plasson, C.; Michaud, D.; Faye, L. Plant-Specific Glycosylation Patterns in the Context of Therapeutic Protein Production. *Plant Biotechnol. J.* **2010**, *8* (5), 564–587.

Gorman, C. M.; Howard, B. H.; Reeves, R. Expression of Recombinant Plasmids in Mammalian Cells Is Enhanced by Sodium Butyrate. *Nucleic Acids Res.* **1983**, *11* (21), 7631–7648.

Hellwig, S.; Drossard, J.; Twyman, R. M.; Fischer, R. Plant Cell Cultures for the Production of Recombinant Proteins. *Nat. Biotechnol.* **2004**, *22* (11), 1415–1422.

Hendricks, J. A.; Keliher, E. J.; Marinelli, B.; Reiner, T.; Weissleder, R.; Mazitschek, R. In Vivo PET Imaging of Histone Deacetylases by 18F-Suberoylanilide Hydroxamic Acid (18F-SAHA). *J. Med. Chem.* **2011**, *54* (15), 5576–5582.

Horn, M. E.; Woodard, S. L.; Howard, J. A. Plant Molecular Farming: Systems and Products. *Plant Cell Rep.* **2004**, *22* (10), 711–720.

Inoue, T.; Eguchi, Y.; Matsumoto, T.; Kijima, Y.; Kato, Y.; Ozaki, Y.; Waseda, K.; Oda, H.; Seiki, K.; Node, K.; et al. Lipocalin-Type Prostaglandin D Synthase Is a Powerful Biomarker for Severity of Stable Coronary Artery Disease. *Atherosclerosis.* **2008**, *201* (2), 385–391.

Kim, T. Y.; Bang, Y. J.; Robertson, K. D. Histone deacetylase inhibitors for cancer therapy. *Epigenetics.* **2006**, (1), 14–23.

Li, S.-O; Eakix, R. E. Synthesis of N-Phosphorylated Derivatives of Amino Acids. **1955**, *77*, 1866-1870.

Liu, X.; Yang, S.; Yu, C.-W.; Chen, C.-Y.; Wu, K. Histone Acetylation and Plant Development. **2016**, *40*, 173–199.

Lusser, A.; Kölle, D.; Loidl, P. Histone Acetylation: Lessons from the Plant Kingdom. *Trends Plant Sci.* **2001**, *6* (2), 59–65.

Ma, J. K.-C.; Drake, P. M. W.; Christou, P. Genetic Modification: The Production of Recombinant Pharmaceutical Proteins in Plants. *Nat. Rev. Genet.* **2003**, *4* (10), 794–805.

Ma, X.; Lv, S.; Zhang, C.; Yang, C. Histone deacetylases and their functions in plants. *Plant Cell Reports*. **2013**, *32*(4), 465–478.

Marks, P. A. Discovery and Development of SAHA as an Anticancer Agent. *Oncogene.* **2007**, 1351–1356.

Morris, G.; Huey, R. AutoDock4 and AutoDockTools4: Automated Docking with Selective Receptor Flexibility. *J. Comput. Chem.* **2009**, *30* (16), 2785–2791.

Mottamal, M.; Zheng, S.; Huang, T. L.; Wang, G. Histone Deacetylase Inhibitors in Clinical Studies as Templates for New Anticancer Agents. *HHS Public Access*. **2016**, *20* (3), 1–43.

Moustafa, K.; Makhzoum, A.; Trémouillaux-Guiller, J. Molecular Farming on Rescue of Pharma Industry for next Generations. *Crit. Rev. Biotechnol.* **2015**, *8551*, 1–11.

Nagata, T.; Nemoto, Y.; Hasezawas, S. Tobacco BY-2 Cell Line as the "HeLa" Cell in the Cell Biology of Higher Plants. *International Review of Cytology*. **1992**, 132, 1–30.

Obembe, O. O.; Popoola, J. O.; Leelavathi, S.; Reddy, S. V. Advances in Plant Molecular Farming. *Biotechnol. Adv.* **2011**, *29* (2), 210–222.

Parham, J. H.; Iannone, M. A.; Overton, L. K.; Hutchins, J. T. Optimization of Transient Gene Expression in Mammalian Cells and Potential for Scale-up Using Flow Electroporation. *Cytotechnology*. **1998**, *28* (1–3), 147–155.

Paul, M.; Ma, J. K. C. Plant-Made Pharmaceuticals: Leading Products and Production Platforms. *Biotechnol. Appl. Biochem.* **2011**, *58* (1), 58–67.

Pires, A. S.; Santos, R. B.; Nogueira, A. C.; Abranches, R. Production of Human Lipocalin-Type Prostaglandin D Synthase in the Model Plant Medicago Truncatula. *Vitr. Cell. Dev. Biol. – Plant.* **2014**, *50* (2), 276–281.

Ruijter, A. J. M.; Gennip, A. H. ; Caron, H. N.; Kemp, S.; Kuilenburg, A. B. P. Histone Deacetylases (HDACs): Characterization of the Classical HDAC Family. *Biochem. J.* **2003**, *370* (3), 737–749.

Salmi-Smail, C.; Fabre, A.; Dequiedt, F.; Restouin, A.; Castellano, R.; Garbit, S.; Roche, P.; Morelli, X.; Brunel, J. M.; Collette, Y. Modified Cap Group Suberoylanilide Hydroxamic Acid Histone Deacetylase Inhibitor Derivatives Reveal Improved Selective Antileukemic Activity. *J. Med. Chem.* **2010**, *53* (8), 3038–3047.

Santos, M. Iões metálicos em medicina: do diagnóstico à terapia. *Sociedade Portuguesa de Química*. Janeiro – Março, **2014**, pp 23–32.

Santos, R. B.; Abranches, R.; Fischer, R.; Sack, M.; Holland, T. Putting the Spotlight Back on Plant Suspension Cultures. *Front. Plant Sci.* **2016**, (*7)* 112–121.

Santos-Martins, D.; Forli, S.; Joa, M.; Olson, A. J. AutoDock4ZN: An Improved AutoDock Force Field for Small-Molecule Docking to Zinc Metalloproteins. J. Chem. Inf. Model. **2014**, 54, 2371-2379.

Schmidt, F. R. Recombinant Expression Systems in the Pharmaceutical Industry. *Appl. Microbiol. Biotechnol.* **2004**, *65* (4), 363–372.

Shirakawa, K.; Chavez, L.; Hakre, S.; Calvanese, V.; Verdin, E. Reactivation of latent HIV by histone deacetylase inhibitors. *Trends Microbiol.* **2013**, 21(6): 277–285

Silverberg, L. J.; Dillon, J. L.; Vemishetti, P. A Simple, Rapid and Efficient Protocol for the Selective Phosphorylation of Phenols with Dibenzyl Phosphite. *Tetrahedron Lett.* **1996**, *37* (6), 771–774.

Strober, W. Trypan Blue Exclusion Test of Cell Viability. *Curr. Protoc. Immunol.* **2001**, *111*, A3.B.1-A3.B.3.

Sun, J. K.; Eun, Y. C.; Yoon, J. C.; Ji, H. A.; Park, O. K. Proteomics Studies of Post-Translational Modifications in Plants. *J. Exp. Bot.* **2006**, *57* (7), 1547–1551.

Terpe, K. Overview of Bacterial Expression Systems for Heterologous Protein Production: From Molecular and Biochemical Fundamentals to Commercial Systems. *Appl. Microbiol. Biotechnol.* **2006**, *72* (2), 211–222.

Twyman, R. M.; Stoger, E.; Schillberg, S.; Christou, P.; Fischer, R. Molecular Farming in Plants: Host Systems and Expression Technology. *Trends Biotechnol.* **2003**, *21* (12), 570–578.

Urade, Y.; Hayaishi, O. Prostaglandin D Synthase: Structure and Function. *Vitam. Horm.* **2000**, *58*, 89–120.

Verdin, E.; Ott, M. 50 Years of Protein Acetylation: From Gene Regulation To Epigenetics, Metabolism and Beyond. *Nat. Rev. Mol. Cell Biol.* **2014**, *16* (4), 258–264.

Walsh, G. Biopharmaceutical Benchmarks 2014. *Nat. Biotechnol.* **2014**, *32* (7), 992–1000.

Walsh, G.; Jefferis, R. Post-Translational Modifications in the Context of Therapeutic Proteins. *Nat. Biotechnol.* **2006**, *24* (10), 1241–1252.

Wilken, L. R.; Nikolov, Z. L. Recovery and Purification of Plant-Made Recombinant Proteins. *Biotechnol. Adv.* **2012**, *30* (2), 419–433.

Xu, J.; Dolan, M. C.; Medrano, G.; Cramer, C. L.; Weathers, P. J. Green Factory: Plants as Bioproduction Platforms for Recombinant Proteins. *Biotechnol. Adv.* **2012**, *30* (5), 1171–1184.

Xu, J.; Ge, X.; Dolan, M. C. Towards High-Yield Production of Pharmaceutical Proteins with Plant Cell Suspension Cultures. *Biotechnol. Adv.* **2011**, *29* (3), 278–299.

Yamaoka, N.; Kodama, H.; Izuhara, Y.; Miyata, T.; Meguro, K. Structure-Activity Relationships of New N-Acylanthranilic Acid Derivatives as Plasminogen Activator Inhibitor-1 Inhibitors. *Chem Pharm Bull.* **2011**, *59* (2), 215–224.

Yan, J.; Chen, J.; Zhang, S.; Hu, J.; Huang, L.; Li, X. Synthesis, Evaluation, and Mechanism Study of Novel Indole-Chalcone Derivatives Exerting Effective Antitumor Activity Through Microtubule Destabilization in Vitro and in Vivo. *J. Med. Chem.* **2016**, *59* (11), 5264–5283.

Yao, J.; Weng, Y.; Dickey, A.; Wang, K. Y. Plants as Factories for Human Pharmaceuticals: Applications and Challenges. *Int. J. Mol. Sci.* **2015**, *16* (12), 28549–28565.

Zhang, Z.; Guo, K.; Bai, Y.; Dong, J.; Gao, Z.; Yuan, Y.; Wang, Y.; Liu, L.; Yue, T. Identification, Synthesis, and Safety Assessment of Forchlorfenuron (1-(2-Chloro-4-Pyridyl)-3-Phenylurea) and Its Metabolites in Kiwifruits. *J. Agric. Food Chem.* **2015**, *63* (11), 3059–3066.

6 APPENDIX

6.1 Solvents distillation

Anhydrous DMF

Addition of calcium hydride (SIGMA-ALDRICH) to distilled DMF, overnight stirring, followed by decantation and distillation under reduced pressure.

Anhydrous DCM

DCM refluxed with phosphorus pentoxide under an inert atmosphere for 2 h and then kept under inert atmosphere. Distilled before each use.

Benzyl alcohol

BnOH was distilled under reduced pressure.

Anhydrous toluene

Distilled over sodium and stored with sodium wire.

Anhydrous CH_3CN

Left over potassium carbonate overnight, distilled and kept over molecular sieves.

Anhydrous CCl_4

Refluxed and distilled over phosphorus pentoxide and stored over molecular sieves.

Anhydrous DIPEA

Distillation under reduced pressure over calcium hydride and kept at a temperature of 0 °C.

Anhydrous MeOH

To 100 mL of distilled MeOH, 5 g of magnesium (pre-dried in the oven) and a minimum amount of iodine were added. Refluxed until the magnesium has been consumed. 900 mL of distilled MeOH were added and kept under reflux for 3 h, followed by distillation

DBU

Fractional distillation under vacuum.

Anhydrous THF

THF was kept for 24 h over calcium hydride before distillation. Sodium wire and benzophenone were added to the distilled THF. The mixture was refluxed under argon for several hours until it acquired a violet colour. The mixture is kept at low reflux and under argon, being only distilled before its utilisation.

6.2 Solutions and buffers

Culture medium Murashing and Skoog

For 1 L of culture medium, 50 mL of MS salt (20 x) without vitamin, 30 g of sucrose (Duchefa Biochemie), 0.2 g KH_2PO_4, 0.1 g myo-Inositol (SIGMA-ALDRICH), 1 mg thiamine (Duchefa Biochemie) and 0.2 mg 2,4-dichlorophenoxyacetic acid (SIGMA-ALDRICH) were added. Potassium hydroxide was added until pH reaches 5.8 and then the solution was autoclaved. Stored at RT.

Buffer NE1

For a final volume of 15 ml, Tris-HCl (25 mM, pH 6.5), sucrose (0.45 M), magnesium chloride ($MgCl_2$, SIGMA-ALDRICH) (5 mM), β-mercaptoethanol (SIGMA-ALDRICH) (5 mM), phenylmethanesulfonyl fluoride (PMSF, AppliChem) (0.5 mM), pepstatin A (AppliChem) (0.364 µM), leupeptin (SIGMA) (1.2 µM) and Triton X-100 (SIGMA-ALDRICH) (0.1%) were added and kept on ice. This solution was prepared before use.

Buffer NE2

For a final volume of 5 mL, HEPES (50 mM, pH 5.7), NaCl (NZYtech) (420 mM), ethylenediaminetetraacetic acid disodium salt dehydrate (VWR®) (0.5 mM), triethylene glycol diamine tetraacetic acid (EGTA, SIGMA-ALDRICH) (0.1 mM) and glycerol (Scharlau) (10%) were added and kept on ice. This solution was prepared before use.

Sample buffer (4 x concentrated) for SDS-PAGE

Tris base (NZYtech) (320 mM, pH 6.8), SDS (NZYtech) (8%), β-mercaptoethanol (20%), glycerol (40%) and bromophenol blue (MERCK) (0.04%) were mixed together and the final volume completed with distilled water. The solution was stored at -20 ºC.

Extraction buffer HE1

For a final volume of 50 ml, sucrose (0.4 M), Tris base (10 mM, pH 8), $MgCl_2$ (10 mM), β-mercaptoethanol (5 mM) and PMSF (0.1 mM) were added and kept on ice. This solution was prepared before use.

Wash buffer HE2

For a final volume of 10 ml, sucrose (0.25 M), Tris base (10 mM, pH 8), $MgCl_2$ (10 mM), Triton X-100 (1%), β-mercaptoethanol (5 mM) and PMSF (0.1 mM) were added and kept on ice. This solution was prepared before use.

Extraction buffer HE3

For a final volume of 10 ml, sucrose (1.7 M), Tris base (10 mM, pH 8), $MgCl_2$ (2 mM), Triton X-100 (0.15%), β-mercaptoethanol (5 mM) and PMSF (0.1 mM) were added and kept on ice. This solution was prepared before use.

PBS (Phosphate-buffered saline, 10 x)

NaCl (1.36 M), potassium chloride (26.9 mM) (JOSÉ M. VAZ PEREIRA, S.A.), Na_2HPO_4 (SIGMA-ALDRICH) (16.8 mM) and KH_2PO_4 (15 mM) were dissolved in distilled water and pH adjusted to 7.6, using a pH Meter Basic 20. The solution was stored at RT.

Tripan blue

Tripan blue (0.4%) was added in PBS 1 x for a final volume of 10 mL.

SDS (Sodium dodecyl sulphate, 10%)

For 1 L of distilled water, 10 g of SDS were dissolved with the aid of heat. The solution was stored at RT.

APS (1.5%) for acrylamide gel

0.15 g of APS was dissolved in 10 mL of distilled water. This solution was unstable and was prepared before use.

Resolving buffer stock for SDS-PAGE

Tris base (3M) was dissolved in HCl (3M) and distilled water. pH was adjusted to pH 8.8, distilled water was added to the final volume and the solution was stored at 4 ºC.

Stacking gel buffer stock for SDS-PAGE

Tris base (0.5 M) was dissolved in HCl (1 M) and distilled water was added to the final volume. pH was adjusted to pH 6.8 and the solution was stored at 4 ºC.

Running buffer stock (10 x)

Tris Base (25 mM), glycine (SIGMA-ALDRICH) (1.92 M) and SDS (0.1%) were mix together and the pH adjusted to 8.3. The solution was stored at RT.

Protein transfer buffer

MeOH (CARLO ERBA) (20%) and running buffer 10 x (10%) were diluted in distilled water (70%) and stored at RT.

PBS-T

Tween® 20 (0.1%) (SIGMA – ALDRICH) was diluted in PBS 1x and stored at RT.

Detection solution Enhanced Chemiluminescence (GE Healthcare)

In an Eppendorf covered with aluminium, peroxidase solution and luminol enhancer (1:1) were mixed together before use.

Detection solution using Femto (ThermoScientific)

In an eppendorf covered with aluminium, SuperSignal West Femto Stable peroxidase buffer and SuperSignal West Femto luminol enhancer solution (1:1) were mixed together before use.